NOVA SCHOOL OF SCIENCE & TECHNOLOGY

DEPARTAMENT OF MATERIALS SCIENCE

NANOZYME+/DRIVING NANOZYMES TOWARDS STEREOCHEMICAL RECOGNITION: APPLICATION TO BIOMOLECULES OF INTERESTS IN HEALTH

ANA RITA AIRES CARDOSO

Master in Health Biochemistry

DOCTORATE IN NANOTECHNOLOGIES AND NANOSCIENCES

NOVA University Lisbon

October, 2023

DEPARTAMENT OF
MATERIALS SCIENCE

NANOZYMES+/DRIVING NANOZYMES TOWARDS STEREOCHEMICAL RECOGNITION: APPLICATION TO BIOMOLECULES OF INTEREST IN HEALTH

ANA RITA AIRES CARDOSO

Master's in health Biochemistry

Adviser: Maria Goreti Ferreira Sales
Full Professor, Coimbra University

Co-advisers: Pedro Miguel Cândido Barquinha
Associate Professor, NOVA University Lisbon

Examination Committee:

Chair: Pedro Miguel Ribeiro Viana Baptista,
Full Professor, **NOVA School of Science and Technology** | FCT NOVA

Rapporteurs: Rosa Fireman Dutra
Associate Professor, Federal University of Pernambuco/Biomedical department

Tito da Silva Trindade,
Full Professor, **Chemistry Department**, University of Aveiro**,**

Adviser: Maria Goreti Ferreira Sales,
Full Professor, Faculty of Sciences and Technology,University of Coimbra

Members: Rúben Miguel Pereira Fernandes
Full Professor, Faculty of Health Sciences, Fernando Pessoa University

Manuela Maria Teixeira Basto de Faria Frasco
Assistant Researcher, Faculty of Sciences and Technology, University of Coimbra

Rita Maria Mourão Salazar Branquinho
Assistant Professor, NOVA School of Science and Technology | FCT NOVA

DOCTORATE IN NANOTECNHOLOGIES AND NANOSCIENCES

NOVA University Lisbon
October, 2023

Nanozymes+/Driving Nanozymes towards stereochemical recognition: application in biomolecules of Interests In health

" O Sofrimento Purifica" Professor Goreti Sales

Dedicatory lorem ipsum.

ACKNOWLEDGMENTS

This dissertation is not only the result of my personal work, but also the result of all the important people who have surrounded me and whom I would like to thank.

I would like to thank my thesis supervisor Prof. Goreti Sales and my co-supervisors Prof. Pedro Barquinha and Prof. Elvira Fortunato for giving me the opportunity to develop this thesis under their close guidance.

Prof. Goreti I deeply thank for the daily encouragement, the confidence in my decisions, the scientific advice in our discussions and the constant enthusiasm. Also, for the inspiration, the patience to listen to me at all moments, for always being there for me and supporting me at all moments, and for being more than just an advisor to me. Prof. Goreti Is a mentor for me.

To all my colleagues in the BioMark group who have contributed directly or indirectly to this work. Especially to "zinha" who always listened to me over 5 years and for all the conversations we had (scientific and non-scientific). I apologise for taking some "Adalgur" in the middle of this process and pressurising with my stress.

For Akmaral Suleimenova who listened to me and found "Wednesday" in my little house (private joke) and for the scientific and non-scientific conversations we had. For supporting me during these two years, for the funny and stressful moments we had.

To Samuel, who supported me in this work and showed me a different way of looking at things.

To all my friends who supported me and were always there when I needed them (because science is full of ups and downs). To Margarete Sousa, Nivaldo Oliveira, Vanessa Ribeiro and Carlos Azevedo, thank you for continuing this crazy, wonderful friendship.

To my family, for their presence in my life, their support in my decisions and their kindness at the right moments.

To my parents for their patience, their presence, their affection and their night shifts. Thank you for this investment, for always letting me dream and for always supporting me in the most difficult moments. Thank you for helping me in all moments with my daughter.

To my sister (Mariana Cardoso) for all the warmth and presence in my life. Also for helping me with Clarinha and listening to me in all moments of my life.

To my uncles and aunts (Né, Fátima, Carlos, João, Edite) and my grandparents who have always supported me and believed in me.

To my dear husband Pedro, for his love, for his unconditional friendship, for being the best partner in all hours and really believing in me when I could not, for being my constant support and my most enthusiastic admirer. I would not be here without you! There are no words to describe how grateful I am. We continue together, always – and I cannot wait to find out what else the future holds for us.

And finally, my best achievement in life, my dear, incredible daughter Maria Clara, who has inspired me to become better and stronger every day since the first day of my life. She is my sweet "Gremlin". I hope that one day science will inspire her too!

"You cannot teach a man anything; you can only help him discover it in himself." (Galileo).

ABSTRACT

A reliable and affordable analytical platform is critical for clinical diagnosis. The electrochemical transduction mechanism in biosensors offers high selectivity, low limit of detection and easy miniaturisation. The present work aims to develop an electrochemical biosensor while exploring alternatives to natural bioreceptors and implementing low-cost and versatile nano-material production. The symbiosis of biosensor technology and nanomaterials improves selectivity and sensibility of the devices.

In this dissertation, four electrochemical biosensors were developed using two different biorecognition elements. Enzymes are used in many biotechnological approaches due to their excellent catalytic features and their ability to recognize a target compound within a complex matrix. Due to their high cost and limited stability, researchers have created artificial catalytic systems to replace natural enzymes. However, these systems employ nanostructured materials that can catalyse a reaction but lack the necessary stereochemical recognition ability.

The catalytic materials are combined with molecularly imprinted polymers (MIP), driving these artificially catalysed reactions into a spatial recognition event. A fundamental system that uses enzymes is the glucose meter, the first line of glucose control among diabetic patients. Thus, an innovative novel glucose enzyme-free biosensor is developed as a proof-of-concept by merging nanomaterials and MIPs in a single platform. The MIP technology offered selectivity to detect and quantify the glucose with dual detection, using electrochemical and optical systems.

In parallel, considering the current pandemic, the technical approach was used to detect human antibodies against severe acute respiratory syndrome coronavirus-2 (SARS-CoV-2). The potential for quantification of complex samples through electrochemical impedance spectroscopy has been successfully demonstrated in a real context, detecting concentrations down to pg/mL. The biosensing principles discussed herein open the way for the development of robust analytical devices that do not rely on natural bioreceptors and have the potential for use in point-of-care (POC).

Keywords: biosensors; electrochemical detection; molecularly imprinted polymers; SARS-CoV-2; Nanozymes

RESUMO

O desenvolvimento de plataformas analíticas precisas e fiáveis são fundamentais para o diagnóstico clínico. O mecanismo de transdução eletroquímica nos biossensores oferece maior seletividade, menor limite de deteção e fácil miniaturização. Este trabalho visa desenvolver um biossensor eletroquímico, explorando alternativas aos biorrecetores naturais e implementando uma produção versátil com a utilização de nanomateriais de baixo custo. A simbiose entre os biossensores e os nanomateriais melhora a seletividade e a sensibilidade dos dispositivos.

Nesta dissertação foram desenvolvidos quatro biossensores eletroquímicos com dois elementos de bioreconhecimento diferentes. As enzimas estão envolvidas em muitas abordagens biotecnológicas devido às suas excelentes características catalíticas e capacidade de reconhecer um composto alvo dentro de uma matriz complexa. Devido ao seu elevado custo e estabilidade limitada, os investigadores criaram sistemas catalíticos artificiais para substituir enzimas naturais. No entanto, estes sistemas empregam materiais com diferentes nanoestruturas capazes de catalisar uma reação, mas não possuem a capacidade de reconhecimento estereoquímico.

A combinação dos materiais catalíticos com os polímeros de impressão molecular (PIM), direciona essas reações catalisadas artificialmente para um reconhecimento espacial. Um exemlo de um sistema fundamental é o medidor de glucose, primeira linha de controlo da glucose entre pacientes diabéticos. Assim, um novo biossensor sem utilizar enzimas naturais para a glucose é desenvolvido como prova de conceito através da combinação de nanomateriais e PIMs numa única plataforma. A tecnologia PIM confere seletividade para detetar e quantificar a glucose com uma dupla deteção, eletroquímica e ótica. Paralelamente, considerando a atual pandemia, os biossensores eletroquímicos foram usados para detetar anticorpos humanos contra SARS-CoV-2. A potencial quantificação de amostras complexas através de espectroscopia de impedância eletroquímica foi demonstrada com sucesso em contexto real., detetando concentrações abaixo de pg/mL. Os princípios dos biossensores discutidos abrem caminho para a criação de dispositivos analíticos robustos que não dependem de biorrecetores naturais e têm um grande potencial em contexto clínico.

Palavras-Chave: Biossensores; Deteção Eletroquímica; Polímeros de Impressão Molecular, SARS-CoV-2, Nanozimas

CONTENTS

LIST OF FIGURES

LIST OF TABLES

ACRONYMS

2019-nCoV	Novel Coronavirus
AA	Ascorbic Acid
ABTS	2,20 -azino-bis(3- ethylbenzothiazoline-6-sulfonic acid)-diammonium salt
ACE-2	Angiotensin Converting Enzyme 2
AI	Aggregation Induced
AIE	Aggregation Induced Emission
APBA	Aminophenylboronic acid
ASSURED	Affordable, Sensitive, Specific, User-friendly, Rapid and Robust, Equipment-free and Delivered to those in need
Au NPs	Gold Nanoparticles
BSA-Ag NCs	Bovine serum albumin-protected silver clusters
CE	Counter electrode
CLIA	Chemiluminescent immunoassay
COF	Covalent organic framework
COVID-19	Corona virus Disease
C-SPEs	Carbon- Screen-Printed Electrodes
CV	Cyclic Voltammetry
DMF	*N*,Ndimethylformamide
DMSO	Dimethyl sulfoxide
DNA	Deoxyribonucleic Acid
DPV	Differential Pulse Voltammetry
ECL	Electrochemiluminescence

EDAC	N-ethyl-N'-(3-dimethylaminopropyl) carbodiimide hydrochloride
E Protein	Envelope Protein
EIS	Electrochemical Impedance Spectroscopy
ELISA	Enzyme-linked Immunosorbent Assay
FAD	Flavin Adenine Dinucleotide
GO	Graphene Oxide
GOx	Glucose Oxidase
HPLC	High-Performance Liquid Chromatography
HRP	Horseradish peroxidase
ISE	Ion-Selective Electrode
ISFET	Ion-Selective Field Effect Transistors
LoC	Lab-on-a-Chip
LOD	Limit of Detection
LSV	Linear Sweep Voltammetry
MPA	3-mercaptopropionic acid
MERS-CoV	Middle East Respiratory Syndrome Coronavirus
M Protein	Membrane Protein
MIP	Molecularly Imprinted Polymer
MOFs	Metal organic frameworks
NHS	N-Hydroxysuccinimide
NPs	Nanoparticles
N Protein	Nucleocapsid Protein
NAAT	Nucleic Acid Amplification Testing
NEB	Non-enzymatic biosensors
NFs	Nanoflowers
NIP	Non-Imprinted Polymer

PB	Prussian Blue
PBS	Phosphate Buffered Saline
POC	Point-of-Care
PPy	Polypyrrol
PSS	Poly(styrene sulfonate)
QDs	Quantum Dots
RBD	Receptor Binding Domain
RE	Reference Electrode
RFV	Relative fluorescence value
rGO	Reduced Graphene Oxide
RNA	Ribonucleic Acid
RSD	Relative Standard Deviation
RT-PCR	Reverse transcriptase-polymerase chain reaction
SARS-CoV-2	Severe Acute Respiratory Syndrome Coronavirus 2
SEM	Scanning Electron Microscopy
SOD	Superoxide Dismutase
S protein	Spike Protein
SPEs	Screen-Printed Electrodes
SWCNT	Single-walled carbon nanotubes
TEM	Transmission Electron Microscopy
TMB	3,3' ,5,5' - tetramethylbenzidine
SWV	Square-Wave Voltammetry
WE	Working Electrode
WHO	World Health Organization
UA	Uric Acid
ZnO-NW	Zinc Oxide Nanowires

SYMBOLS

C_{dl}	Double-layer capacitance
I	Current
I_D	Raman intensity of carbon D band
I_G	Raman intensity of carbon G band
R_{ct}	Charge-transfer resistance
R	Solution resistance
V	Potential
X	Average value of blank signal
Z'	Real component of impedance
Z''	Imaginary component of impedance
Z_W	Warburg impedance
σ	Standard deviation

CHAPTER 1

Motivation and aim of the thesis

1

MOTIVATION AND AIM OF THESIS

1.1 Scientific Context

The requirement for low-cost, rapid and precise sensing platforms for point-of-care (POC) use is constant in modern life.

The detection of glucose remains a matter of constant concern since it is relevant to diagnose or follow-up several diseases, as diabetes [1]. The relevance of glucose biosensors makes it a target for worldwide commerce, with increasing demand each year as more people is being diagnosed with diabetes and preventive care is spreading better [2]. The glucometer is the most common example that utilises the electrochemical modality due to its capacity to monitor glucose levels in diabetes with amperometric techniques [3]. Another important example of monitoring needs in POC emerged with the Novel Coronavirus (2019-nCoV), which was labelled a pandemic by the World Health Organization (WHO) due to its rapid spread. The capacity of response to the pandemic was intensively related to the use of lateral-flow tests.

Biosensors are proving to be extremely helpful in improving life quality in various domains ranging from water, food control, environmental and healthcare monitoring.

In 2022, the global biosensors market was valued at USD 28.6 billion, and it is predicted to reach USD 58.37 billion between 2023 to 2032 [4]. **Figure 1.1** depicts the evolution and anticipated growth of the North American biosensor market by application. The variety of medical applications, the growing number of diabetes patients, the high demand for compact diagnostic devices, and the quick technical advances are all driving demand for biosensors.

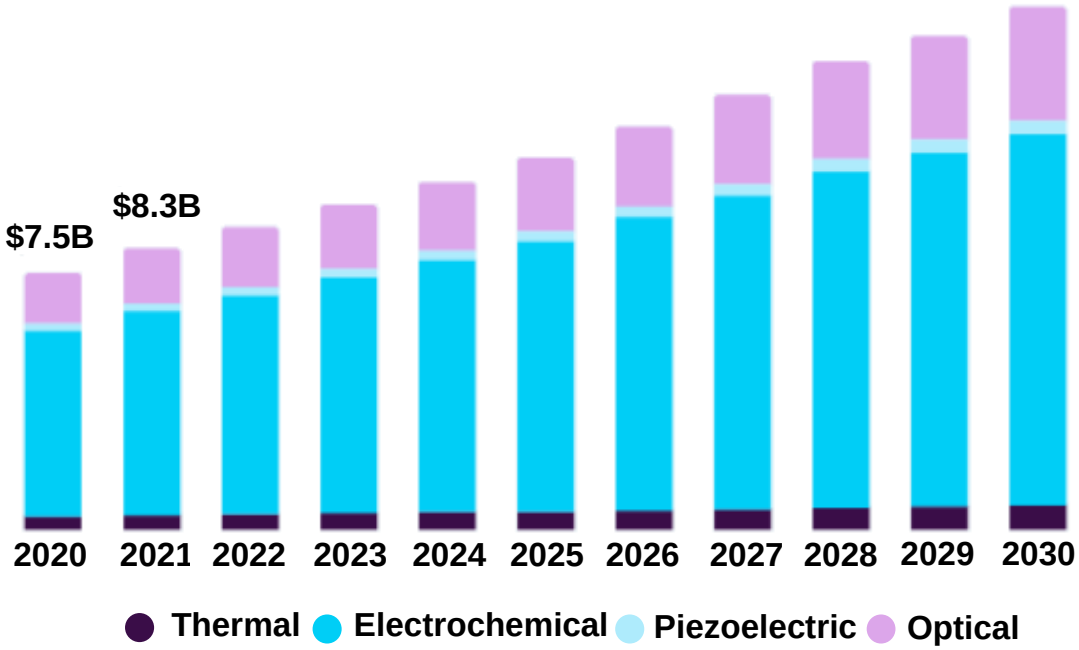

Figure 1.1: North America biosensors market growth by application. Values in USD million. Adopted from Grand View Research – biosensors market, 2022.

Glucose meters have been in the market for several decades and have evolved throughout several generations. The recent generation of glucose meters in the literature has lower cost and long-term stability then previous versions but lacks the necessary selectivity to allow accurate application in serum samples [5], [6]. Recently, nanozymes have emerged to replace the function of natural enzymes, but their affinity for the substrate still lacks spatial recognition [6]. This regard, MIP materials may help meeting spatial recognition requirements. These materials are host-tailored polymers, where a given target analyte acts as a mould when a polymeric network forms around it.

Overall, producing materials with catalytic activity properties that hold spatial recognition ability should allow the production of artificial enzymes with similar features to the natural-enzymes [7]. This was tried a few times, almost two decades ago, when MIP-technology and the nanoscale of materials were yet to face substantial developments [8]. Today, it is clear that the nanoscale control of materials is a crucial event, including the recent developments of MIP materials and the nanoscale manipulation of catalytic elements. For instance, the addition of charged species only at the rebinding site of MIPs has been shown to improve the affinity of a given target compound (which may be a protein [9] or a small molecule [10]), confirming that the nanostructural control is a crucial event.

Overall, the advent of dimensioning artificial enzymes that hold similar capacities to the natural one may revolution the biotechnology market. The procedure may be explore in many technological processes that use enzymes, significantly impacting society.
Moreover, this plan occurred in the middle of the pandemics. This was time of global uncertainty, in which many of us wanted to help. This was the case of this plan. Thus, to contribute some way to a better management of the pandemic, attempts are made to monitor the circulating antibodies against the virus. Quantifying the levels of antibodies may allow stratifying the population and distinguishing who has an active immune response against the virus from who has not.

1.2 Objectives

Due to the relevance and several advantages of the electrochemical transduction mechanism on biosensing, such as low detection limits, wide linear response range, excellent stability, and repeatability, this thesis seeks to explore novel technologies. that may benefit from different nanomaterials.

The main goals of this work are:

- Design and integration of a sensitive carbon nanomaterial, directly assembled on an electrochemical sensing platform;
- Fabrication of low-cost and innovative conductive nanomaterial to be fully integrated as biosensing platforms;
- Integration of catalytic nanomaterials and bioreceptor material, especially using molecular imprinting technology, on an electrochemical biosensor surface;
- Ultimately, catalytic molecular imprinting technology is fabricated to mimic the biological activity of relevant biomarkers.

1.3 Thesis Outline

This thesis is organized into eight chapters.

- **Chapter 1**: describes the motivation and the main objectives of this work, containing a summary description of the structure of the thesis.

- **Chapter 2** provides some fundamental background regarding the design and principle of biosensor devices, emphasizing aspects of particular relevance to the present work. A brief state-of-the-art applied to the selected biomarkers (glucose and Severe Acute Respiratory Syndrome Coronavirus 2 -SARS-CoV-2) is also described. An overview of the commonly used nanozymes and nanomaterials and their main applications is addressed herein.

- **Chapter 3** presents the main results concerning the development of a sensitive electrochemical biosensor having the Spike protein (S protein) on carbon-based screen-printed electrodes (C-SPEs) for monitoring in POC antibodies against SARS-CoV-2, an essential tool for epidemiological tracking of Coronavirus disease 2019 (COVID 19) and establishing vaccination schemes. In an innovative and straightforward approach, highly conductive support is combined with the direct adsorption of S protein to enable an extensive antibody capture. The high conductivity was ensured by using carboxylated carbon nanotubes on the carbon electrode, employing a simple and quick approach, increasing the surface area.

- **Chapter 4** shows the main results of an innovative, simple, and ultra-sensitive biosensor for monitoring antibodies against SARS-CoV-2 in POC. Protein-based exfoliation of graphite can provide stability, low toxicity, and high-quality graphene for applications with a biological interface. Herein, a cost-effective green technology resulting from the mechanical exfoliation of graphite into graphene in the presence of SARS-CoV-2 S protein was developed. The functional graphene-S protein nanosheets were prepared by a simple ultrasonic method. The carbon surface of the working electrode (WE) was modified with the biographene that enabled a subsequent binding of a layer of S proteins for enhanced capturing of the antibodies against SARS-CoV-2 in serum with great sensitivity. This strategy could be applied to numerous bioconjugates, combining the structural, electrochemical, and multifunctional properties of biographene for synergistic improvement of biosensors.

- **Chapter 5** describes the design, fabrication and main results of a non-enzymatic electrochemical glucose sensor. This sensor was developed using dual detection, optical and electrochemical signals, with nanoparticles (NPs) of gold produced in-situ based on MIPs in carbon SPEs (C-SPE/Au NPs/MIPs/Py-COOH) offering a high selectivity to

the sensor. This approach is straightforward, and the gold nanoparticles (Au NP) was electrodeposited *in situ*, improving the sensor's sensitivity. The formation of the Au NPs was investigated by scanning electron microscopy (SEM) and electrochemical techniques were used to confirm the successful fabrication of the sensor. Overall, this alternative is a promising tool for following glucose levels in serum. Besides, this biosensing device showed good sensitivity, reproducibility, accuracy, and rapid response time, contributing to quick glucose detection.

- **Chapter 6** focused on generating novel artificial enzymatic materials combining catalytic activity and spatial recognition abilities. This is done by merging MIP with nanozyme technologies. Such artificial enzyme materials, herein named as NANOZYME+, make use of (i) the ability MIP materials to establish a spatial recognition of the substrate, as in natural enzymes, and combine this with (ii) nanozymes, introducing catalytic properties at the "active site" where recognition takes place. As a proof-of-concept, this work is applied to generate innovative ENZYME-FREE SENSING devices used to diabetes.

- **Chapter 7** summarizes the main conclusions of this work and highlights potential applications for future research work.

- **Chapter 8** shows the scientific outputs of the candidate during the PhD period.

CHAPTER 2

Introduction

This chapter, detail background aspects related to this thesis. A brief background concerning biosensors' fundamental principles, followed by electrochemical devices and their applications in the health context, such as glucose and SARS-CoV-2, is presented and discussed. Afterwards, some theoretical concepts about molecular imprinting technology are provided, and the relevance of nanozymes is presented.

Some of the contents present in this chapter were adapted from:

Marques, A. C*., Pinheiro, T*., Martins, G. V., **Cardoso, A. R***.; Martins, R., Sales, M. G., Fortunato, E. Non-Enzymatic Lab-on-Paper Devices for Biosensing Applications. In Comprehensive Analytical Chemistry, Elsevier, 2020, 89, 189–237.
*Equal first authors

Cardoso, A. R*., Frasco, M*., Serrano, V*., Fortunato, E., Sales, M. G. Molecular Imprinting on Nanozymes for Sensing Applications. Biosensors 2021, 11, 152. https://doi.org/10.3390/bios11050152
*Equal first authors

Pinheiro, T *., **Cardoso, A. R***., Sousa, C. E. A., Marques, A. C., Tavares, A. P. M., Matos, A. M., Cruz, M. T., Moreira, F.T.C., Martins, R., Fortunato, E., Sales, M. G., Paper-Based Biosensors for COVID-19: A Review of Innovative Tools for Controlling the Pandemic. ACS Omega 2021, 6, 44. https://doi.org/10.1021/acsomega.1c04012
*Equal first authors

2.

INTRODUCTION

Biosensors are devices that convert the interaction of a biorecognition element with a target analyte into a measurable signal. These devices combine the specificity of interaction of an analyte of interest with a biological/chemical component, called (bio)recognition element, with the sensitivity of a transducer that converts such interaction into a measurable signal [11] (**Figure 2.1**).

The specificity/sensitivity of a biosensor is directly dependent on the specificity/sensitivity of the (bio)recognition element for the target compound, which constitutes a crucial part of the biosensor [12]. Typically, these (bio)recognition elements are enzymes, biomolecules, organelles, cells, proteins, among others. However, synthetic recognition elements have been used as biomimetic materials to mimic a specific biological property, offering higher stability and reproducibility than their natural counterparts [13]. Additionally, changes in the intrinsic properties of several nanomaterials when in contact with the target analyte have also been used in the last decade as a biosensing detection mechanism [14]–[16].

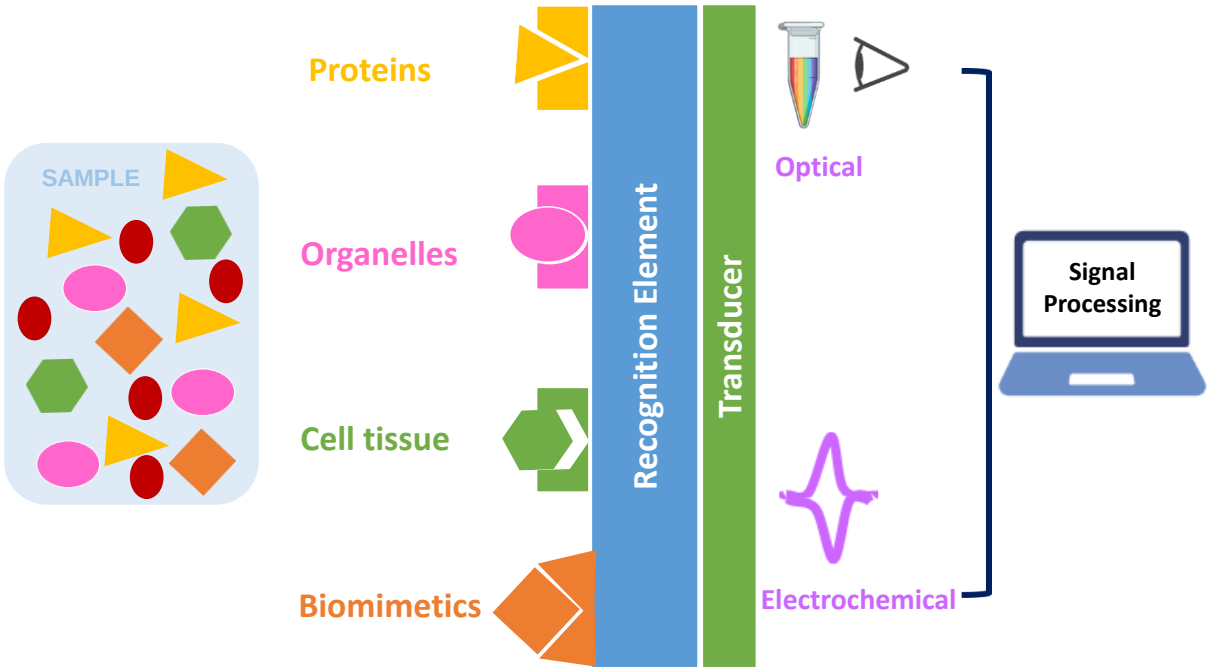

Figure 2.1: Biosensing device schematic representation with biorecognition and transduction elements.

POC biosensors allow rapid detection of several analytes and have become relatively common in developed countries, the best example being the rapid pregnancy test. POC tests are highly needed in developing countries because they show the potential to complement or even replace standard laboratorial testing. This emergency need for POC testing has also became clear in the course of the current pandemics, the COVID-19, in which it would be essential to have tests in the clinical context that would allow the doctor establishing safe and fast clinical decisions. In a whole, POC testing leads to reduced number of travels to clinical services and, consequently, medical expenses, in addition to providing means of screening in regions without access to medical and hospital infrastructures [17]. WHO, has established guidelines for the development of diagnosis for use in economically disadvantaged regions, known under the acronym ASSURED (Affordable, Sensitive, Specific, User-friendly, Rapid and Robust, Equipment-free and Delivered to those in need) [18]. Biosensors are prone to meet these guidelines. They are POC devices that have the potential to be used in numerous fields, since they can be tailored to measure several target molecules, with different transduction principals and a multitude of nanomaterials, in which biomimetic structures can be used.

For biosensing applications, the most conventional approaches employ biological recognition elements, as enzymes, antibodies or Deoxyribonucleic Acid (DNA) probes, to produce catalytic and affinity biosensors, with high performance and fast response times [19] The transduction

methods used in these devices are mostly optical (colour signals, fluorescence) and electrochemical (**Figure 2.2**). For signal readout and analysis, external readers such as scanners and smartphone-based technologies have been applied [20], as well as some equipment-free quantitative readouts methods [21].

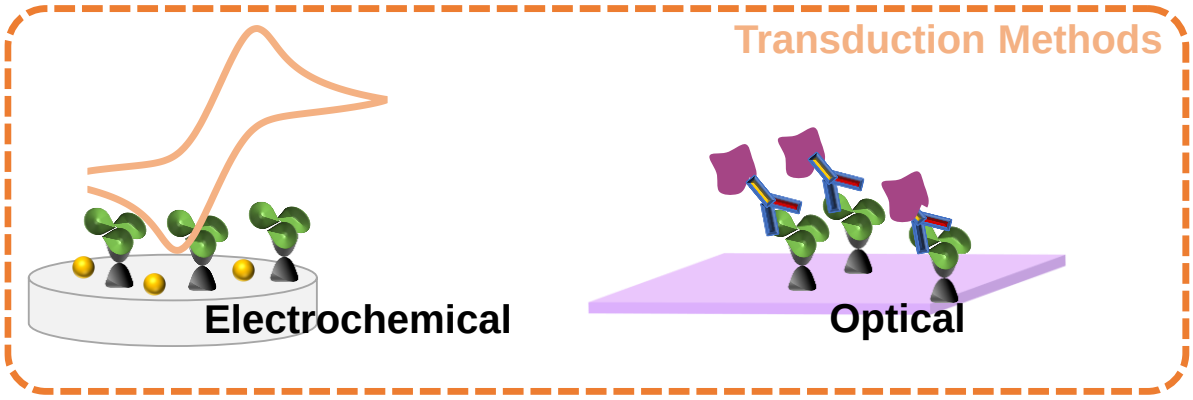

Figure 2.2: The most transduction methods use: Electrochemical and optical.

2.1 Electrochemical Biosensors

Electrochemical biosensors involve reading electrical-based properties around a redox reaction at the surface of a given electrode. Generally, this requires an electrochemical cell that is composed of two- or three-electrodes. The cell includes a working electrode (WE), a reference electrode (RE) and/or a counter electrode (CE). It is on the WE that the detection of a given compound is made possible, by means of a direct or indirect redox reaction occurring at the cell. In general, electroactive species may undergo electrochemical oxidation or reduction at the WE surface, which implies an electron transfer process. This electron transfer occurs between the electroactive molecule and the WE and can be followed via current measurements. Overall, the magnitude of current measured is related to the ongoing redox reaction, which depends on the kind of electroactive species involved, the background medium in which the electroactive species exists, and the electrochemical/ambient conditions employed to monitor the redox event [22]. Usually, the area of the CE is larger than that of the WE, to avoid limitation in the kinetic process involving current measurements [23], [24]. The RE is used to input pre-set potential differences into the WE.

Electrochemical biosensors have several beneficial features, including portability, cost effectiveness, small size and simplicity. Inexpensive electrodes can be integrated with simple electronics to accomplish rapid measurements and easy-to-use portable systems. Their ability to

detect the concentration of an analyte within a complex sample in real time is extremely valuable for medical diagnosis, food quality control and environmental monitoring [25].

Considering the overall organization of the electrodes, one may find microfluidic cells, lab-on-a-chip devices (LoC), SPEs, containing from macro to nanosized electrodes. They can be obtained by different methods, many times involving the deposition of a conducting ink by means of casting, spray-drying, spin-coating, drop-coating, or printing on a suitable substrate. These methods may enable mass production, offering high reproducibility and low-cost features [26], [27]. Over the years, different types of nanomaterials like carbon nanotubes (single and multi-walled) and graphene nanostructures have also been included in the production of electrochemical biosensors to improve the signal sensitivity and decrease the limit of detection (LOD), opening new avenues for biosensing applications [28]. The incorporation of these nanomaterials with different electrochemical strategies on eco-friendly substrates like paper allow the production of sustainable and low-cost sensing platforms for biomolecule detection in POC context [29]. According to the type of transducer, electrochemical biosensors can use of different techniques, as potentiometric, conductimetric, amperometric (that also includes voltammetric), and impedimetric [30].

Potentiometric readings are usually based on polymeric membrane ion-selective electrodes (ISEs) or ion-selective field effect transistors (ISFETs). They measure potential differences against a RE and monitor the potential changes against the logarithm concentration of a given ion. This approach has been employed for assessing directly the concentration of relevant ions in physiological fluids [31], as H^+, NH_4^+, or penicillin, among others, or indirectly by assessing the concentrations of neutral species that are involved in reactions with other ionic species, as is the case of glucose [32].

Conductimetric-based readings measure the electrical conductivity of a given sample solution, which is related to the ionic content (kind and concentration of ions). This may employ interdigitated microelectrodes combined with conducting polymers that may act as an electrochemical transducer converting biological to electrical signals [19].

Amperometric readings concern current or charge measurements upon the application of a constant potential at a WE, against the RE. They are usually linked to low LoDs, since the background signals are kept a minimal level [22], [33] Chronoamperometry is an approach widely employed that measures the steady-state current generated on the cell as a function of time, when the applied potential over the WE is maintained. Changes in current occur as a result of the electrode's diffusion layer - a stationary thin layer of solution in contact with the electrode surface - expanding or contracting [34].

In voltammetric readings, the potential value applied is changed in time and the current collected for each potential value monitored. The occurrence of electrochemical oxidation or reduction events at given potentials are evidenced by current changes, being the area of the current peaks observed related to the electron transfer involved. The voltammetric sensors are widely used by research groups in biosensing analysis, allowing them to directly correlate the resulting current measured at a constant potential value with the bulk concentration of the analyte species. There are different voltammetric techniques, from which the most common are cyclic voltammetry (CV), square wave voltammetry (SWV), differential pulse voltammetry (DPV), stripping voltammetry, polarography, or linear sweep voltammetry (LSV) [35].

CV is the often used as a voltammetric technique for primary research on the electrochemical behaviour of electrode for characterizations. CV measurements allow monitoring current variations while the potential applied on the WE is reversibly varied under a fixed scan-rate value. The electron transfer rate between the electroactive species and the electrode surface determines a redox process's reversibility [35]. Furthermore, CV is a widely used tool for assessing the reversibility of redox reactions through the simple measurement of voltammograms at different scan rates. Thus, a precise linearity between the peak current and the square root of the scan-rate is one of the prerequisites of reversible electrochemical processes. In addition, this consequence is an inherent aspect of a diffusion-controlled process. In irreversible systems, however, the linear potential sweep and CV produce an identical voltammetry profile since no reversal peaks arise when the sweep direction is changed [36].

SWV has been recognized as an important method for sensitive detection of significant biomolecules such as proteins, nucleic acids, and so on. In general, the excitation signal in SWV is formed of an amplitude symmetrical square-wave pulse paired with a step-height staircase waveform, with the forward pulse of the waveform equal to the staircase step [36]. Furthermore, the net current is calculated by subtracting the forward and reverse currents. The key advantages of this voltammetric approach include a higher scan-rate during analysis, less consumption of electroactive species, and improved performance due to electrode surface passivation [36].

Impedimetric readings make use of electrochemical impedance spectroscopy (EIS) to monitor the response of an electrochemical cell against an applied potential (or under open-circuit), in which the frequency dependence may reveal underlying chemical processes. Generally, the measurements can be applied under Faradaic or non-Faradaic conditions [37]. Herein, the focus was on the Faradaic processes that require a redox marker species.

EIS is routinely used for characterising functionalised electrode surfaces, enabling sensitive measurements related to surface phenomena or variations of bulk properties. Data can be represented as Nyquist (the imaginary impedance Z" plotted against the real impedance component Z') and Bode plots (both the logarithm of absolute impedance |Z| and the phase shift ϕ plotted against the logarithm of the excitation frequency). Nyquist plots, also known as Cole-Cole plots, are one of the most used methods for evaluating impedance information because they allow an easy prediction of circuit parts and for graphical extrapolation to derive the R_Ω parameter (**Figure 2.3**) [38], [39].

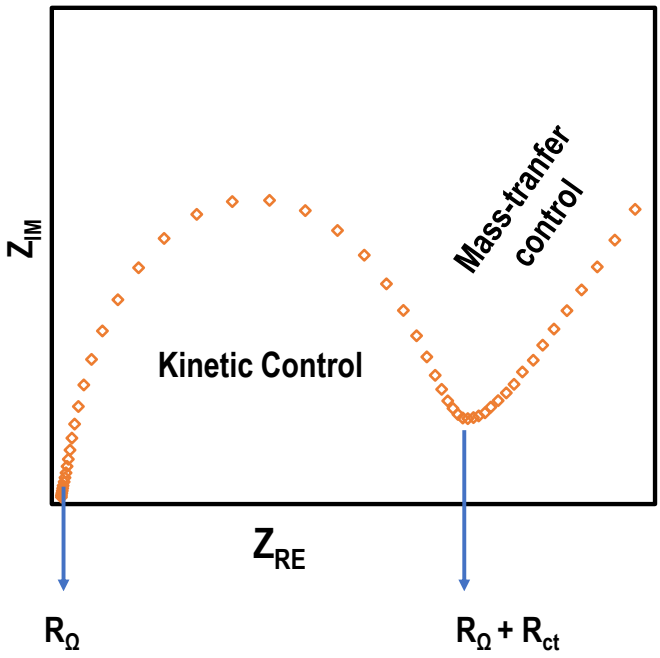

Figure 2.3: General Nyquist plot represented for an electrochemical system, having real impedance (Z_{RE}) plotted *versus* imaginary impedance (Z_{IM}), with solution resistance (R_Ω) and charge transfer resistance (R_{CT}) indicated.

Typically, the impedance data is fitted to an analogous electrical circuit representing the physical process in the interface system. As a result, any process that occurs in an electrochemical cell can be represented by equivalent circuits made up of various combinations of resistors (R), capacitors (C), and/or inductors (L). In electrochemical biosensors, the most common data fitting makes use of the equivalent Randle's circuit. This includes (1) the solution resistance, R_s, which is impacted by ionic concentration, ion type, and electrode area; (2) the resistance to charge transfer, $R_{ct,}$ which is proportional to the electron transfer; (3) the double-layer capacitance. C_{dl}; (4) and the Warburg impedance, $Z_{w,}$ which is linked to diffusion processes occurring under steady state conditions [40]. The Nyquist plot for a Randle's cell at higher frequencies

comprises a single temporal semi-circle curve displaying the charge transfer process and a diagonal line indicating the diffusion process (Warburg impedance), while at lower frequencies [41].

Usually, EIS measurements are conducted in the presence of both reduced and oxidized forms of a redox probe, which undergo redox reactions at the electrode surface under these conditions. An electrochemical reaction can typically occur on the electrode surface via two unique limiting mechanisms: kinetically controlled (charge transfer based) and diffusion controlled (mass transfer based). Thus, the reactions occurring at the electrode-electrolyte interface include a quick mass-transfer reaction, a gradual charge-transfer response, and, eventually, an interface diffusion phenomenon.

To summarize, EIS has been broadly open to various areas of expertise, such as metal corrosion, electrochemical synthesis of materials, and biosensor devices [41]–[43]. Numerous applications of EIS in biosensing can be found in the literature, which includes the quantification of DNA hybridisation, antigen-antibody and protein-protein interactions and other mechanisms [38], [39].

2.2 Common Applications of Biosensors

Electrochemical biosensors are highly involved in POC applications, for being linked to low-cost devices with simple analytical procedures. They have also been benefiting from the huge advances in the way nanomaterials have been tailored and integrating their assembly. In a whole, electrochemical biosensors allow developing new tools in response to global efforts and alliances that aim to fight current and future pandemics and screen chronic diseases, allowing earlier detection and medical action to improve treatment outcomes.

These global developments in terms of biosensing have been mostly linked to diabetes, through glucose monitoring, or the corona virus disease 2019 (COVID-19), caused by the severe acute respiratory syndrome coronavirus-2 (SARS-CoV-2). Thus, these two specific applications were the main focus of this plan, accounting the use of different nanomaterials that may be employed, with or without catalytic action.

2.2.1 Glucose

The WHO and the International Diabetes Federation estimated that the 415 million adults that had diabetes in 2015 will increase up to more than 640 million people in 2040 [44]. Diabetes *Mellitus* is a chronic metabolic disorder in people worldwide [44]. This disorder causes large fluctuations in blood sugar levels because the pancreas does not produce enough or doesn't properly use insulin to regulate glucose metabolism (type I), or the cells do not respond to this production (type II) [44] [45]. Furthermore, Diabetes has been associated with many other pathologies, such as coeliac disease, cystic fibrosis, tuberculosis and heart disease, resulting in many complications like retinopathy leading to blindness, nephropathy leading to renal failure, peripheral nerve damage with increasing risks of extremity (foot) ulcers amputation, cardiovascular diseases or even cancer [46], [47]. As there is no cure, Diabetes has been managed by preventing and delaying chronic disorders, by following a diet control agenda, exercising, and monitoring blood glucose levels [48].

There are today many works focusing on developing new methods for monitoring glucose [49], because this is essential for controlling diabetes. Several biosensors have been developed to monitor blood glucose levels, and the implementation of microsystem technologies contributed to further advancements in the development of biosensors [50]. Biosensors have evolved in the last decades to assess blood glucose levels [51]. The first effective biosensor was an enzyme-based electrode to measure the blood glucose level, proposed by Clark and Lyons in 1962 [52], but this approach has evolved within time. The enzyme-based glucose biosensors are now divided into three types [49]: the first generation (the use of oxygen as co-substrate and also on the formation and liberation of H_2O_2) [53]; the second generation (replaced oxygen detection by redox mediators, which transfer electrons effectively) [54]; and the third generation (direct transfer of electrons between enzyme and electrode, in the absence of mediator) [55].

There are several transduction schemes for the direct or indirect detection of glucose on a biosensor. This includes reading electrochemically-active species (typically when the electrochemical species such as electrons are utilized or produced in the bio-interaction process) or optical properties (of the intrinsically fluorescent or coloured compounds, their coenzymes or co-substrates), which may include a wide range of nanomaterials to improve the performance of the biosensor [56]. The first colorimetric sensor was 1965 based on colorimetric detection of hydrogen peroxide liberated by oxidation of glucose-by-glucose oxidase (GOx). The first

functional electrochemical biosensor was developed in 1967, by Updike and Hicks [57]. Later on, in the period 1974-1975, thermal transducers in enzymatic biosensors were also developed. The most studied and marketed detection methods for glucose are electrochemical enzyme sensors using GOx [58]. The use of GOx ensures the selectivity of the method, enhancing the ability of the biosensor to discriminate glucose among other compounds in complex samples. But the use of GOx for oxidizing glucose also brings limitations, because enzymes are very sensitive to a wide range of parameters, as medium composition, temperature, pH, which conditions storage capacity and reduces the lifetime of the biosensor.

Thus, a wide range of alternative approaches for glucose sensing not requiring an enzyme have emerged in time [59]. In these, the oxidation of glucose at sufficiently low potentials is granted by a catalytic material, usually of inorganic nature. Several studies of non-enzymatic glucose oxidation employed metal catalysts, such as Au, Pt, Cu, Ni or single polycrystalline metals (Au, Pt and boron doped diamond), in solution or as NPs [60]. Such enzyme-free sensors offer improved reliability by eliminating drift related to enzymatic degradation [61]. However, these sensors using enzyme-free catalytic materials show an unspecific response for other sugars (saccharides) and other co-existing compounds, as ascorbic acid (AA) and uric acid (UA) [62]. This is a result of the lack of spatial constraints when the catalytic event takes place.

But a spatial recognition of a given substrate may be established by means MIP technology. In principle, a combination of MIP and catalytic materials would eliminate the lack of selectivity of the enzyme-free catalytic materials, by allowing a stereochemical recognition of glucose upon binging. MIPs also show some advantages, being of quick response, low-cost and easy to produce. Also, a target molecule is imprinted in a functional polymer so that it is possible to concentrate the target molecule and undergo an easier quantification process [63].

2.2.2 SARS-CoV-2

A novel human coronavirus, named SARS-CoV-2, emerged in December 2019, in Wuhan, Hubei Province, prompted a pandemic declaration of the Corona Virus Disease (COVID-19), by the WHO on March 11, 2020. By 4th October 2023, the global numbers of the pandemics indicated more than 771 million cases of infection worldwide, from which almost 7 million people died. More updated information may be found here [64].

SARS-CoV-2, as other coronaviruses, is an enveloped virus, with a viral genome enclosed in an helicoidal capsid. Spike (S) and envelope (E) proteins are the principal viral envelope proteins, while nucleocapsid (N) protein, along with Ribonucleic Acid (RNA) molecule, compose the viral

nucleocapsid (**Figure 2.4**). SARS-CoV-2 infects human cells through Angiotensin Converting Enzyme 2 (ACE-2), to which the viral protein S can bind (**Figure 2.4**).

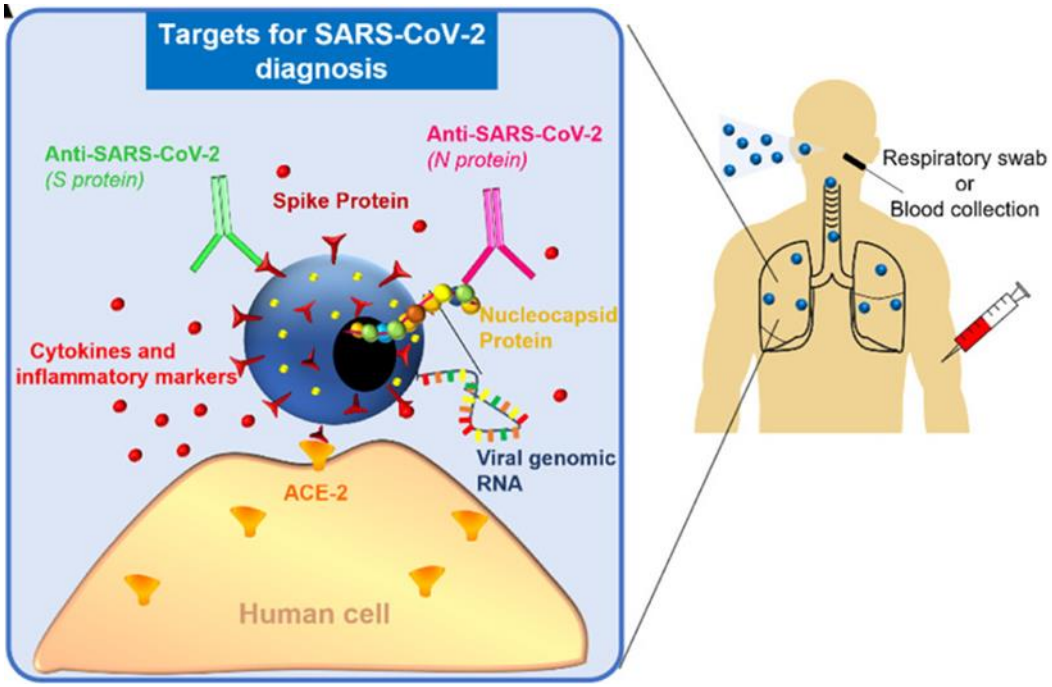

Figure 2.4: Possible targets for SARS-CoV-2 infection diagnosis, which include viral genomic material and specific viral antigens, namely, the spike and nucleocapsid proteins, as well as organism response markers to the presence of the virus, through antibody production and inflammatory response. Respiratory or serological samples collected via swab of syringe are typically used for detecting the infection or an immunological response.

Medical diagnosis of COVID-19 is accurately achieved by targeting the genetic material of the virus. This involves nucleic acid amplification testing (NAAT), which may use real-time RT-PCR (reverse transcriptase-polymerase chain reaction), due to the possibility for highly sensitive and specific assay performance that allows for qualitative, early infection identification in a high-throughput, laboratorial setting [65], [66]. Although current gold standard methodologies for SARS-CoV-2 viral RNA identification have been readily employed worldwide and have been instrumental for reliable infection identification, [67], [68] they pose impediments toward wide testing of people as a key action to control the spread of the virus [69]. These methods rely on specific reagents that may be readily available in some countries, but may lack in other areas of the world, creating a gap between the need for testing and the availability of currently, very highly needed materials [70], as well as on specialised personnel and equipment able to carry out these tests [71]. They are also time consuming and performed in a centralised fashion, usually with different collection and test performance locations, increasing the time until the final test result, limiting contact tracing and treatment of patients that in some cases will only perform tests after symptom onset [72], [73]. Other analytical limitations, such as the possibility

for false positives and negatives that have been observed, or differences between test kits' analytical performance have been a concern regarding these nucleic acid amplification diagnosis assays.

Thus, alternative POC testing devices and biosensors can give a significant contribution to the set of diagnostic and virus identification tools already in action [74]. These devices are more simple to operate and interpreter, with improved cost-effectiveness and more easily employed in areas with lower accessibility to centralised healthcare (either far from bigger urban centres or underdeveloped areas of the world, where well-equipped laboratories are less common) [75]. Similarly, to the development of therapeutic approaches and vaccine development for SARS-CoV-2, there is a challenge of rapidly investigating and developing new highly accessible biosensing tools that bring multidisciplinary contributions in POC use.

Upon the interaction of SARS-CoV-2 with the human organism, there is an immunogenic response toward viral antigens that varies during the stages of viral infection, from the asymptomatic phase into the onset of symptoms and convalescence [76]. Immunological response monitoring against COVID-19 involves identification and quantification of specific antibodies for SARS-CoV-2, mostly immunoglobulins IgG, IgM, and IgA. At a given moment, which depends on each individual, the immunological response against the infection of SARS-CoV-2 is triggered and leads to increased levels of IgM (and IgA in saliva) and IgG [76], [77]. Specific IgG and IgM are detected in serum from 0 to 8 days of infection, by complex laboratory methods [78], supporting that immunoglobulin levels change with each individual and within time. In a recent study, 50 and 81% of patients were positive for IgM and IgG, respectively, when first screened, having positive responses increased to 81 and 100% five days after the first measurement [79]. In general, the changing levels of immunoglobulins through time are very relevant from a clinical perspective because they can provide information about how patients handle the infection and when immunity was acquired after negative testing to the virus. The main antibodies circulating against SARS-CoV-2 target S or N proteins, and the dynamic progression of their levels change in patients at different disease stages. It has been found that the levels of N antibodies are higher in patients with a need for intensive care treatment, meaning that knowing the ratio of N and S antibodies may turn out an excellent tool for prognosis of disease outcomes [80]. Thus, serological detection of antibodies has been an important route in the control and study of this pandemic because it may serve as a diagnostic tool for present and past infections [81], as well as aiding to better control the population immunity. Electrochemical based analytical devices have also been reported for the selective detection of SARS-CoV-2 antibodies (both IgG and IgM), combining the sensitivity of the electroanalytical methods

with the inherent bioselectivity of the biological component [82]. Overall, the specific use of electrochemical biosensors for detecting the virus or the antibodies against it has been very useful and helpful for an effective COVID-19 management, although technological improvements are still needed and being forged [83]–[87].

2.3 Molecular Imprinting Technology

Although MIP technology traces back from the 30s and has been well known since the 70s for adsorption of compounds that have been imprinted at a molecular scale within a polymeric network [88], [89], it was only in the twenty-first century that MIPs were successfully employed to update conventional bio-recognition procedures in sensing.

The general concept behind the MIP is to build a synthetic polymer receptor via template-guided synthesis. In general, the typical steps for the synthesis of MIP materials can be described as schematically represented in **Figure 2.5**. This includes the following steps: (1) the template or print molecule is mixed with functional monomers that get positioned spatially around the template and guide the assembly; (2) the polymerisation takes place to create a crosslinked matrix around the template; (3) the template is removed from the polymer network leaving a complementary cavity that retains the spatial features, i.e., size and shape, and bonding preferences of the template. It is expected that the imprinted polymer so obtained is able to selectively rebind the template in the complex samples **Figure 2.5** [90]. Different interactions between the template and functional monomers can be established in the process of imprinting, namely noncovalent (e.g., hydrogen bonds, ionic interactions, and van der Waals interactions), covalent, and semi-covalent bonding [90]–[92].

Initially, the utilization of covalent interactions allowed the binding sites of the monomer could be used in the correct stoichiometric ratio to the template molecule, allowing for more control of the imprinted cavities. Non-covalent imprinting became popular later on due to its flexibility and simplicity of operation, involving interactions via hydrogen bonding, ionic bonding and van der Waals forces. To be effective, non-covalent binding requires many binding sites established between monomers and template, to allow efficient complexation upon the rebinding stage. Due to its versatility, the noncovalent approach is today the most widely applied method for preparing MIP materials.

The best conditions for MIP synthesis can be studied by computational modelling and combinatorial methods [93], [94]. Several parameters are relevant to verify the recognition properties

of the MIP and its successful application, namely in sensors. Those include the adsorption capacity, imprinting factor, selectivity factor, and response time [95], [96].

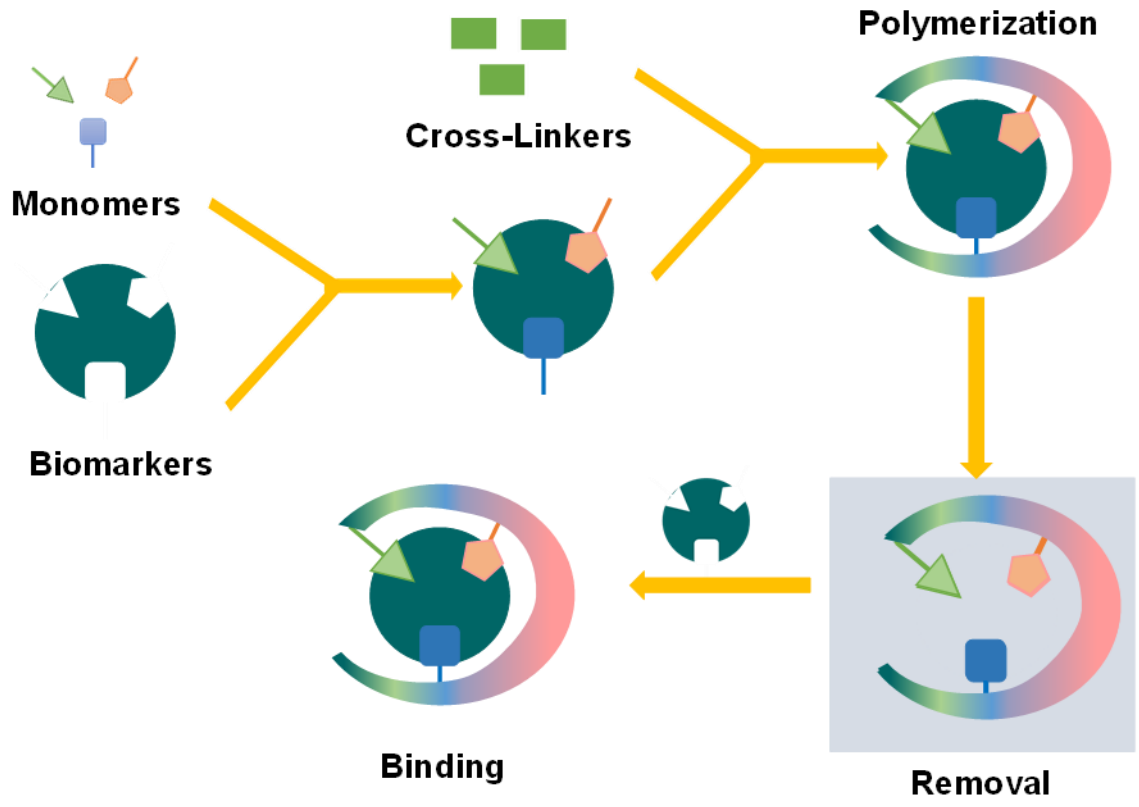

Figure 2.5: Schematic representation of Molecular Imprinting technology.

Concerning the polymerization methods, different synthetic routes can be used for MIP preparation. The most common are free radical polymerization [97] and sol–gel process [98]. In free radical polymerization, it is possible to select among bulk polymerization (that includes mechanical grinding and sieving) and more complex techniques, for example, to originate particles (e.g., suspension, precipitation, emulsion, and seed polymerizations), which are also commonly used [99]. When MIPs are combined with electrochemical detection, electropolymerization is the preferred approach [100], with main advantages relating to direct formation of the polymer film on the surface of the transducer in a wide range of substrates [101]–[103] allowing the production of both conductive and nonconductive polymers [104]. Besides the mentioned methods, it is also possible to use other strategies for MIP synthesis, such as surface imprinting, living polymerization, solid-phase MIP nanoparticles, along with various novel technologies that have emerged [105], [106]. The methods chosen for MIP production with desirable properties and the final configurations clearly depend on the target molecule (e.g., the whole target or a small fragment as an epitope, small, or large macromolecules) and application, also

considering the costs and simplicity of the processes. MIPs are a thriving research subject, and comprehensive reviews can be found in the literature covering methods of polymer fabrication and imprinting strategies, range of applications, and integration in biosensing devices [99], [107]–[110].

The ability to tailor the imprinted sites with functional groups, allied with the robustness and stability of polymer materials, led to considerable research efforts to expand the applications of MIPs to a catalytic action. Many different approaches have been explored (e.g., noncovalent imprinting, chemical reactions) and catalytic MIPs have been prepared using analogues of substrates, transition states, or products as templates [111]–[115]. Since the first important developments, considerable advances in the field have allowed to prepare more flexible and adaptative structures [116], [117]. Imprinted polymers have been combined with amino acids, peptides, metals among others in synergic strategies to realize the potential of artificial enzymes [118]–[120].

2.4 Enzymes and Nanozymes

Enzyme-based biosensors have standout due to the simplicity of operation, compactness, and high selectivity, being extensively used in enzyme-catalysed reactions for electrochemical and optical transduction [20], [121]. However, enzyme-based biosensors suffer from inherent disadvantages and issues that limit their use in many settings. Some of the shortcomings of enzymes for biosensing applications are that native enzymes show hard and costly purification processes from limited natural sources, leading to an increase in price of such platforms and devices, going against the low-cost and abundance of paper as a substrate for these applications [122], [123]. Although highly selective, enzymes suffer from stability issues related to the chemical environment surrounding the electrocatalytic reactions. Due to the intrinsic nature of proteins, most enzymes are constrained by temperature and pH variation within tolerable limits before their activity decreases and denaturation occurs [124]. For example, GOx for glucose detection and horseradish peroxidase (HRP) for enzyme-linked immunosorbent assay (ELISA) holds extensive studies and a wide range of applications, as it has always attracted research due to its tremendous potential [125]. However, it operates optimally within a 2–8 pH range, below 44°C and with ambient humidity conditions [124].

Consequently, enzymatic biosensors cannot operate in harsh chemical and thermal environments, resulting in a more limited use in disposable, single-time applications. Also, their production must be controlled because enzymes may suffer from harsh fabrication conditions.

Furthermore, enzyme immobilisation in active substrates, especially in electrochemical sensing, is highly challenging, with the need for additional fabrication strategies. Poor enzyme immobilisation paired with instability of enzymes affects shelf life and consequently, leads to rigid storage requirements [124].

Overall, enzyme-based biosensors are very relevant and have important applications in biosensing. However, the disadvantages related to poor stability and reusability, along with high costs for preparation and purification, have led to efforts in designing synthetic mimics [126]. The research in this field spreads from semisynthetic approaches (e.g., genetic modification of natural enzymes) to artificial systems (e.g., cyclodextrins, metal complexes, porphyrins, dendrimers, polymers) [127], [128].

Due to these shortcomings, non-enzymatic sensors have recently been explored and developed, to replace enzymes and remove the necessary enzymatic bioactivity by more stable, reproducible, and simple materials and approaches, showing great promise for high performance sensor development [129]. Non-enzymatic biosensors (NEB) mostly use nanostructured materials to substitute enzymes and perform electrocatalytic reactions or other transduction mechanisms, such as change in optical properties, taking advantage of high surface area, morphology and electron transport of these nanomaterials [130].

These biomimetic materials are characterised by unique features and have several advantages compared with natural enzymes. The artificial enzymes are low-cost, have easy mass production, high stability (especially at high temperature), and long-term storage feasibility [128]. The progress in the field of nanomaterial-based artificial enzymes or nanozymes has been fast since the first discovery of the unexpected peroxidase-like activity of ferromagnetic nanoparticles [131]. Thus, nanozymes are considered alternatives to natural enzymes and the prospective biomedical applications are vast, ranging from disease diagnostic and imaging to therapeutics [132], [133]. Considering biosensing devices and the current technological advances, synergistic effects are expected to achieve ultrasensitive methods, such as colorimetric, fluorometric, chemiluminescent, surface-enhanced Raman scattering, and electrochemical [132], [134], [135] with special emphasis on the electrochemical-based devices, which offer great advantages in terms of portability and feasibility of point-of-care use. Despite these enthusiastic perspectives, poor substrate selectivity, low efficiency and limited catalytic types are challenges to be tackled. In a biomimetic convergence, MIPs are synthetic highly selective receptors, which have been integrated with nanozymes to improve the desired features, with special outcomes for sensor design [136].

2.4.1 Design of Nanozymes

As natural enzymes are efficient biocatalysts, there has always been great interest in mimicking the proven high substrate specificity and superior catalytic activities. Moreover, the development of synthetic approaches could overcome the disadvantages of natural enzymes related to high-cost preparation and purification, low stability, and difficulties in storage and reuse [125], [126]. Thus, allied with advances in nano- and biotechnology, artificial enzyme mimics have been extensively studied [132], [137]. The term "nanozyme" appeared for the first time in a work by Scrimin, Pasquato, and co-workers in 2004 to describe the excellent catalytic properties of a multivalent system comprising ligand-functionalised thiols on Au NPs [138]. Since the notable discovery of the intrinsic catalytic activity of magnetic Fe_3O_4 NPs as peroxidase in 2007, nanozymes refer to nanomaterials with enzyme-like characteristics [131], [137].

The field has been expanding quickly and nanomaterials with enzyme-mimicking activities [136] including noble metals (Au, Ag, Pt) [123], [139], carbon-based materials (Carbon nanotubes, quantum dots (QDs), reduce graphene oxide) [140] and metal oxides (ZnO, NiO, MnO_2) [141] mostly due to their high catalytic activity [19] and have attracted great interest and led to important benchmarks [136].

Nanomaterials as enzyme mimics present many advantages in comparison with natural enzymes. Either as single or multi-components like composites or doped materials, nanozymes have high surface-to-volume ratio, tuneable catalytic activity, and plenty of surface reactive species [128], [131]–[133], [135], [137], [138], [142], [143]. These features are combined with cheaper and simpler manufacturing processes, long-term stability, and robustness to harsh environments. However, some other traits are not so favourable, such as toxicity in biological systems and lack of selectivity, and the catalytic activities of most nanozymes is still low, which may limit the range of applications. Thus, nanozymes as artificial catalysts are a likely choice, but the field still faces many challenges Figure 2.6 [136].

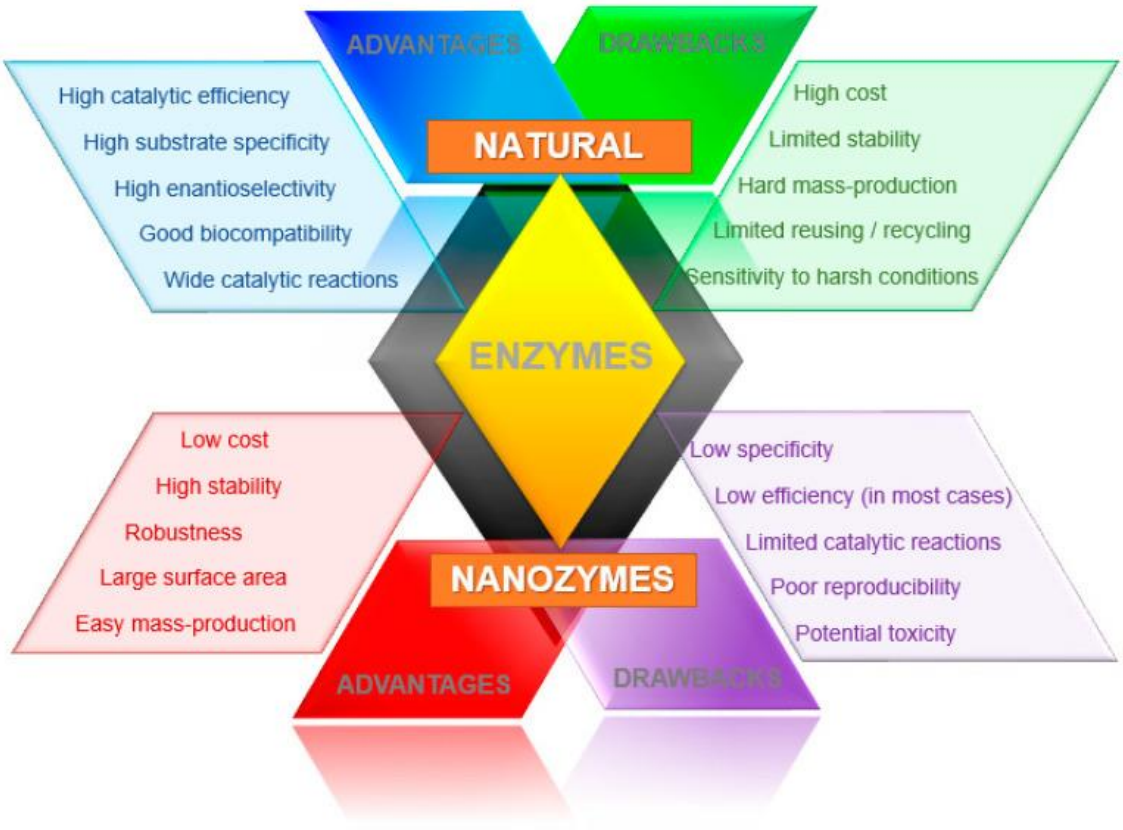

Figure 2.6: Comparison of some characteristics between nanozymes and natural enzymes.

2.4.2 Classification and Enzyme-Like Activities

Regarding artificial enzyme mimics, several nanomaterials with inherent catalytic activity have been studied as highly stable and low-cost approaches. These nanomaterials can be categorised in main groups regarding their composition, namely into metal, metal oxide, carbon-based materials, and their hybrids [144]. A variety of nanomaterials has been studied as artificial enzyme mimics, including CeO_2 NPs, Fe_3O_4 NPs, Pt nanomaterials, Au NPs, bimetal and trimetal NPs, graphene oxide, carbon nanotubes, fullerene derivates, QDs, metal organic frameworks (MOFs) as some common examples [126], [132], [145]–[147] (**Figure 2.7**).

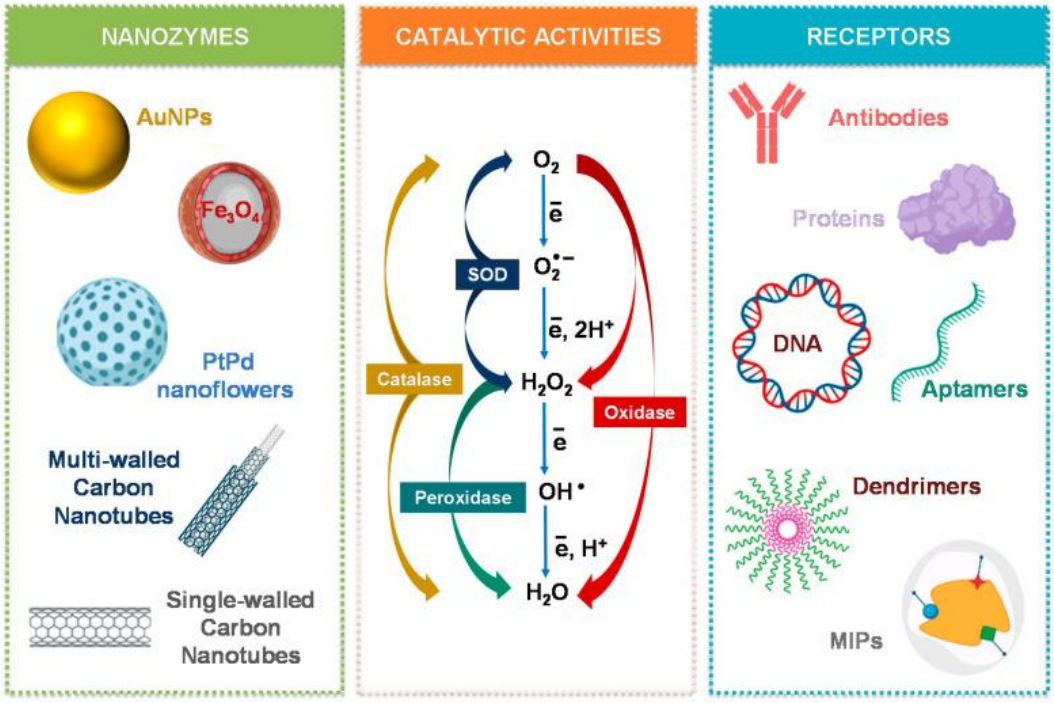

Figure 2.7: Schematic illustration of some nanomaterials mimicking enzymes, the most studied enzyme-like activities, and common ligands to tune the catalytic efficiency and selectivity of nanozymes [148].

The discovered nanozymes so far can broadly function as oxidoreductases, namely as peroxidase, oxidase, superoxide dismutase (SOD), and catalase mimics [137]. Other enzyme-like activities by carbon-based materials, Zr- and Cu-based MOFs and Au NPs modified with catalytic monolayers have also been reported, displaying for example hydrolase activity, which catalyses chemical bond hydrolysis (e.g., nuclease, esterase, phosphatase, protease, and silicatein)[132], [137]. Laccase-like activity has been demonstrated in Cu-based MOFs based on guanosine monophosphate coordinated copper [149]. Multi-nanozymes where two or more types of enzymes are mimicked can also be observed in some nanomaterials like Au, Pt, and CeO_2 [137], [150], [151]. These capabilities can be expanded by using bimetallic NPs that can achieve not only single- but also multiple-enzyme mimicking, or nanocomposites to benefit from their synergistic effects and enhanced catalytic performance [152], [153].

2.4.2.1 Peroxidase

Peroxidases, such as HRP, are widely used in biosensor devices and they catalyse the oxidation of substrates by a peroxide, such as H_2O_2. After finding the novel properties of Fe_3O_4 magnetic NPs, their peroxidase-like activity was used in the detection of H_2O_2 and glucose [154]. The nanozyme catalysed the oxidation of the substrate 2,20 -azino-bis(3- ethylbenzothiazoline-6-sulfonic acid)-diammonium salt (ABTS) by H_2O_2 to the oxidised colored product. Moreover, by

combining this reaction with the catalytic oxidation of glucose by using GOx, it was possible to develop a colorimetric assay for glucose detection [154]. Since then, the field has evolved rapidly and metals, metal oxides, MOFs and carbon-based nanomaterials have been studied as peroxidase-like mimics [155], [156]. In a work by Cui et al., 2015, a simple colorimetric biosensing platform was proposed based on growing Prussian blue (PB) on the microporous MOF MIL-101(Fe), forming uniform octahedral nanostructures with highly efficient catalytic activity for H_2O_2 [155]. PB crystals are made of iron ions coordinated by CN bridges, possess a high surface area, also exhibiting intrinsic high peroxidase-like activity. Moreover, the outer surfaces of these PB/MIL-101(Fe) nanostructures were successfully modified, rendering them biocompatible while maintaining their activity [155] (**Figure 2.8**).

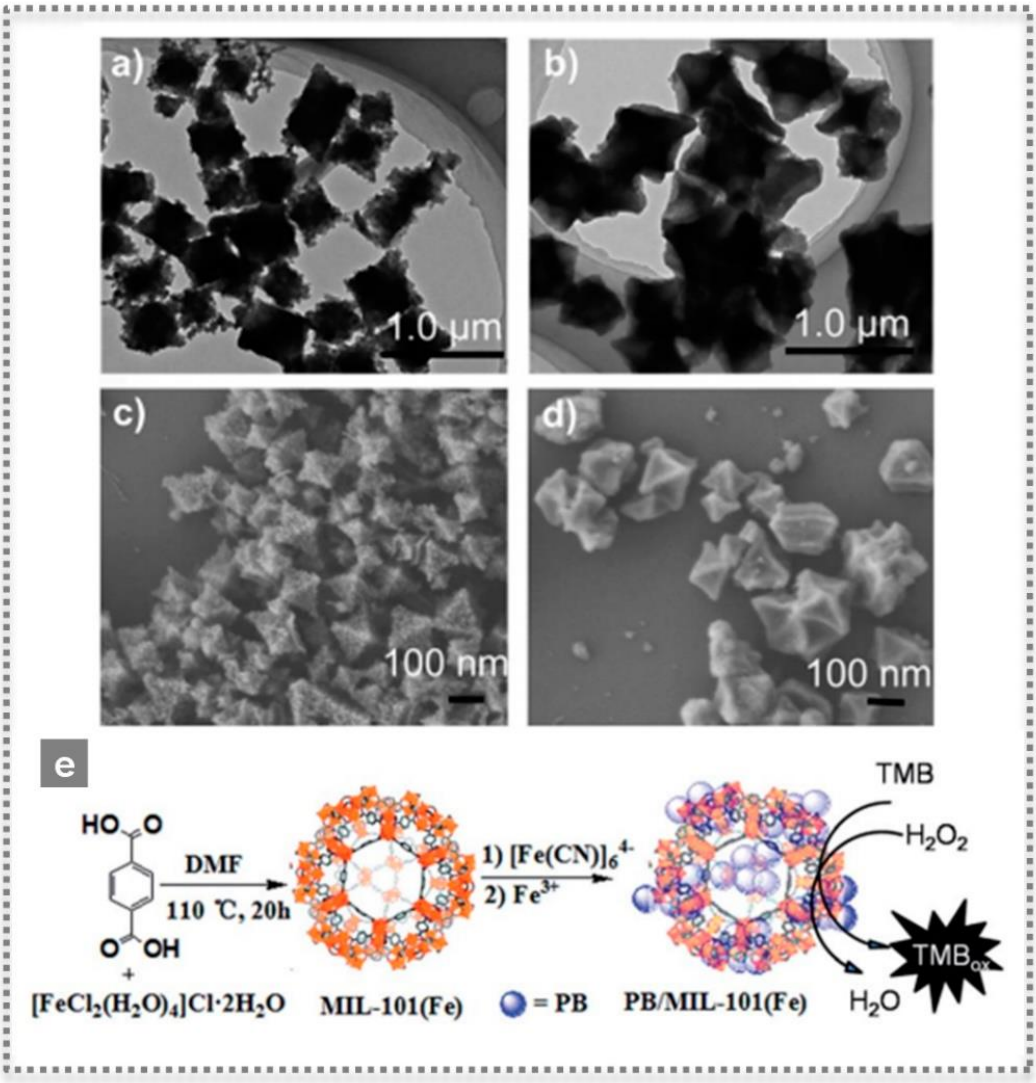

Figure 2.8: Characterization by Transmission electron microscopy (TEM) (a,b) and Scanning Electron Microscopy (SEM) (c,d) of microporous MOF MIL-101(Fe) as-prepared (a,c) and after introducing Prussian blue, PB/MIL-101(Fe)

(b,d), as highly efficient peroxidase-like mimics, and scheme illustrating the synthesis of PB/MIL-101(Fe) (e) (Reproduced with permission [155] Copyright 2015, The Royal Society of Chemistry).

Another interesting example was the application of a peroxidase-like activity to successfully detect thrombin in plasma by preparing a fibrinogen-modified bismuth-gold (Fib-Bi-Au) NPs [157]. The Fib-Bi-Au NPs catalysed the oxidation of Amplex Red in the presence of H_2O_2, and this simple fluorescence-based assay enabled detecting thrombin with LOD of 2.5 pmol L^{-1} and revealing a promising clinical application [158] (**Figure 2.9 A**). The majority of nanozymes applied in detection exhibit peroxidase-like activity; thus, numerous examples are found in the literature with a broad range of nanomaterials [132], [159], [160]. Recently, a covalent organic framework (COF) nanozyme has been developed by incorporating an iron porphyrin unit in the COF backbone as the active center and L-histidine as the substrate binding site for selective chiral recognition. The peroxidase-like activity was shown to be enantioselective and with higher activity than the natural HRP, while both the activity and selectivity can be easily modulated by changing the doped amino acids and their content [160].

2.4.2.2 Oxidase

Oxidase-like nanozymes are those that catalyse the oxidation of substrates with molecular oxygen. Natural enzymes are usually selective for a given substrate, hence their names such as GOx. Nanomaterials such as Au NPs, MnO_2, or CeO_2 exhibit oxidase-like activity, but they lack selectivity to a given substrate [137], [161], [162]. Still, oxidase-like nanozymes are integrated in sensors with proper coupling to biomolecules pertaining to the target. For instance, a colorimetric sensor for mercury ions and DNA molecules relied on the oxidase-like activity of bovine serum albumin-protected silver clusters (BSA-Ag NCs). This activity was stimulated by mercury showing high catalytic activity towards 3,3' ,5,5' - tetramethylbenzidine (TMB), in a "switched-on" state [163]. Moreover, as mercury ions are known to bind with two DNA thymine bases, forming base pairs, the sensor could detect DNA molecules. A hairpin structure containing mercury ions was disrupted in the presence of the target DNA, releasing the ions that switched on the oxidase mimicking activity of BSA-Ag NCs. The target DNA could be detected as low as 10 nmol L^{-1}, with a linear range from 30 to 225 nmol L^{-1} [164] (**Figure 2.9 B**). In a recent work, the oxidase-like activity of Cu/Co bimetallic MOF functionalised with an aptamer was used to detect a protein on the surface of exosomes [120]. The prepared $CuCo_2O_4$ nanorods were surface-modified with CD63 aptamers resulting in catalysis inhibition. The aptamers disassembled upon exosome recognition originating a recovery of the oxidase-like activity.

This colorimetric method enabled the detection of exosomes in a range of 5.6 × 10^4 to 8.9 × 10^5 particles µL $^{-1}$, with a detection limit of 4.5 × 10^3 particles µL $^{-1}$ [165] (**Figure 2.10**).

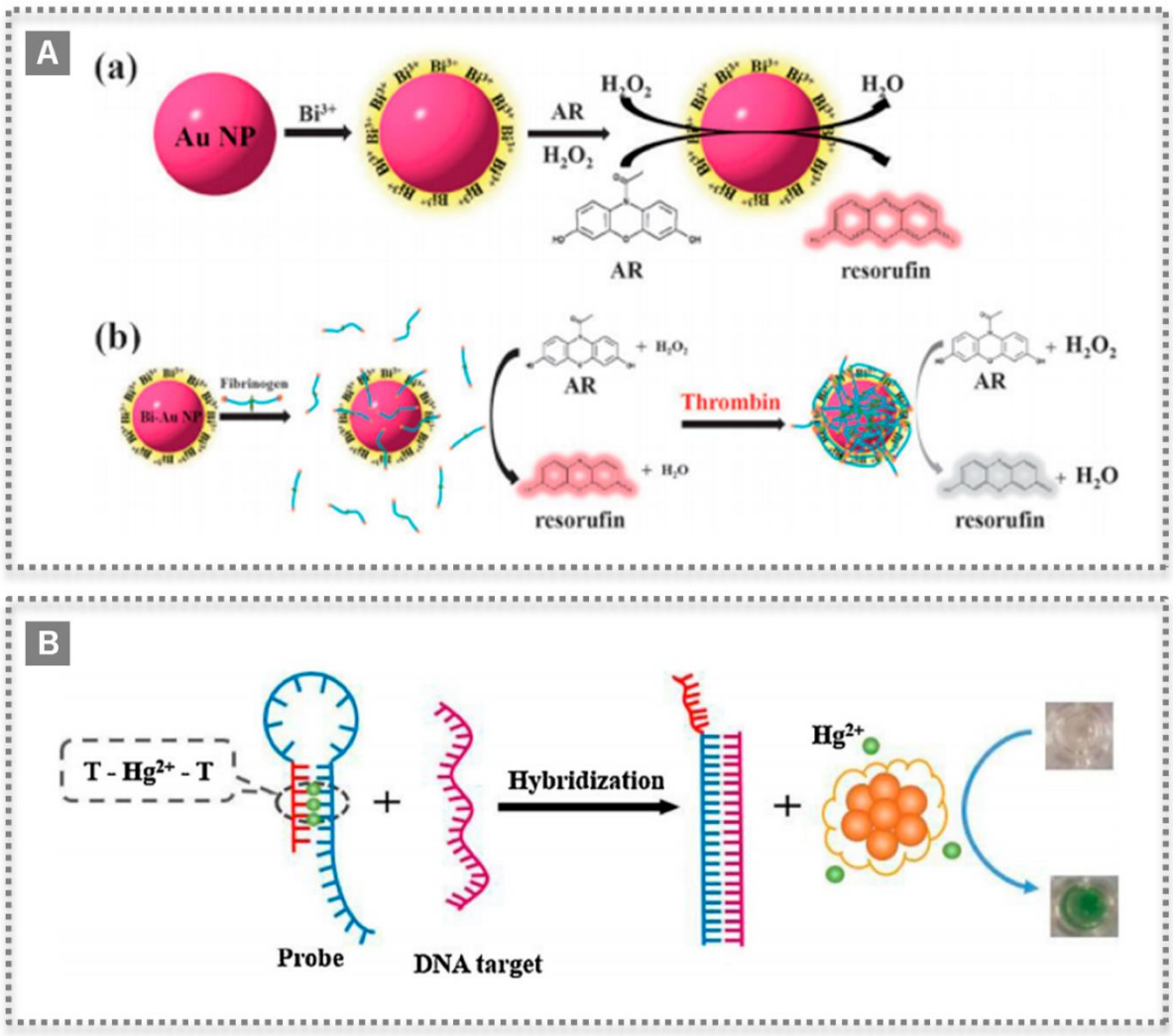

Figure 2.9: Nanozyme bioconjugates for sensing applications: (A) Scheme of bismuth-Au NPs preparation and peroxidase-like catalyzing mechanism for reaction with Amplex Red (AR) (a), and further modification with fibrinogen as probe for detection of thrombin (b). (Reproduced with permission [158] Copyright 2012, The Royal Society of Chemistry); (B Colorimetric biosensor based on oxidase-like activity of bovine serum albumin-protected silver clusters, which is switched on selectively by mercury ions and applied to detect DNA. (Reproduced with permission [164], Copyright 2015, Elsevier B.V.)

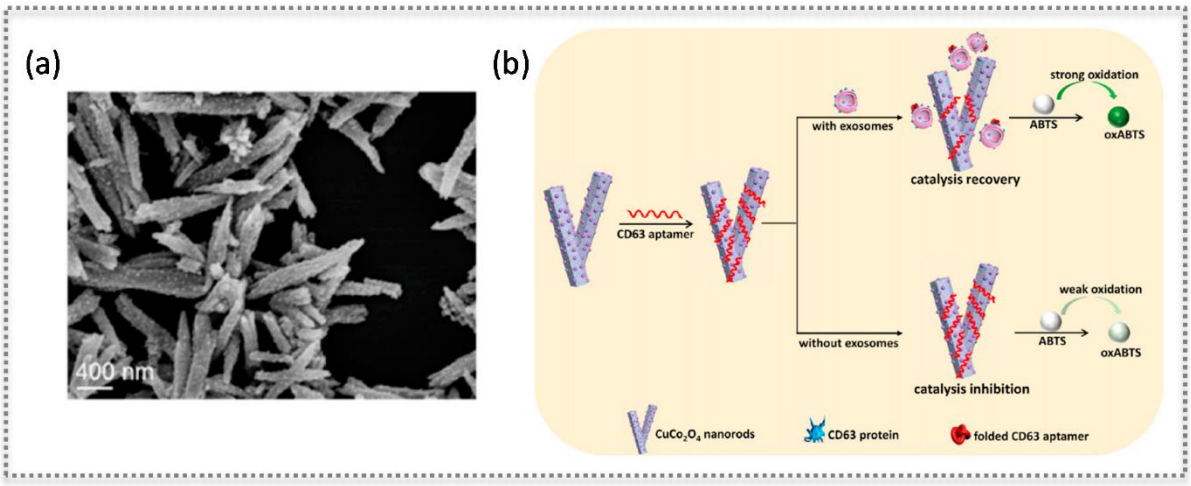

Figure 2.10: Nanozyme based on $CuCo_2O_4$ nanorods: SEM characterization (a) and scheme showing the modulation of oxidase-like activity of the nanorods by the adsorption of the aptamer that recognizes CD63 protein on exosomes (b), as a label-free sensing approach. (Reproduced with permission[165], Copyright 2020, Elsevier B.V.).

2.4.2.3 SOD and Catalase

Both SOD and catalase enzymes are involved in protecting cells from oxidative damage, and likewise to other enzyme mimics, CeO_2, Au NPs, among other nanozymes, are artificial alternatives with many potential therapeutic applications [144], [166]. Because of their antioxidant properties, many works study the potential benefits of nanozymes with catalase and SOD activities for cell and tissue protection against oxidative stress, in cancer therapy, and as anti-inflammatory and antibacterial agents [167], [168].

The symbiosis between electrochemical biosensors and nanozymes has been successfully developed and mostly used in the clinics and other areas. The huge advantage of this combination was a higher sensitivity, shorter detection time and better signal readout [169].

Recently, nanozymes, are a particular type of nanomaterial, widely used in electrochemical sensors as electrode modifiers, nanocarriers, and/or catalytic labels [170]. According to Campuzano *et al.*, 2020 [170] there are huge growth of development of electrochemical biosensor involving nanozymes, especially peroxidase-like activity and used mainly as catalytic labels. This approach provides an improvement in several aspects, as analytical performance, and practical use.

The peroxidase-like activity nanozymes is the most employed in electrochemical sensors. The main goal of this sensor was the electrochemical detection of H_2O_2 generated during the oxidation of certain substrates [152]. So, the using of nanozymes, nanomaterials exhibiting

enzyme-like catalytic features offers higher efficiency, lower cost, easier production and higher stability in electrochemical biosensors.

One of the major drawbacks of nanozymes is the lack of selective recognition of the substrate in contrast to the corresponding natural enzymes. Thus, various methods have been pursued to improve the selectivity of nanozymes. One approach has been to couple peroxidase-like nanozymes with oxidases, producing H_2O_2 only in the presence of specific substrates [171]. Surface modification with proper ligands or bioreceptors as antibodies, aptamers, and oligonucleotides, through bioconjugation or physisorption, has also been attempted [125]. In this context, the combination of nanozymes with MIPs has opened a new avenue to overcome this technological challenge [172]. The area of biomimetic catalysis is vast, and there are comprehensive literature reviews focusing on types of nanomaterials, classification, catalytic mechanisms, activity, and applications of nanozymes [142], [167], [173]–[175].

As mentioned previously, over the past decades, MIPs have proven excellent features in mimicking natural recognition events for a myriad of applications. The most compelling examples concern the replacement of natural antibodies in diagnostic-based immunoassays [8], [176]. The molecular imprinting technology has matured to the point of reaching similar or even surpassing the required characteristics in terms of selectivity, robustness, and cost-effective production without involving animal research [92]. Thus, the combination of "plastic" molecular recognition with advances in sensor fabrication has been offering selective and sensitive methods. These devices are promising for low-cost and rapid detection and monitoring of biomarkers of disease (e.g., protein, nucleic acids, metabolites, virus) and compounds of interest in environmental and food analysis [177]. Besides sensors [178], MIPs have several applications, e.g., in drug delivery, tissue engineering, biocatalysis, bioimaging, extraction, among others [179]–[181]. Given the known advantages of these synthetic materials, research on building catalytic activity into MIPs has for long been considered an exciting area [176].

Molecular imprinting technology is extremely versatile as demonstrated by the possibility of imprinting within the nanosized environment of doubly cross-linked micelles [182], [183] (**Figure 2.11**). In this, the imprinting is confined within the boundary of surfactant micelles. The obtained MIP NPs have a hydrophobic/hydrophilic core-shell morphology and are water-soluble, making this micellar imprinting very useful for a variety of template molecules [182]. Such imprinted NPs can also be post-functionalized to present catalytic properties. In addition, the catalysis can be fine-tuned owing to the facile modification of size, shape, and depth of the binding pockets. The technology was demonstrated to deploy very efficient artificial phosphodiesterase and esterase-like activities [182], [183].

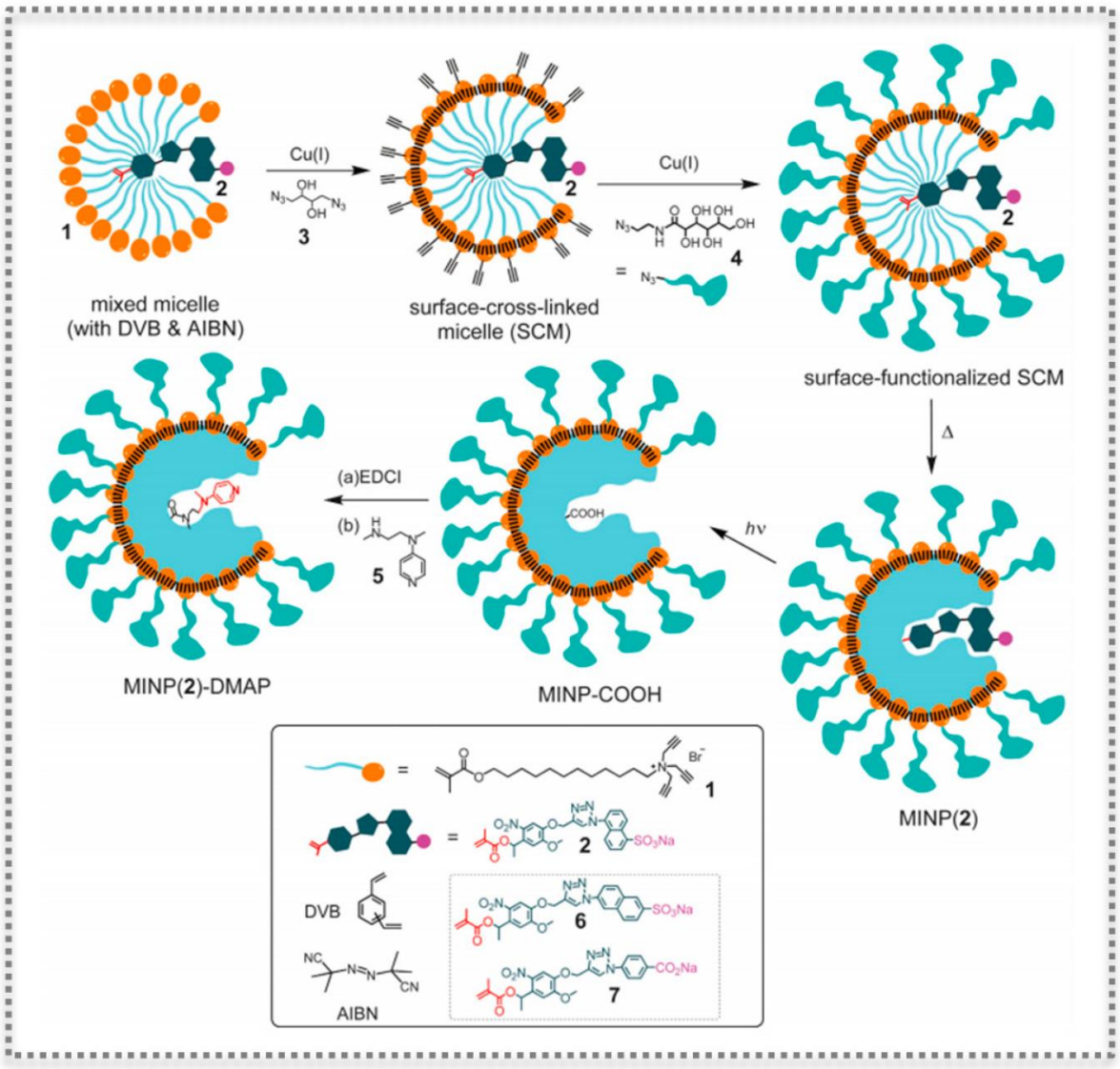

Figure 2.11: Preparation of catalytic molecularly imprinted NPs (MINPs) functionalized with the transacylation catalyst 4-dimethylaminopyridine (DMAP), as a method to molecularly imprint within cross-linked micelles. (Reproduced with permission [182] Copyright 2017, Wiley-VHCA AG).

2.4.3 Nanozymes@MIPs

Recent advances on tailored MIPs on nanozymes represent a novel avenue for additional advances in the field. The synergistic catalysis arising from integrating two different artificial enzymes was first advanced as a strategy for the formation of disulfide bonds in peptides [184]. In this study, imprinted polymeric microzymes and inorganic (Fe_3O_4) nanozymes were integrated in one process resulting in high product yields and excellent selectivity [184].

Further works expanded the concept based on coating the nanozymes with the MIP layer containing binding pockets to improve the selectivity and the catalytic performance of nanozymes

[82]. Generally, the nanozymes do not present selective recognition, and a specific bioligand (e.g., antibody, aptamer) is conjugated on the nanozyme. The use of such ligands may compromise the high stability and low cost of nanozymes. Furthermore, the natural ligands available may not cover the range of emerging analytes [185], [186]. These drawbacks can be addressed by growing artificial substrate recognition sites on the nanozymes by molecular imprinting technology. The MIP layer provides the selectivity, but it has been reported that the catalytic activity of various nanozymes is also enhanced. Considering nanozymes as heterogenous catalysts, the substrate must diffuse to the catalyst surface, and after the reaction, the product desorbs, enabling enzyme regeneration [187] Interestingly, if the MIP is grown on the nanozyme, the several steps of catalysis could be enhanced or inhibited by the polymer layer. Thus, a surface science approach supported the study of the three reaction steps to explain the enhanced catalytic activity in the presence of the MIP. This work suggested that the substrate concentration near the nanozyme surface was enriched by the imprinted polymer with faster transportation kinetics. Moreover, the activation energy was lower, and the MIP did not retain the products, facilitating enzyme turnover [187].

For most nanozymes@MIPs, the imprinted polymer is grown to entrap the nanozyme. An example of such strategy has been presented by creating substrate binding cavities on three classic nanozymes with peroxidase- and oxidase-like activities [185] (**Figure 2.12**). The imprinted nanogels, prepared by aqueous precipitation polymerization, were synthesized on Fe_3O_4 NPs with peroxidase-like activity, but also on CeO_2 mimicking oxidase activity and Au NPs mimicking peroxidases [185]. The substrate binding pockets enabled achieving remarkable specificity and the enhancement of the activity of nanozymes. In the case of Fe_3O_4 and CeO_2, two substrates were imprinted, namely, TMB and ABTS, that when oxidized show a blue and a green color, respectively. The imprinted substrates for Au NPs were TMB and dopamine [185]. The prepared MIP appeared to be porous, allowing an efficient substrate diffusion. Interestingly, and in accordance with some reports in the literature, surface modification of nanozymes can enhance their activity [185]. The MIPs, which were properly engineered with functional charged monomers, highly enhanced the selective substrate recognition and the catalytic activity. The improvement caused by the MIP was consistent among the various nanozymes and substrates analyzed, suggesting that nanozyme@MIP may be a general method to obtain desired selectivity and activity [185].

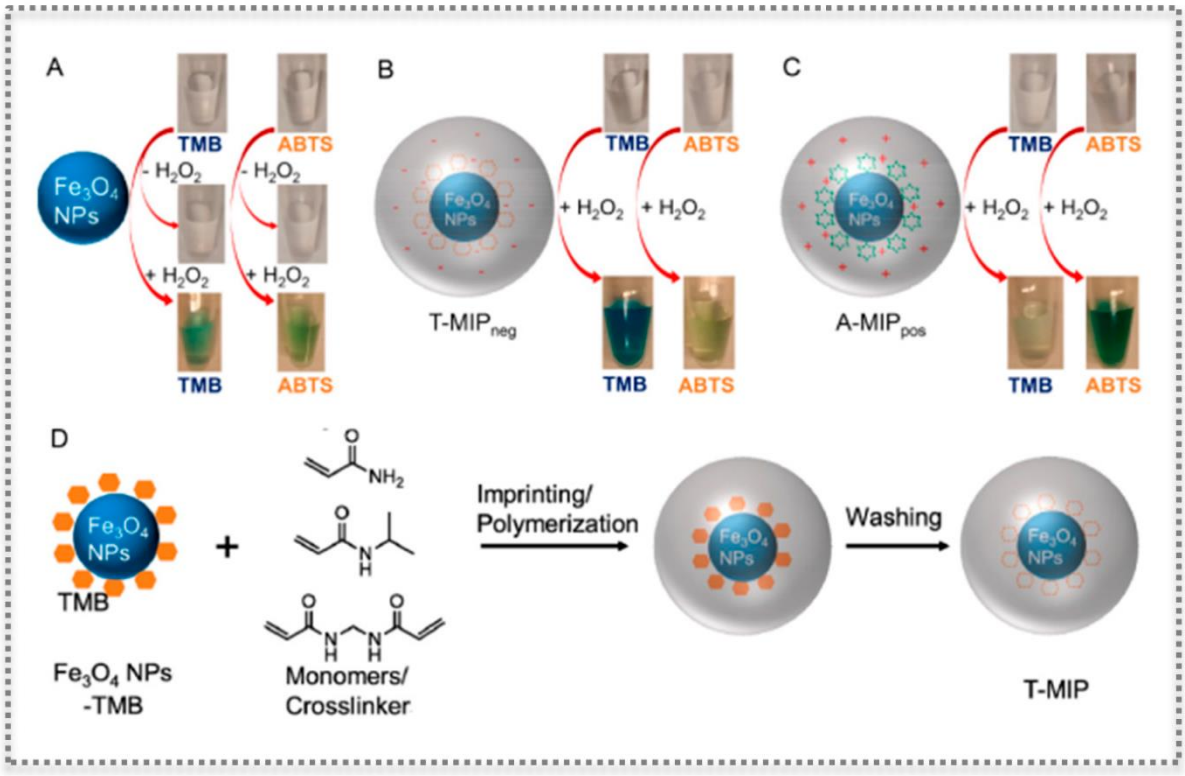

Figure 2.12: Molecular imprinting on nanozymes: Photographs and schemes showing bare Fe_3O_4 nanozyme (A), with an anionic MIP layer (T-MIPneg) (B) and with a cationic MIP layer (A-MIPpos) (C) for oxidizing two substrates (TMB and ABTS), as well as scheme of imprinting the nanogel (D). (Reproduced with permission [185], Copyright 2017, American Chemical Society).

Other examples in the literature can be found, such as growing a polypyrrole (PPy) based MIP on Fe_3O_4 nanozymes using methylene blue (MB) as substrate [85]. In this study, the Fe_3O_4@PPy composite presented superior catalytic properties for MB in the presence of sodium persulfate, a sulfate radical-based oxidant, in comparison with bare Fe_3O_4 nanozymes. Interestingly, Fe_3O_4@PPy could still degrade more than 80% of MB after five recycling cycles [188].

The versatility of imprinted nanozymes was tested when trying to develop a universal sensor for multiplex detection. This study used peroxidase-like metal (Pt, Ru, and Ir) nanozymes to fabricate cross-reactive sensor arrays to detect a variety of analytes [186]. The sensor arrays allowed to discriminate several small biothiol molecules, proteins, and cells. Other successful traits were related to the ability of identifying unknown samples, as well as discriminating bio-thiols in serum and proteins in human urine [186].

The use of Au NPs in the construction of imprinted nanozymes, as a novel method for enhanced selective detection of glucose, was conceived by employing aminophenylboronic acid (APBA) in the MIP shell [189]. The affinity to glucose is assured by the boronic group in APBA, which can bind to adjacent hydroxyls of saccharides under alkaline conditions. Moreover, to

improve the catalytic activity, heptadecafluoro-n-octyl bromide nanoemulsion was introduced to provide oxygen, which resulted in efficiency gain of about 270-fold [189]. These Au NP-based GOx mimics are very promising considering the importance of glucose monitoring.

The oxidase-like activities of other metal NPs have been explored, such as the case of Au–Pt alloy [190]. This alloy was coupled to magnetic microspheres to enhance the stability and ensure their magnetic separation. The affinity to substrate was accomplished by preparing a MIP containing APBA as polymer shells with imprinted sites for glucose. Having a GOx-like activity, the imprinted nanozymes had about 200-fold higher catalytic efficiency than Au NPs [190]. Recently, PtPd nanoflowers (NFs) exhibiting peroxidase-like activity were synthesized by a surfactant-directing method and further surface-modified with a MIP layer [191]. The MIP was prepared by aqueous precipitation polymerization and contained imprinted pockets for TMB (**Figure 2.13**).

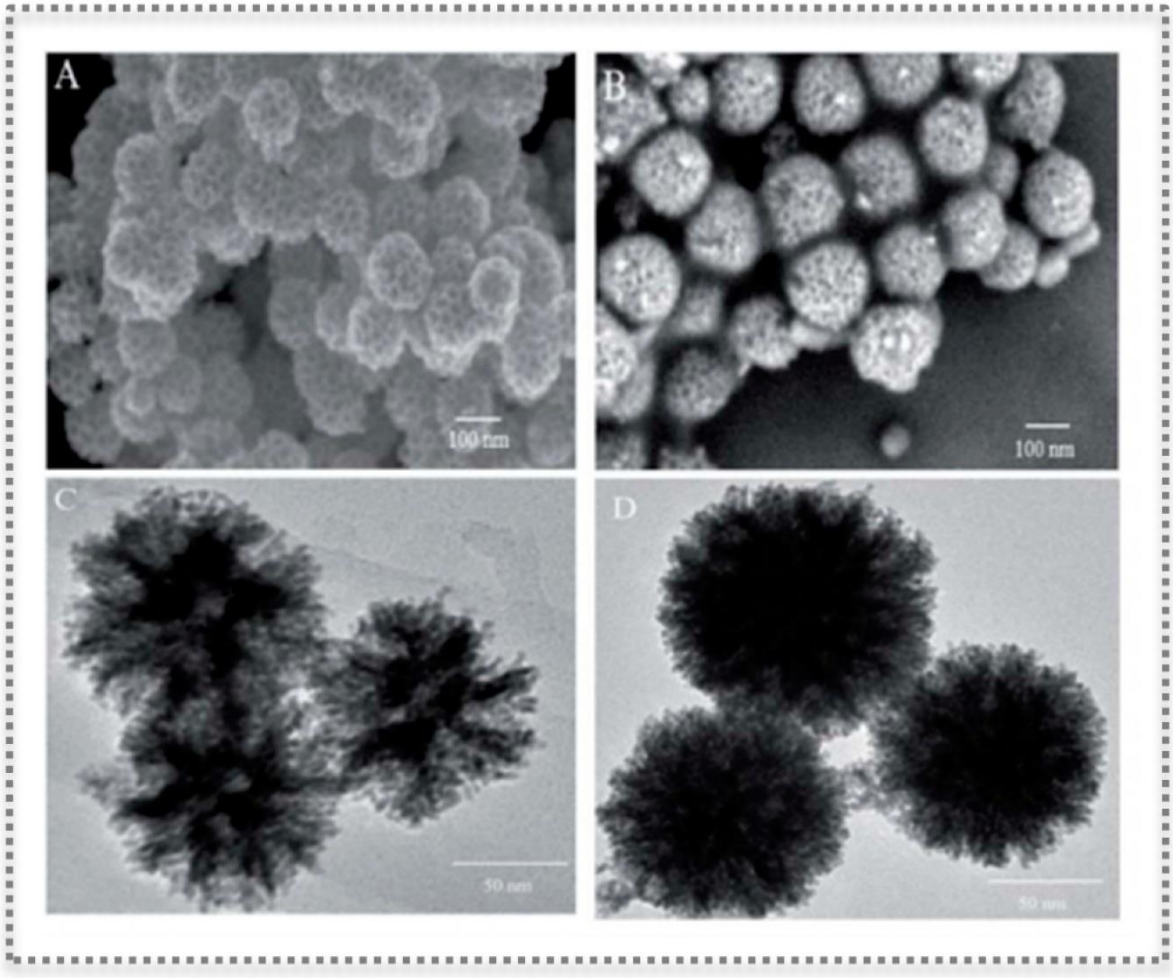

Figure 2.13: Characterization of molecular imprinting on PtPd NFs showing spherical nanostructure with flower-like morphology and mesoporous on the surface: SEM images of PtPdNFs (A) and T-MIP-PtPd NFs (B); TEM imagens of PtPd NFs (C) and T-MIP-PtPd NFs (D). (Reproduced under the terms and conditions of the Creative Commons

The final composite (T-MIP-PtPd NFs) had better catalytic properties, achieving a linear range of 0.01–5000 μmol L^{-1} and a detection limit of 0.005 μmol L^{-1} for colorimetric detection of H_2O_2. A sensitive colorimetric detection of glucose was also possible through a cascade reaction employing GOx [191]. The research on nanocomposites to gain from a synergistic effect has been investigated using a combination of PtCu bimetallic NPs and poly(styrene sulfonate) (PSS) functionalized graphene (Gr). Moreover, the surface of PtCu/PSS-Gr was covered by a MIP for detection of the flavonoid puerarin. The peroxidase-like activity of the MIP@PtCu/PSSGr was applied in the colorimetric detection of puerarin reaching a LOD of 1 × 10^{-5} mol L^{-1} and with a linear range of 2 × 10^{-5} to 6 × 10^{-4} mol L^{-1} [192]. As proposed by this study, the PSS-Gr had good dispersity, stability, and a large surface area, which supported the dispersion of PtCu NPs, i.e., preventing any possible agglomeration that could lead to reduced enzymatic activity. Additionally, as the PtCu/PSS-Gr nanocomposite was covered by the MIP, without the target analyte puerarin, the small H_2O_2 passes through the polymer and reaches the peroxidase-like enzyme, generating hydroxyl radicals that trigger the oxidation of TMB. However, when puerarin is present and specifically binds the imprinted sites, it acts as barrier to H_2O_2, leading to decreased catalytic reaction[192].

Photooxidase mimics are activated by light for the oxidation of the substrate in the presence of dissolved oxygen [193]. Among the variety of nanomaterials that have been used as photooxidase mimics, the graphite carbon nitride (g-C_3N_4) is an emerging visible-light-active organic semiconductor with intrinsic fluorescence properties. Hence, applications of g-C_3N_4 in photocatalysis and photoluminescence-based biosensing are growing [193]. A recent study demonstrated the interesting properties of surface molecular imprinting on g-C_3N_4 nanozymes for improved detection of L-cysteine in serum [193]. The enzymatic activity was first probed upon blue LED irradiation, leading to oxidation of the chromogenic substrate like TMB without destructive H_2O_2. Most interestingly, the MIPg-C_3N_4 nanozyme, i.e., having TMB imprinted sites on the surface of g-C_3N_4, showed to suppress the matrix interference from serum samples, enhancing both substrate selectivity and enzyme activity in comparison to bare g-C_3N_4. Superior properties in terms of enzyme affinity to TMB, in comparison to other inorganic nanozymes, were also suggested in this study [193].

Electrochemiluminescence (ECL) detection has been highly investigated in sensor development. Nonetheless, common ECL reagents have a few disadvantages (e.g., high toxicity, low stability, and environment-sensitive luminescence efficiencies) and aggregation induced

emission (AIE) materials can overcome these limitations in some practical applications [194]. Additionally, nanozyme amplification has been proposed to offer unique advantages to ECL, and an aggregation-induced (AI)-ECL assay combined with Co_3O_4 nanozymes has been developed for the detection of antibiotic residues, namely, chloramphenicol [194]. In this sensor, the strong and stable signal relied on COF materials with AI-ECL groups (COF-AI-ECL), while the Co_3O_4 nanozymes worked as the amplification element. The synthesized COF-AI-ECL and Co_3O_4 were cross-linked to the surface of a gold electrode, followed by the construction of a MIP for selective recognition of chloramphenicol. The sensor showed a detection limit of 1.18 × 10^{-13} mol L^{-1}, and a linear range of 5 × 10^{-13} to 4 × 10^{-10} mol L^{-1}. Each sensor component offered improved sensitivity and selectivity features even when using complex matrix samples, essential to tracing antibiotic residues in food safety control [194].

The possibility of having a sensitive fluorescence system for selective detection of the myc toxin patulin motivated the development of a system based on Ag NP/flake-like Zn based MOF nanocomposite (AgNPs@ZnMOF) as an efficient support for MIP [194]. The Ag NPs were created inside the nano-pores of flake-like Zn MOF and the peroxidase-like activity of Ag NPs was greatly improved by the high surface area of MOF while the MIP for patulin ensured the selectivity. The fluorescence intensity, resulting from the product of catalyzed H_2O_2-terephthalic acid reaction, decreased linearly with increasing concentrations of patulin in a range of 0.1–10 µmol L^{-1} and a detection limit of 0.06 µmol L^{-1} [194].

In bioanalytical chemistry, the use of immunoassays is widespread, and the ELISA is considered the gold standard in many applications, owing to the highly sensitive detection [195]. Noneth less, the research on biomimetic alternatives is very attractive, namely, for reducing production costs and enhancing the reagent stability. Innovation at this level can occur both by using MIPs, also known as synthetic antibodies, and by employing nanozymes as catalytic labels. This biomimetic approach has been proposed for detecting an organophosphate pesticide [195]. In this work, the 96-well array format was accomplished with the synthesis of MIP microspheres by precipitation polymerization, followed by immobilization on the plate by "grafting to" method, assisted by ionic liquid as binder [195]. The nanozyme label relied on the peroxidase-like activity of Pt NPs and was prepared in two steps. First, BSA-hapten conjugates were synthesized and the final Pt@BSA-hapten probe was obtained by mixing with a colloidal solution of Pt NPs. Colorimetric and surface-enhanced Raman scattering were used for signal detection because the substrate TMB was oxidized to a blue TMB^{2+}, which also possesses a Raman signal. The proposed method showed a LOD of 1 ng mL^{-1} for triazophos [195]. Various biomimetic alternatives to common ELISA assays have been proposed. The detection of sulfadiazine, an

antibacterial compound whose residues in food and environment from misuse are of health concern, was studied using Au@SiO_2 and Au@Pt@SiO_2 NPs [196], [197].

The nanocomposites as labelling markers had the intrinsic peroxidase-like activity of Au NPs or Au@Pt bimetallic materials, and the SiO_2 NPs offered large surface area and ease of surface functionalization. This ideal combination was further improved by preparing MIP films for selective recognition and reusability, allowing to develop assays whose results were comparable to those obtained by High-performance liquid chromatography (HPLC) [196], [197]. Other configurations have been proposed, such as the use of Pt@SiO_2 NPs and a MIP for highly sensitive and selective detection of histamine with a LOD of 0.128 mg L^{-1} [198].

The multiplicity of sensor design has been expanded by the report of a three-component functional cell-mimicking structure bearing a nuclear Fe_3O_4 peroxidase-like activity, a shell layer of a stimuli-responsive molecularly imprinted hydrogel representing the cytoplasm, and a lipid bilayer membrane [199] (**Figure 2.14**).

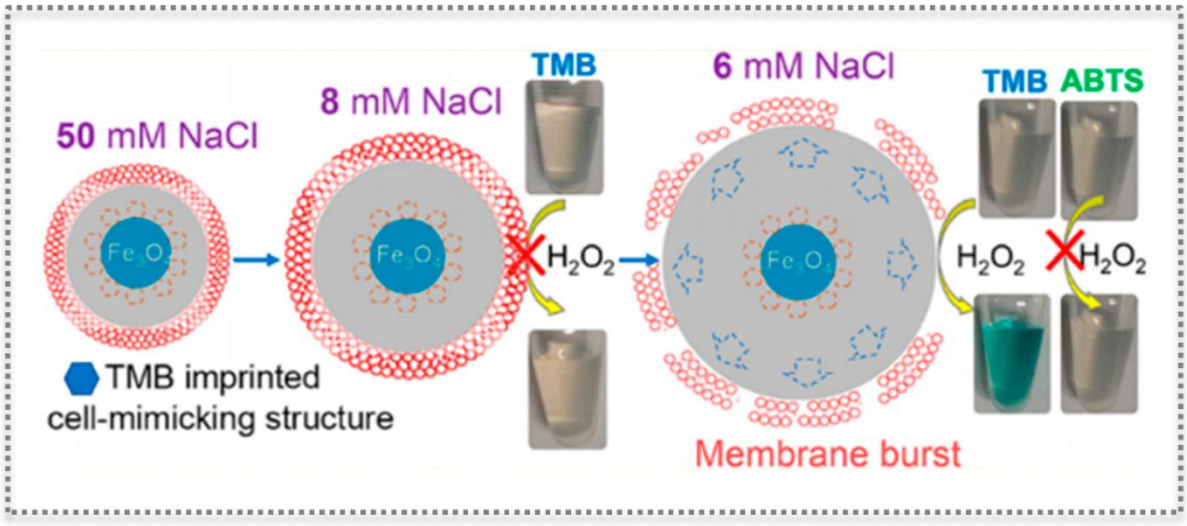

Figure 2.14: Cell-mimicking protocell of three components with a peroxidase-like iron oxide core as nucleus, a molecularly imprinted hydrogel shell as cytoplasm, and a lipid bilayer for biomedical applications. (Reproduced with permission [199], Copyright 2017, American Chemical Society).

Each component of the tripartite system had unique functions to deploy an interesting switch-like colorimetric system. The core Fe_3O_4 ensures the oxidation of the chromogenic substrate TMB (and similar, like ABTS) in the presence of H_2O_2. In turn, the MIP layer selectively recognizes TMB and is simultaneously sensitive to salt concentration by swelling or shrinking [199]. Finally, the elasticity of the lipid membrane keeps up with the swelling of the anionic MIP gel when lowering the sal concentration, until there is no more tolerance to volume change and the lipid layer bursts.

Thus, the gradual "analog" gel volume change was reflected in a "digital" colorimetric output because the burst of the membrane allows access to TMB that is oxidized to produce color. Interestingly, controlled access to TMB can also be achieved by using melittin, a membrane-perturbing amphipathic peptide, which introduces channels in the membrane. The selectivity is ensured by the imprinted gel, while this approach enlarges the potential applications of the system [199].

In summary, nanozymes have emerged as the next generation of enzyme mimics to overcome the existing challenges and broaden the application of synthetic catalysts. Despite the demonstrated advantages, the lack of specificity has always been a problem that hindered a faster and broader application of nanozymes. The synergy gained by using molecular imprinting technology to create selective substrate binding sites on nanozymes has been reasoned as a solution to solve the obstacle of missing specificity. Simultaneously, MIPs are also biomimetic, low-cost, and stable materials that can be produced on a large scale. The intrinsic catalytic activity of nanozymes can be improved by designing nanomaterial cores and proper surface functional groups, also benefiting from nanocomposites and doped nanomaterials. Concurrently, this diversity in composition, sizes, shapes, and surface properties calls for rigorous characterization and standardization of activity if practical implementation is foreseen. MIP technology is also resourceful, contributing with the possibility to obtain on-demand tailorable functional moieties and stimuli-responsive nanostructures. This biomimetic convergence is a hot research topic and new insights into functional engineered nanozymes@MIPs in the development of biosensing devices are expected to find auspicious biosensing applications soon. Once they have surpassed the current limitations and achieved the enhanced catalytic activity and specificity, imprinted nanozymes can be incorporated in portable, low-cost, and time-saving assays for novel point-of-care applications. These POC applications linked to low-cost devices that rely on synthetic materials are a huge opportunity for developing new tools that allow global efforts and alliances in combating the current and future pandemics, as well as screening for chronic diseases, allowing earlier detection and earlier medical action, to improve treatment outcomes.

CHAPTER 3

An ultra-sensitive electrochemical biosensor using the Spike protein for capturing antibodies against SARS-CoV-2 in point-of-care

The results presented in this chapter were published in **Cardoso, A. R.**, Alves, J. F., Frasco, M., Serrano, V., Mateus, D., Sebastião, A. I., Matos, A. M., Carmo, A., Cruz, M. T., Fortunato, E., Sales, M. G., An ultra-sensitive electrochemical biosensor using the Spike protein for capturing antibodies against SARS-CoV-2 in point-of-care. Materials Today Bio 2022, 16, 100354, 1-10. https://doi.org/10.1016/j.mtbio.2022.100354

3.

AN ULTRA-SENSITIVE ELECTROCHEMICAL BIOSENSOR USING THE SPIKE PROTEIN FOR CAPTURING ANTIBODIES AGAINST SARS-COV-2 IN POINT-OF-CARE

3.1 Introduction

In just two decades of the 21st century, numerous viral epidemics/pandemics have occurred that have been recognised by the WHO. These include Severe Acute Respiratory Syndrome Coronavirus (SARS-CoV, 2003), Chikungunya (2005), Influenza A (H1N1) (2009), Middle East Respiratory Syndrome Coronavirus (MERS-CoV,2012), Ebola (2014, 2019), and Zika (2015/2016) [1]. Such frequent outbreaks are evidence that future pandemics can be expected [200]. In this context, zoonotic viruses are considered the leading potential pathogens, for which there are neither effective vaccines nor drugs. The most compelling example is the recent outbreak of SARS-CoV-2, which triggered COVID -19 with devastating effects worldwide [201].

The highly contagious properties led to a rapid increase in the number of infected individuals. The high prevalence of asymptomatic individuals has also led to a high rate of transmission of the disease. Although there are no accurate quantitative data in the literature, reports suggest that approximately 30% of the population exposed to the virus is asymptomatic and transmits the disease. In addition, the signs of COVID -19 are nonspecific and include respiratory symptoms, fever, cough, dyspnoea, and viral pneumonia that require biochemical testing for diagnosis. Although the inherent infectious properties of the virus cannot be altered, it is possible to improve the biochemical tests that are currently being conducted worldwide to stratify the population, monitor the level of immunity in the community, and conduct viral surveillance [202]. Separating those infected (who must remain in quarantine) from those who have an

immunological response against the virus (antibodies) is essential for controlling pandemics and improving the global economic scenario. This will allow a portion of the population to return to their "normal" activities without risk. In addition, in order for currently available vaccines to be administered, it must be demonstrated that antibodies against SARS-CoV-2 have formed, and it must be known how they develop in individuals over time and how they subside over time. This is especially important at the community level, but difficult to implement at the global level [203]. Overall, monitoring of antibody levels is necessary to guide antiviral treatment, infection control, epidemiologic measures, and vaccination.

Serologic testing is essential for evaluating the qualitative and quantitative results of immune responses and has proven to be a valuable tool since the onset of infection. These tests are important public health tools to limit the risk of exposure and unintentional spread of the virus. This could be critical to limit the global spread of the disease and allow for the establishment of checkpoints for people in transit, including airports. In addition, a global antibody test would also allow stratification of populations by no, weak, moderate, or strong immune response, which is particularly important for achieving our "normal" life [204], [205]. Therefore, tools should be available to detect SARS-CoV-2 antibodies in the general population at different time points for each individual. Current methods include ELISA tests, which are neither rapid enough to allow immediate action nor sensitive enough to detect early stages of viral infection and disease onset. They also require laboratory facilities and specific equipment and reagents. In addition, some of these reagents are expensive and not available to meet global needs [206], [207].

Alternative rapid systems using biosensors have also been developed. These could be ideal modern tools as they have the potential to develop simple and inexpensive devices with low limits of detection for anti-SARS CoV-2 antibodies. Currently, lateral flow assays are the most popular biosensors for SARS CoV-2 serological assays because they have several advantages, such as ease of use and rapid response time. However, they have limited sensitivity and sensing capability compared to biosensors and are also more expensive [206]. In contrast, electrochemical biosensors can provide efficient, rapid, and accurate analysis, for which many papers have been published in the literature using this technology [208]. However, electrochemical biosensors also face some challenges that delay technology transfer to reach commercialization at the point-of-care [209].

Recent works on antibody detection can use renewable materials as substrates [210], optical techniques with special engineered antibodies [211] or plasmonic-based readout devices [212] and specially designed nanostructure arrays [213]. Overall, these works provide good analytical

properties but require several steps for electrode assembly, which can be very complex and/or require specialised and expensive instrumentation.

Therefore, a simple biosensor for serological monitoring of SARS-CoV-2 antibodies is still lacking in the literature, which is particularly important to allow scaling up to an industrial production and their global use.

The performance of an electrochemical biosensor depends on the characteristics of the electrode's interface and external conditions. Immobilization capacity, sensitivity, conductivity or specificity of the biosensor may be affected by the electrode's surface area and material composition [214], [215] Therefore, nanomaterials emerge as a promising resource to modify the electrode's interface to enhance its efficiency characteristics, improving the biosensor analytical performance. Carbon nanomaterials are particularly suitable for carbon electrodes and engineering their atomic properties allow for a variety of carbon allotropes that might answer to a diverse range of applications [216]. Carboxylated single-walled carbon nanotubes (SWCNTs), formed by a nanoscale graphene sheet folded around itself, are characterized by strong covalent bonding, high tensile strength, improved electron transfer, high surface area-to-weight ratio and porosity (important for protein immobilization) and good thermal stability (which may have a positive impact on the reproducibility of the sensor) [214], [217], [218].

Additionally, engineered NPs may also be used as electrochemical labels. Cadmium telluride quantum dots (CdTe QDs) are colloidal semiconductor fluorescent nanoscale crystals that can be easily modified with biomolecules such as antibodies, generally improve the stability of the sensor as well as its photoelectric properties [219]–[221], and present good interaction with carbon nanotubes [222], making these nanoparticles an interesting electrochemical probe for our biosensor.

Thus, this article presents a sensitive electrochemical biosensor that, although assembled using an amazingly simple procedure, can detect small amounts of antibodies in human serum (and in much smaller amounts than conventional methods). The biosensor uses commercially available SPEs with a carbon WE containing *p*-phenylenediamine and protein S. Analytical properties are evaluated, and the devices are tested in human serum and further validated using a commercial benchmark method restricted to laboratory facilities. Electrochemical detection is performed in two ways: with an iron redox probe or with anti-IgG labelled with QDs.

3.2 Experimental Section

3.2.1 Reagents and Solutions

All chemicals were of analytical grade and ultrapure Milli-Q water laboratory grade (conductivity <0.1 μS/cm) was used. Chemical reagents included potassium hexacyanoferrate III ($K_3[Fe(CN)_6]$) from Carlo Erba; potassium hexacyanoferrate II ($K_4[Fe(CN)_6]$) trihydrate from Panreac; carboxylated single-walled carbon nanotubes (SWCNT); *N*-ethyl-*N*′-(3-dimethylaminopropyl) carbodiimide hydrochloride (EDAC), *p*-phenylenediamine, phosphate buffered saline (PBS, 0.01 mol/L, pH 7.4), *N,N*-dimethylformamide (DMF) were purchased from Sigma-Aldrich; *N*-hydroxysuccinimide (NHS) was acquired from Merck; recombinant SARS-CoV-2 S protein, S1 subunit, Host Cell Receptor Binding Domain (RBD), rabbit anti-SARS-CoV-2 S protein antibody, and rabbit anti-SARS-CoV-2 N protein antibody were obtained from RayBiotech.

3.2.2 Apparatus

Electrochemical measurements were performed using a PalmSens4 potentiostat/galvanostat controlled by PSTrace 5.8 software. Commercial carbon SPEs (C-SPEs) from Metrohm DropSens (DRP-110) were used. These contain a three-electrode system, including: (a) a carbon counter electrode, (b) a silver RE, and (c) a 4 mm diameter carbon WE. The C-SPEs were connected to a PalmSens switch box that allows connection to the potentiostat.

3.2.3 Electrochemical measurements

CV was performed in the range of -0.3 to + 0.7V at a scan rate of 50 mV/s. EIS was performed in open circuit with a sinusoidal potential perturbation with an amplitude of 0.01 V and 50 data points logarithmically distributed over a frequency range of 0.1–100000 Hz. The SWV data require a sampling potential of -0.3 to +0.7 V, with a frequency of 2 Hz and a step height of up to 2.5 mV. For the EIS data, Nyquist plots were used to represent the spectra obtained, showing the frequency response of the electrolyte system and plotting the imaginary component (Z´´) of the impedance against its real component (Z'). The EIS data were fitted to the typical Randles equivalent circuit, typically employed in impedimetric biosensors, and being composed herein of solution resistance (Rs), double layer capacitance (Cdl), and charge transfer resistance (Rct) [223]–[226]. RS is the resistance between the working and RE. RCT is the electron transfer resistance across the electrode-electrolyte interface. Cdl is the specific capacitance at the

interface of the electrolyte and the electrode and is characterized by the non-faradaic charge that arises from the surface. Analysing the collected data, circuit elements displayed errors below 5%. In general, the electrical properties at the WE surface were monitored by CV, EIS, and SWV studies using a redox probe solution of 5.0 x 10^{-3} mol/L $[Fe(CN)_6]^{3-}$ and 5.0 x 10^{-3} mol/L $[Fe(CN)_6]^{4-}$ in PBS buffer pH 7.4.

3.2.4 Preparation of C-SPE biosensor

The approach used to build the current biosensor is described in **Figure 3.1** and was inspired by our previous work on malaria and Zika diagnostics [227], [228]. The first step involves the dispersion of carboxylated SWCNT in DMF (1.0 mg/mL) during 60 min. Then, the WE was incubated with 1.16 µL of the SWCNT solution and dried at 72 °C for 30min (**Figure 3.1 A**). In the next step, the carboxyl groups on the surface of SWCNT were activated with a solution of EDAC and NHS (0.025 mol/L EDAC and 0.0125 mol/L NHS) for 90 min in a humid chamber at room temperature. The *p*-phenylenediamine (0.02 mol/L) was then bound to the SWCNT by incubation for 60 min to obtain an amine layer on the WE (**Figure 3.1 B**). Finally, S protein (0.019 mg/mL) was bound to the amine layer for 40 min at room temperature and in a humid environment (**Figure 3.1 C**). All solutions were prepared in PBS buffer pH 7.4, unless otherwise indicated. Subsequently, the analytical performance of the biosensor was determined by detecting antibodies bound to the S protein (**Figure 3.1 D**).

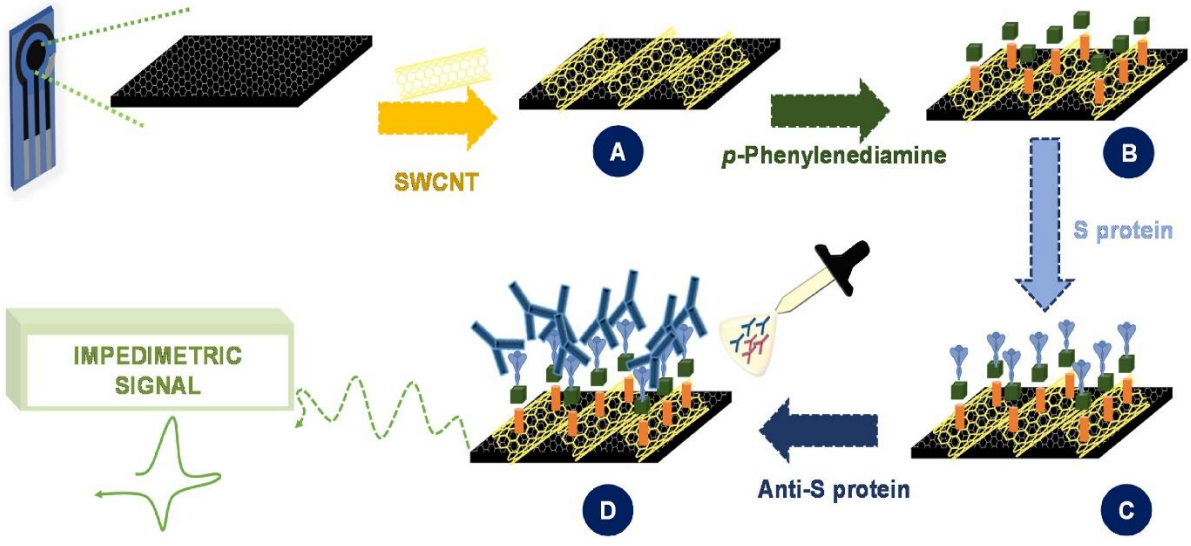

Figure 3.1: Schematic representation of the C-SPEs and the functionalization of the WE: (A) addition of carboxylated SWCNT; (B) modification with *p*-phenylenediamine through EDAC/NHS coupling reaction; (C) binding of S protein and (D) electrochemical detection of anti-S protein antibody.

3.2.5 Characterization by Raman spectroscopy

Each step of the sensor design was followed by Raman spectroscopy by direct analysis of the material in a Thermo Scientific DXR Raman spectroscope equipped with a 532 nm laser. The average signal-to-noise ratio (peak height/RMS noise) was allowed for 900 s of measurement time, after up to 2 min of photobleaching, with up to 3 mW of laser power and a 50 μm slit aperture.

3.2.6 Ethics statement

Human serum was collected at Centro Hospitalar e Universitário de Coimbra (CHUC) from patients with or without a clinical history of COVID -19 and without concomitant comorbidities (cardiovascular, autoimmune, or respiratory disease). Positive samples were collected randomly during routine blood analysis by the clinicopathology service of the University Hospital of Coimbra (Patients details is shown in **Table 3.1**. The collected human samples were immediately frozen until use. This study was approved by the CHUC Ethics Committee (Process number OBS.SF.220-2021), always ensuring the protection of personal data through anonymization (General Data Protection Regulation 2016/679).

Table 3.1 - Clinical information for all patients used in experimental work.

Patient number	Age	Patient's comorbidities	Symptom-based disease duration (days)	COVID-19 severity	Relapsing	SARS-CoV-2 vaccination
9	57	Chronic obstructive pulmonary disease	20	Moderate	No	No
11	34	None	15	Mild	No	No
12	41	None	20	Mild	No	No
16	60	None	10	Mild	No	No
17	61	Type 2 diabetes	14	Moderate	No	No
30	68	Obese; Type 2 diabetes,	30	Severe	No	No
33	55	None	20	Moderate	No	No

3.2.7 Analytical performance of the biosensor

The analytical performance of the sensor layer was evaluated by incubation with increasing standard concentrations of antibody solutions (anti-S protein) ranging from 1 pg/mL to 10 ng/mL prepared in PBS buffer pH 7.4. Each standard was incubated for 40 min at room temperature in a humidified environment. After incubation with each standard concentration, the sensor was washed and its impedimetric properties were analysed by EIS using the iron redox probe. The analytical response of the biosensor was also evaluated in negative human serum, i.e., serum without anti-S protein antibodies, which served as a control and was spiked with known standard concentrations of anti-S protein antibodies. Standards were prepared in negative human serum diluted 500-fold in PBS buffer pH 7.4, and the incubation time was set at 40 min. All assays were performed in triplicate. The LOD corresponded to the $x + 3\sigma$, where x is the average value of the EIS blank signals (obtained in the absence of anti-S protein) and σ is the known standard deviation of the EIS blank signal in successive measurements [229]. Biosensor selectivity was evaluated by incubation with the anti-N protein antibody in the same concentration range used to determine the calibration curve with the anti-S protein antibody. Similarly, the incubation time was set at 40 min and all electrochemical assays were performed in triplicate.

3.2.8 Analysis of human serum samples by VIDAS®

Immunoassay tests were performed using the VIDAS® equipment from Biom erieux (Marcy l'Etoile, France). This instrument performs an automated qualitative ELISA for the detection of specific anti-SARS-CoV-2 IgG in human serum, which requires the use of the VIDAS SARS - CoV-2 IgG 423834-02® kit (BioMerieux, Marcy l'Etoile, France). This kit contains the disposable solid phase strips, solid phase vials containing humanized recombinant SARS-CoV-2 antigen, the standard (with humanized recombinant anti-SARS-CoV-2 IgG antibody), and the positive (also with humanized recombinant anti-SARS-CoV-2 IgG antibody) and negative controls (without the humanized recombinant anti-SARSCoV-2 IgG antibody) (https://www.biomerieux-diagnostics.com/vidas-sars-cov-2). In addition, the solutions used to generate the standard curve were obtained by successive dilutions of the purified anti-SARSCoV-2 S-protein S1 recombinant antibody from BioLegend (San Diego,CA, USA). The different solutions of the purified anti-SARS-CoV-2 S-protein S1 recombinant antibody were prepared. Then, 100 µL of these solutions were added to a designated spot on the kit strip and the automated qualitative ELISA was performed. First, the instrument dilutes the contents of the container. Then, the coated

antigen captures the SARS-CoV-2 specific IgG, and a wash step follows to remove the unbound components. In a second step, the mouse monoclonal antibodies conjugated with alkaline phosphatase specifically recognize the IgG present in the contents. Again, the device performs a wash step to remove the unbound components. Finally, the instrument performs an incubation step by adding the substrate 4-methyl-umbelliferyl phosphate to the sample/standard, which is hydrolysed to the fluorescent product 4-methylumbelliferone. The fluorescence of this product is measured at 450 nm and a relative fluorescence value (RFV) is generated (**Figure 3.2**) [230].

3.2.9 Correlation of VIDAS® signal with standard anti-S solutions

Even though VIDAS® gives an RFV value, the information it provides is only qualitative. It is considered a positive result if the test value (which is the quotient between the RFV of the sample and the RFV of the instrument standard 1) is equal to or above 1.00, and negative if it is below 1.00 [230], [231]. However, the RFV values are proportional to the concentration when anti-S standard solutions are analysed by VIDAS®.This allows the conversion of RFV values to concentration. To this end, anti-S standards of 0; 1.0; 5.0; 10.0; 25.0; 50.0; 100; 250 µg/mL were analysed by VIDAS®.

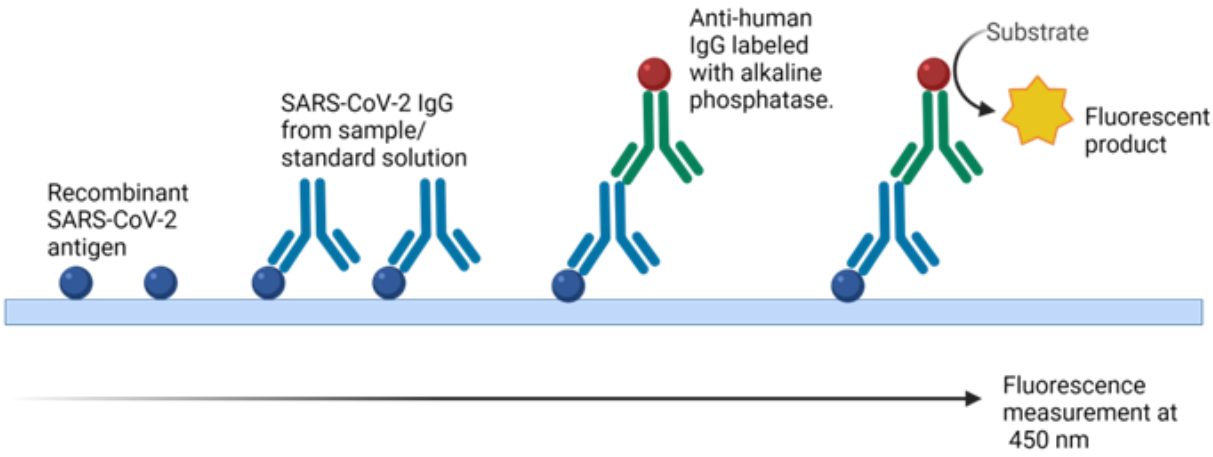

Figure 3.2: Schematic representation of the VIDAS® mode of operation.

3.2.10 Analysis of human sera with the electrochemical biosensor

The positive serum samples were tested to evaluate the biosensor response compared to the VIDAS® results. The serum samples only had to be diluted beforehand (500-fold dilution in PBS, pH 7.4) to fit within the linear range of the sensitive biosensor and avoid interference from the serum matrix. All assays were performed in triplicate.

3.2.11 Synthesis of quantum dots and conjugation with anti-human IgG antibodies

Red emitting cadmium telluride quantum dots capped with 3-mercaptopropionic acid (MPA) CdTe@MPA QDs were prepared according to a previous protocol with minor modifications [23]. Conjugation of antibodies with red emitting CdTe@MPA QDs was performed as follows. A solution of QDs (2.5 mg/mL) in PBS 0.01 mol/L pH 7.2 was incubated with goat anti-human IgG (51.02 µg/mL), EDAC (1.25 mg/mL), and NHS (1.50 mg/mL) for 3 h at room temperature in a total volume of 100 µL. Then, 30 mL of glycine (10 mmol/L) was added and the reaction mixture was incubated at room temperature for 30 min. Finally, the resulting solution was centrifuged at 8500 rpm for 3 min in the Amicon™ Ultra-0.5 centrifugal filter device. The filtrate solution was discarded, and the membrane was inverted to collect the anti-human IgG@QDs conjugates at the final concentration of 51.02 µg/mL. The procedure was repeated for the preparation of anti-human IgG@QDs at 10.10 µg/mL and 101.01 µg/mL (**Figure 3.3**).

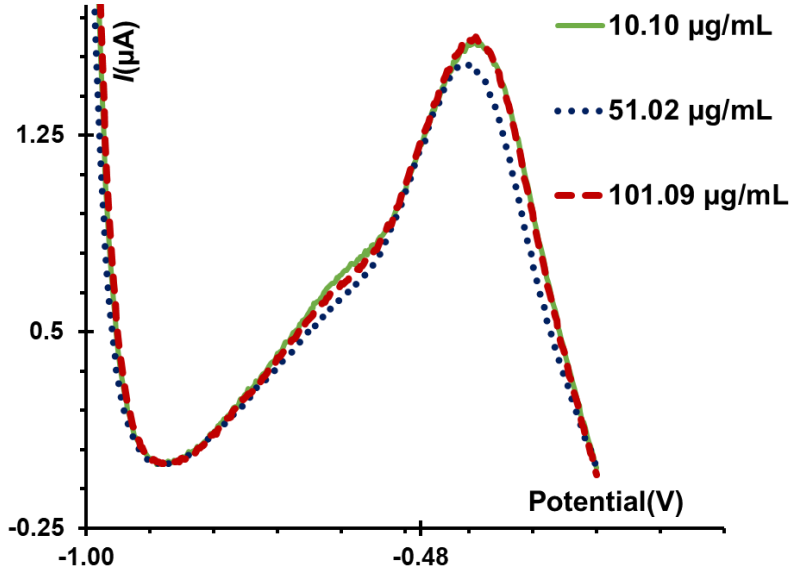

Figure 3.3: Current intensity of the electrochemical biosensor measured by SWV for different concentrations of anti-human IgG@QDs (10.10 µg/mL, 51.02 µg/mL and 101.09 µg/mL).

3.2.12 Secondary anti-human IgG@QDs as electrochemical labels

First, different concentrations of secondary goat anti-human IgG antibodies (10.10, 51.02, and 101.01 µg/mL) labelled with CdTe QDs were each incubated on one of the three sensor-modified surfaces with the maximum positive serum concentration detected by our biosensor (752 ng/mL) to select the optimal concentration for signal detection (Figure 3.3). The composite WE surface of five other biosensors was incubated with PBS pH 7.4 for 40 min at room temperature until stabilized. Then, positive serum solutions diluted in negative serum (107, 150, 188, 250, and 752 ng/mL) were incubated on each of the five composite sensors. The selected concentration of QDs-labelled IgG antibody conjugates was then added to our device to label the primary antibodies present in the positive serum by incubating it at room temperature for 90 min. Instead of a redox probe, a solution containing 0.1 mol/L KCl as electrolyte was used to allow a more practical direct reading. The parameters of the SWV method had a potential range of -1.0 V to -0.2 V, with a potential step of 2.5 mV with an amplitude of 0.02 V at a frequency of 2 Hz.

3.3 Results and Discussion

3.3.1 Biosensor assembly and characterization

The biosensor was constructed in three steps: Carboxylation of the carbon substrate, subsequent amination of this surface, and adsorption of S-protein. The preparation of an aminated surface directly on the carbon substrate could combine the first two steps and further simplify the procedure, but this was tried in several other ways that did not show sufficiently satisfactory results in terms of electrochemical stability to be a convincing electrochemical biosensor for global application. The electrochemical features of the C-SPEs in each of these steps were followed by CV, EIS and SWV tests, with a standard iron redox probe, whose typical data are shown in Figure 3.4. Carboxylation of the carbon WE on the C-SPEs was performed by casting carboxylated SWCNTs. As expected, the electrochemical properties showed that the electrical properties of the sensing layer were improved after modification with carboxylated carbon nanotubes. The effectiveness of this step was more evident in the EIS and SWV data, with a lower Rct value of~549 Ω and a higher current of ~48.62 µA, respectively, compared to the original readings. After this modification, amination of the WE with *p*-phenylenediamine was achieved by an EDAC/NHS coupling reaction between the carboxyl groups of SWCNT and an

amine group of *p*-phenylenediamine [232]. Subsequently, the S-protein was incubated on the amine layer, which resulted in a decrease in current at both CV (~83.68 µA) and SWV (~33.98 µA). In addition, a significant increase in Rct (1038.67 Ω) was observed. These results suggest that the S-protein recognition layer was successfully formed on the electrode.

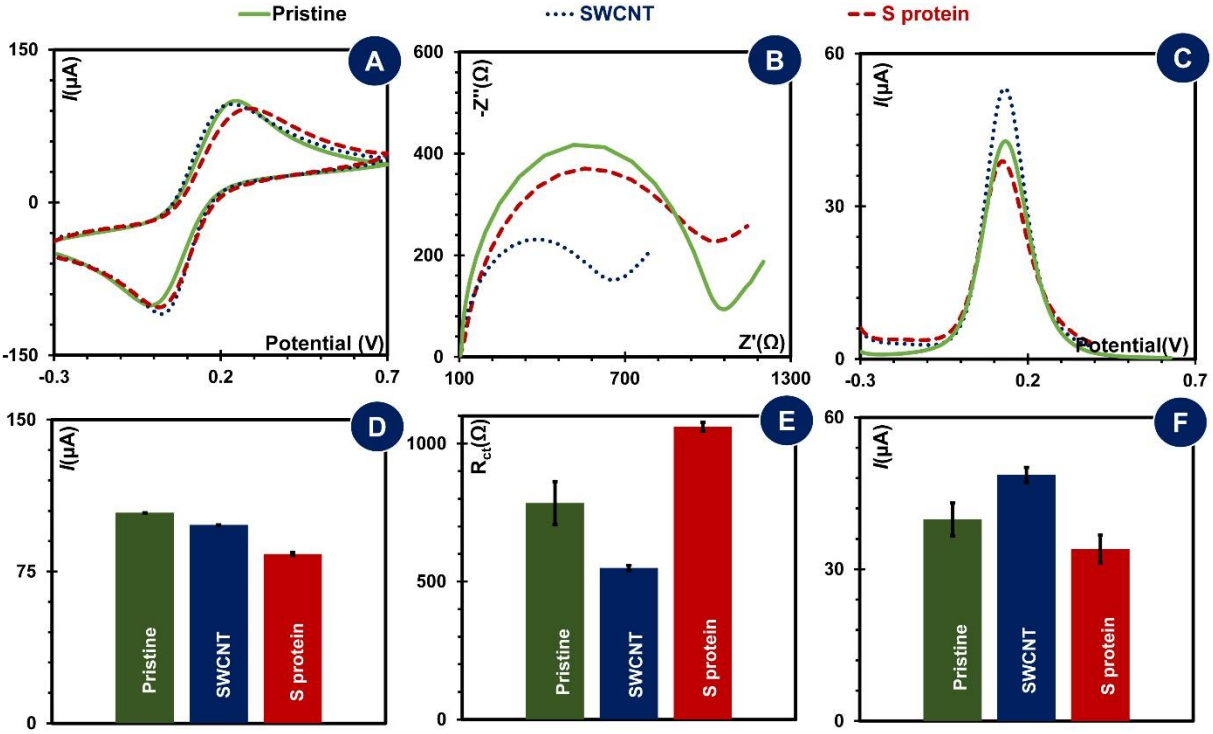

Figure 3.4: Electrochemical data collected upon the biosensor construction, using CV (A), EIS (B) and SWV (C) measurements. Data includes pristine C-SPEs, after modified with SWCNT and S protein. Graphics D and F show the current peak's intensity, and graphic E presents the Rct values with the respective error bars, highlighting the reproducibility of three independent devices.

The chemical modification of each step of the biosensor construction was followed by Raman spectroscopy **Figure 3.5**. The typical G and D bands of the C-SPE were located at 1583.0 cm^{-1} and 1350.8 cm^{-1}, respectively, indicating the presence of a graphitic nanomaterial with sp2 and sp3 carbon-hybridization systems. Incubation of the carboxylated SWCNT onto the WE significantly changed the Raman spectra obtained. The G and D bands were now at 1590.62 cm^{-1} and 1342.21 cm^{-1}, respectively, with the D band decreasing more than tenfold compared to the G band.

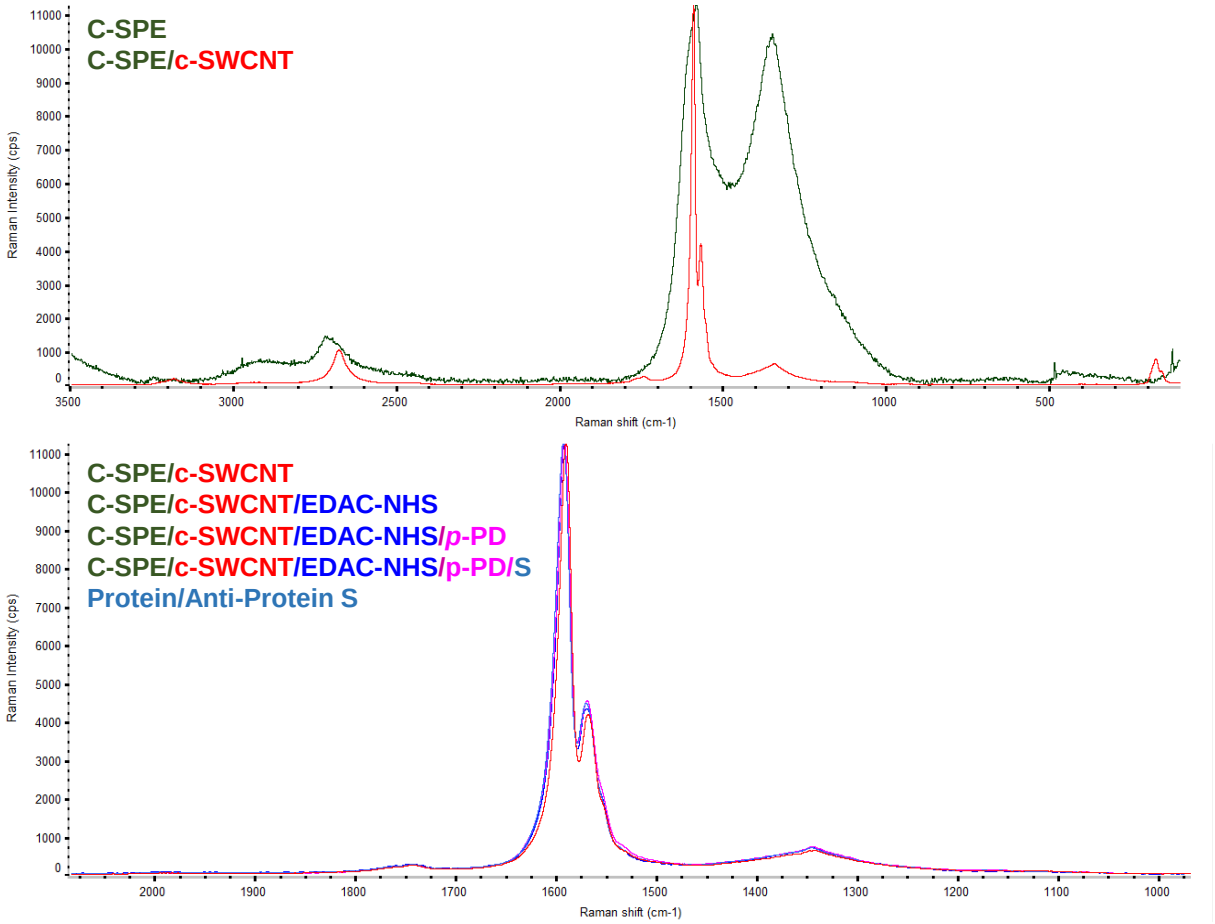

Figure 3.5: Raman spectra for each stage of chemical modification of the WE of the C-SPE (green/top) throughout the biosensor construction, including the modification with carboxylated SWCNT (c-SWCNT, red/top), and the successive addition of EDAC/NHS, *p*-phenylenediamine, S protein and anti-S protein antibodies (substantially superimposed and difficult to distinguish).

Overall, this confirmed the presence of the carbon nanotubes on the C-SPE [233]. Subsequent addition of EDAC/NHS, p-phenylenediamine, S-protein, and anti-S-protein antibodies did not result in significant changes in Raman spectra, also confirmed by calculating the ratios of the intensities of G and D bands **Table 3.2**. Overall, the significant change in Raman spectra was observed only after the incubation of the carboxylated SWCNTs, with only minor changes in the D-band and G-band observed in the subsequent phases of the biosensor assembly.

Table 3.2: Raman intensity of the G and D brands on the spectra of the biosensor, following the consecutive steps of modification.

Material	G Band	D Band	I_G/I_D
C-SPE	226.93	208.14	1.09
+ c-SWCNT	11370.16	631.09	18.02
+ EDAC/NHS + p-PD	5054.32	322.83	15.67
+ S protein + Anti-S protein	1475.73	91.52	16.12

3.3.2 Analytical performance in PBS buffer

The analytical properties of the biosensor were evaluated by testing increasing concentrations of the anti-S protein antibody, followed by EIS measurements and the generation of calibration curves. The typical Nyquist plots of the EIS measurements are shown in **Figure 3.6A**. They show a positive correlation between the increase in Rct and the successive increase in antibody concentration. These results indicate that the impedimetric resistance, i.e., the diameter of the semicircles in the Nyquist plots, increases with increasing amount of antibody that recognizes and binds the S protein. The sensor showed a linear range between 1.0 pg/mL and 10.0 ng/mL, while higher concentrations saturate the sensor layer **Figure 3.6B**. The reproducibility of the sensor system was confirmed by performing three independent calibrations, with new biosensing units. The relative standard deviation (RSD) of the slope was ~2.6%, with an average slope of 280.47 Ω/decade. The squared correlation coefficient of the calibrations was >0.99. The reproducibility of the electrochemical response was excellent, proving that the system is reproducible, considering that the RSD values ranged from 0.5% (minimum) to 1.11% (maximum) in a linear trend. Overall, these results showed a highly sensitive response to anti-S protein antibodies with a LOD of 0.77 pg/mL.

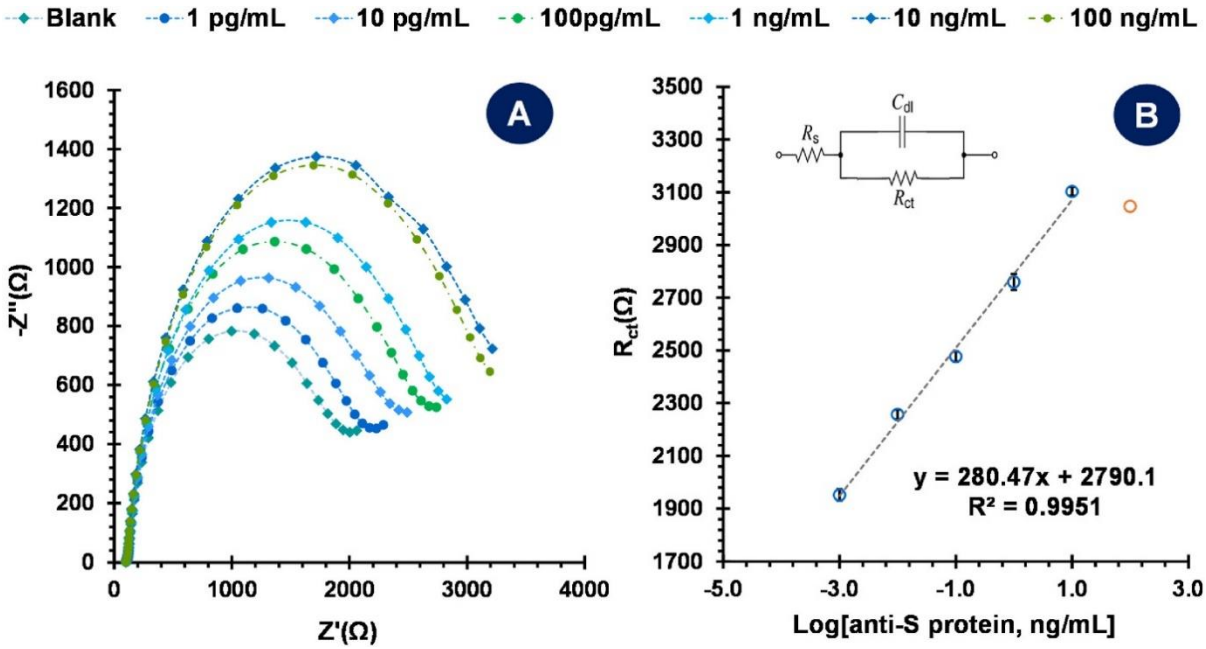

Figure 3.6: EIS measurements of the calibration with anti-S protein antibodies (1.0 pg/mL – 100 ng/mL) in PBS buffer: Nyquist plots (A) and the corresponding calibration curve (B). Readings were performed with the redox pair 5.0 x10^{-3} mol/L $[Fe(CN)_6]^{3-}$ and 5.0 x 10^{-3} mol/L $[Fe(CN)_6]^{4-}$ prepared in 0.01 mol/L PBS buffer pH 7.4.

3.3.3 Selectivity of the biosensor

The biosensor had a recombinant S protein on the surface of the WE so that it should bind selectively to anti-S protein antibodies. This selective binding may be confirmed by examining the response of the biosensor to other competing compounds. Since infected humans also have anti-N protein antibodies, it was considered here to evaluate the selectivity by checking the cross-reactivity of the biosensor with these specific antibodies. Distinguishing between antibodies to S and N proteins is also critical for tracking COVID -19. Technically, anti-N proteins are expected to interfere little to not at all with the measurement of anti-S proteins. In this study, the selectivity of the biosensor was evaluated by examining the response to individual solutions of anti-N and anti-S protein antibodies prepared in the same concentration range over the concentration range of the linear response. The data collected considered the Rct values obtained in each EIS measurement, and the average values were plotted in **Figure 3.7**. In general, in the presence of the anti-N protein antibody, the biosensor showed a uniform response (like the blank) over the entire concentration range tested. This contrasted with the increasing Rct values of the biosensor in the presence of the increasing concentrations of anti-S protein antibody.

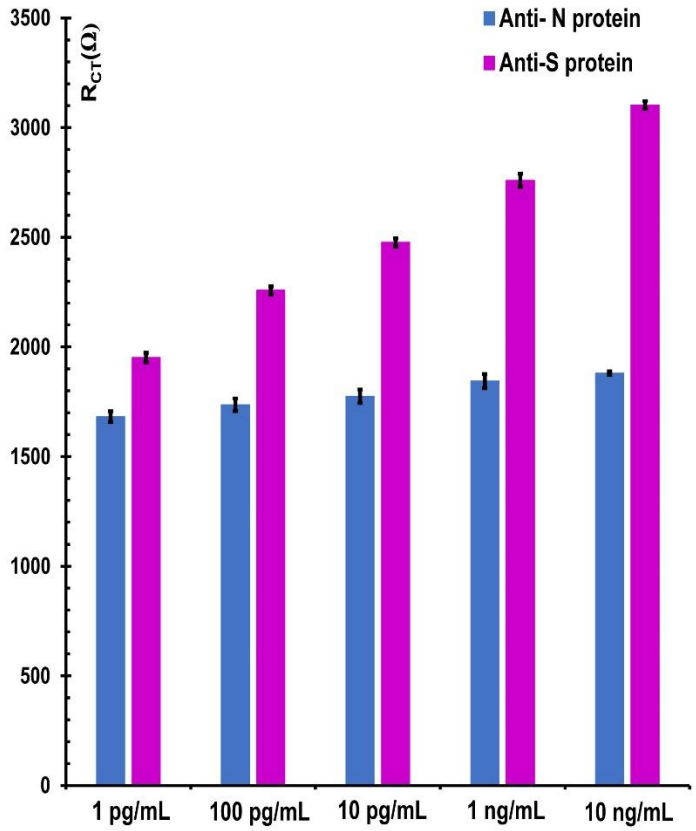

Figure 3.7: EIS response of the biosensor in the form of Rct values after the incubation of anti-S or anti-N protein antibodies, ranging from 1.0 pg/mL to 10 ng/mL.

Overall, the data suggest that the current biosensor is not affected by the presence of the anti-N protein antibody and that it responds accurately to the anti-S protein antibody. These are interesting results, as any analytical tool capable of distinguishing spike-from nucleocapsid-specific immunity can help to study the immunological response of post-infected or vaccinated individuals [208], [234].

3.3.4 Analytical performance in spiked human serum

The analytical performance of the sensing layer was evaluated using negative human serum spiked with anti-S protein antibodies to provide more realistic information in the context of real-world applications. The negative serum was diluted 500-fold to better match the sample to the linear trend of the biosensor. The EIS measurements were used to evaluate the biosensor response, and the calibration curves were plotted as Rct versus the logarithm of concentration (**Figure 3.8**). Rct values increased with increasing antibody concentration (**Figure 3.8 A**), and a linear trend was confirmed in the range of 1.0 pg/mL and 10 ng/mL. The average slope was 1825.5 Ω/decade, which was greater than that of the buffer, indicating that sensitivity

increased. This likely reflects the higher complexity of the sample matrix (including higher ion and protein content), as the absolute Rct values were higher than those of the buffer at comparable concentrations. Overall, the biosensor provided reproducible responses, with RSDs of slope of ~4.0. The squared correlation coefficient of all calibrations was also >0.99, confirming the quality of the linear trend (**Figure 3.8 B**). Overall, these results showed a sensitive response to detect anti-S antibodies with a very low LOD. Although tested in a more complex matrix, LOD was not significantly different from LOD in PBS buffer pH 7.4 and was 0.70 pg/mL. This LOD is in the range or even lower than recent findings reported in the literature for other electrochemical biosensors, mostly also containing nanomaterials that improve the sensitivity (**Table 3.3**). Considering the detection of antibodies in infected humans and because the serum was diluted 500-fold, the biosensor can be used to analyse human sera from 0.5 ng/mL to 5000 ng/mL. This is a wide concentration range that will simplify future application procedures, although more concentrated solutions may saturate the biosensor and require additional dilution. However, further testing was performed with positive samples, as the level in the serum of a healthy person (negative serum) is quite different from that of a person with COVID -19.

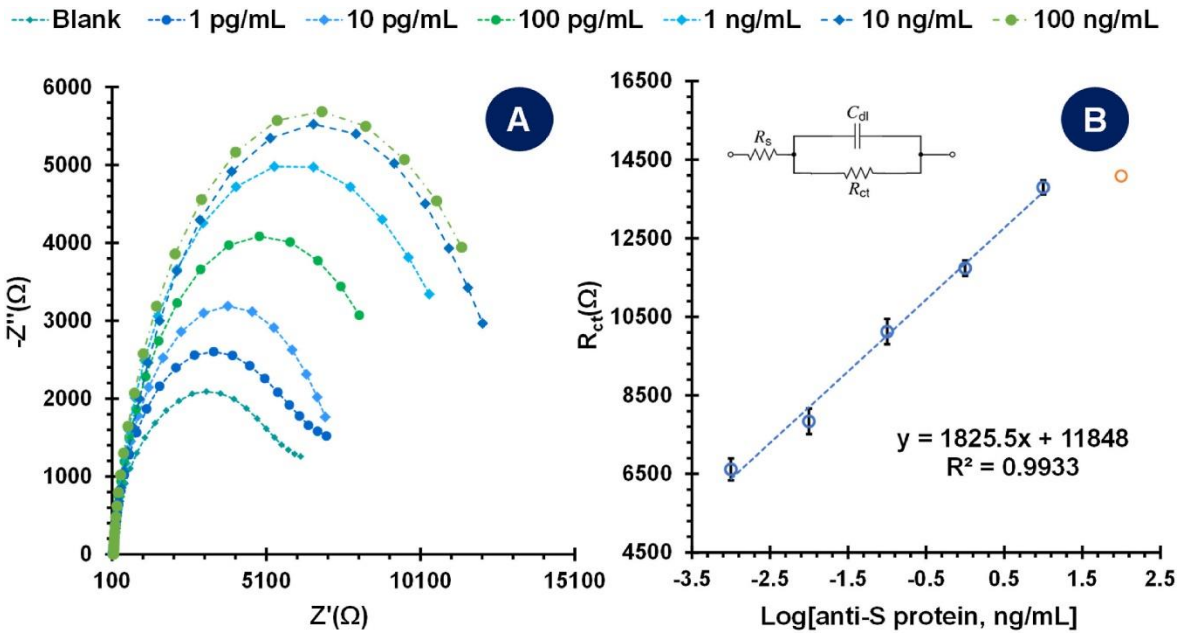

Figure 3.8: EIS measurements of the calibration with anti-S protein antibodies (1.0 pg/mL – 100 ng/mL) spiked in negative human serum (500-fold diluted in PBS buffer): Nyquist plots (A) and the corresponding calibration curve (B). Readings were performed with the redox pair 5.0 x 10^{-3} mol/L $[Fe(CN)_6]^{3-}$ and 5.0 x 10^{-3} mol/L $[Fe(CN)_6]^{4-}$ prepared in 0.01 mol/L PBS buffer pH 7.4.

Table 3.3: Electrochemical biosensors for detection of SARS-CoV-2 antibodies.

Biosensor design	Advantages	LOD*	Refs.
Paper/GO	Eco-friendly Low-cost	1 ng/mL	[210]
Paper/ZnO-NW	Eco-friendly Enhanced sensitivities and sensing ranges	*10 ng/mL.(*)	[235]
Gold Nanoparticles on 3D electrodes/rGO	Label-free Regeneration ability	1 pM	[236]
Gold electrode	Rapid Label-free	*0.1 µg/mL.(*)	[237]
Gold clusters	Higher sensitivity Non-invasive samples (saliva or oropharyngeal swab)	0.01 ag/mL	[238]

GO: graphene oxide; **ZnO-NW**: zinc oxide nanowires; **rGO**: reduced graphene oxide. (*) Lowest tested concentration.

3.3.5 Analysis of positive sera samples

The ability of the electrochemical biosensor to determine antibody levels in different positive human samples was tested by analyzing the same samples with both the biosensor and VIDAS®. Since VIDAS® only provides qualitative data (positive or negative) in terms of antibody levels in sera, we generated a standard curve using different standard solutions of purified anti-SARS-CoV-2 S1 recombinant protein antibodies. The RFV values obtained for these antibodies (expressed in arbitrary units) were correlated with the logarithm of the antibody concentration, enabling the extraction of quantitative data from this commercial method. The data obtained are shown in **Figure 3.9** and consider only the concentration range of the antibodies, which have a linear behaviour. The anti-S-SARS CoV-2 IgG concentration in the sera could be now calculated by intersecting this curve, which gives an idea of the range of anti-S protein IgG antibody concentrations in the COVID-19 positive population. The samples included in this comparative study contained different ranges of antibody concentrations (n=5), as expected given the quite variable RFV concentrations in VIDAS®. The concentrations chosen for this purpose are well above the capabilities of the biosensor and range from 5 to 230 µg/mL. Prior to

analysis, samples were treated according to the method used. For VIDAS®, the procedure provided by the commercial instrument was used, while for the biosensor only an appropriate dilution was performed.

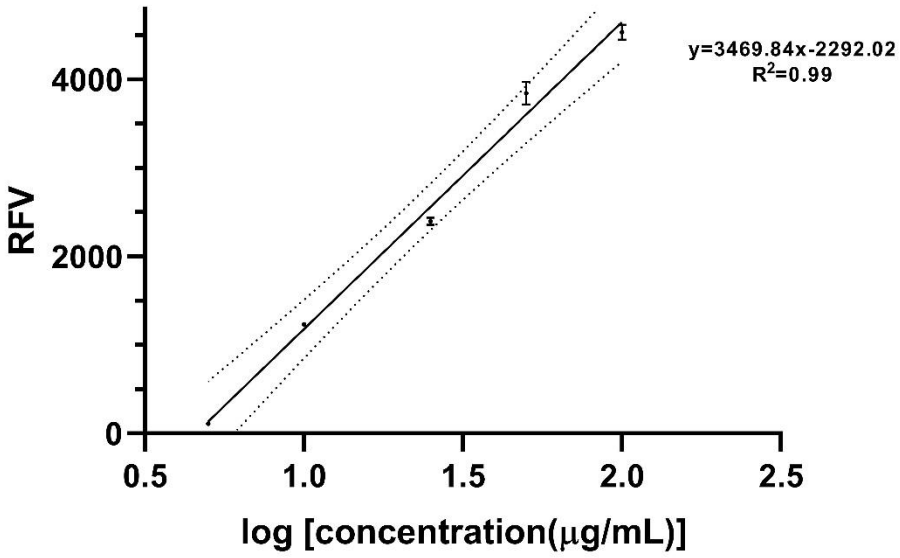

Figure 3.9: Standard curve of the correlation between the obtained RFV and the respective logarithm of the standard concentration (μg/mL) (mean ± error). The dashed lines represent the 95% confidence intervals. Note that the higher and lower concentrations are not shown because they were removed due to deviations from linearity.

The concentrations of these samples obtained with VIDAS® and the biosensor are shown in **Table 3.4**. The concentrations obtained with the biosensor were extracted from the correlation of the log concentration of antibodies known to be present in the samples with the Rct values of each of these positive samples (**Figure 3.10**). This was done to provide a valuable correlation between the positive sera and the electrochemical method, which proved necessary to eliminate the effect of the sample matrix now containing additional biomolecules required to combat the disease. Attempts were made to compare the readings with the concentrations of antibodies diluted in negative sera, but the data obtained were not reliable. It was also noted that the Rct values increased well beyond the usual calibration ranges, which indeed confirmed some influence of the positive samples, but these had no significant effect upon the concentration of antibodies yielding a linear trend. Overall, the relative errors in this analysis ranged from -10.2 to +15.3%. Considering that these are human samples, these results can be considered accurate [239], [240]. Furthermore, these are excellent results considering that the samples were highly diluted in the biosensor measurements and that the two methods have very different operating principles. This also indicates that the biosensor can be considered an

important alternative to current methods, especially when lower amounts of antibodies are involved.

Table 3.4: Analytical data obtained with the electrochemical biosensor by EIS readings and by the comparison methods, VIDAS® of different positive sera samples.

Samples	C_{VIDAS} (µg/mL)	C_{EIS} (µg/mL)	% error
1	5.4	5.2	-2.9
2	6.3	5.9	-5.7
3	51.6	59.4	+15.3
4	29.4	31.0	+5.5
5	230.7	207.2	-10.2

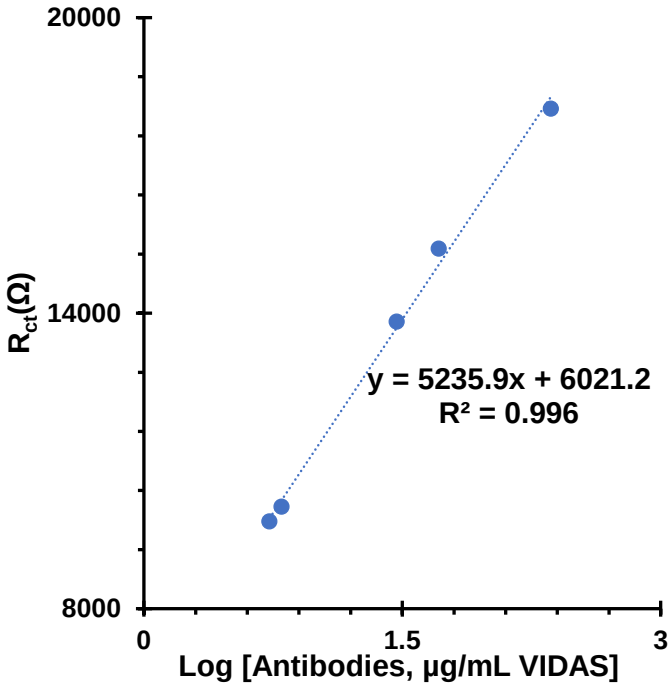

Figure 3.10: Correlation between the results of several dilutions of positive serum analysed by VIDAS® and the Rct readings of the biosensor (as obtained by EIS measurements).

3.3.6 Comparison of method capabilities to low antibody concentrations

From the data obtained, it appeared that the biosensor was able to detect much lower concentrations of antibodies than VIDAS®. To confirm this, a positive human sample with a concentration of approximately 225.66 µg/mL was diluted down to different concentration levels and evaluated using both methods. VIDAS® was only able to measure concentrations up to 2256 ng/mL, which corresponds to a 100-fold dilution of the original sample. At higher serum dilutions, corresponding to 150, 107, and 83 ng/mL, the analytical signal in VIDAS® was similar, indicating that the concentration was equal to or lower than 2.3 µg/mL and that further concentration differences could not be distinguished. Overall, VIDAS® was unable to discriminate between antibody concentrations below 2.3 µg/mL. This is a fairly high concentration and confirms the limited ability of the comparative method to provide accurate data for lower antibody concentrations (the commercial method works well but only provides reliable data for higher concentrations).

In contrast, serial dilution of this sample resulted in a linear trend against antibody concentration by EIS. This was achieved when the concentration incubated on the biosensor ranged from 70 to 752 ng/mL, with clearly distinguishable values for concentrations of 150, 107, and 83 ng/mL. The electrochemical biosensor was thus able to detect differences between samples that had much lower concentrations than those analysed by VIDAS®, down to 70 ng/mL. Validation of the data obtained by EIS was not performed because we were not aware of any method suitable for comparison at such low concentrations. This unique feature of the proposed devices could be a valuable tool for future epidemiological studies and for understanding changes in antibody levels associated with vaccination (as a recommendation for clinicians on when to recommend a new vaccine dose).

3.3.7 Alternative electrochemical analysis of human sera

Considering the good results obtained in testing positive human serum with the electrochemical biosensor, another proof-of-concept was explored by developing and using NPs as electrochemical markers bound to secondary antibodies. These secondary antibodies bind the anti-S protein antibodies recognised on the surface of the biosensor and generate an electrochemical signal. For this purpose, the secondary antibodies were labelled with CdTe QDs, which are nanoscale colloidal semiconductor crystals that have electrochemical properties (**Figure 3.3**) [222]. The electrochemical results of the QDs were investigated in terms of metal oxidation by

SWV, moving from -1.0 V to positive potentials. In a proof-of-concept study, different concentrations of anti-human IgG antibodies labelled with CdTe-QDs were tested to evaluate their effects on current measurements at the sensor surface (**Figure 3.11**). The most diluted and the most concentrated solutions of the IgG antibodies produced similar current values (1.60 µA and 1.63 µA, respectively). Therefore, considering the fluorescence values obtained for the different concentrations of QDs-labelled IgG antibodies, we decided to label the primary antibodies with the lower concentration of IgG antibodies (10.10 µg/mL), as this could be a more dispersed solution containing a higher ratio of CdTe-QDs nanocrystals for each IgG antibody (thereby amplifying the signal). In this approach, the biosensor was first incubated in a solution containing diluted positive serum (107, 150, 188, 250, or 752 ng/mL) and then in a solution containing anti-human IgG@QDs of 10.10 µg/mL. The SWV data obtained for these concentrations are shown in **Figure 3.11 D** and reflect the metal oxidation readings. The current signals decreased with increasing antibody concentration, yielding a linear trend when the peak height values were plotted against the log concentration of the antibody (150 ng/mL to 752 ng/mL). In principle, one would expect that a higher amount of anti-S antibody would lead to a higher number of IgG@QDs conjugates, which in turn should lead to a higher current value due to the higher amount of QDs. However, the system may undergo opposite effects during the incubation of the IgG@QDs conjugates. While the antibodies block the electrical surface and decrease the current signals, the current value of the observed peak increases with increasing number of QDs. Since this leads to opposite effects and the linear trend has a negative slope, it was obvious that the anti-IgG dominated the signal obtained. In any case, this proof-of-concept approach is an alternative way to read the electrochemical response if one wishes to obtain a more selective response. Alternatively, direct electrochemical measurements using the iron redox probe already outperform conventional methods such as VIDAS® in terms of LOD and sensitivity.

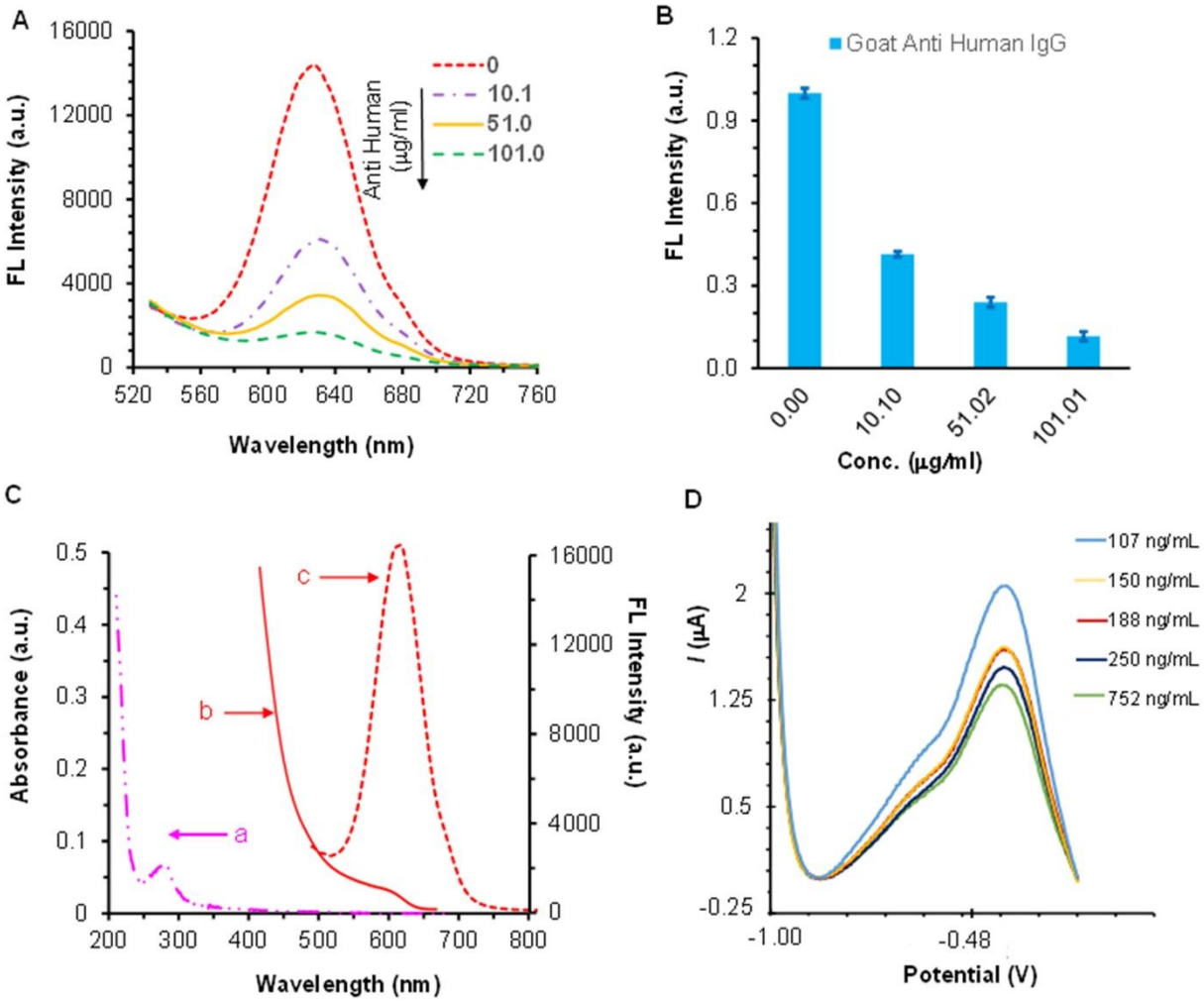

Figure 3.11: (A and B) Fluorescence signals of red emitting QDs in the presence of increasing concentrations of goat anti-human IgG, in PBS 0.01 mol/L pH 7.2. (C) UV–vis absorption spectra of goat anti-human IgG in PBS 0.01 mol/L pH 7.2 (a) and the UV/vis spectra of red emitting QDs 2.5 mg/mL in PBS 0.01 mol/L pH 7.2, (b) along with the correspondent fluorescent spectra (c). (D) SWV voltammograms of different concentrations of positive serum containing primary antibodies conjugated with a 10.10 ng/mL concentration of IgG secondary antibodies labelled with CdTe QDs.

3.4 Conclusions

A rapid serological test to diagnose and/or monitor immunity after SARS-CoV-2 infection or vaccination remains a challenge given current technologies. ELISA-based methods are not very sensitive and reliable quantitative information is scarce. Here we demonstrate the successful development of a simple, innovative, highly sensitive and selective biosensor for the detection of antibodies to the S protein in human serum. This novel electrochemical biosensor can be used post-infection or postvaccination when circulating antibody concentrations are lower and

cannot be detected by conventional ELISA methods. Its detection capabilities significantly outperform commercial methods available on the market and are comparable or better than other electrochemical methods described in the literature.

It is important to note that a cross-response of the biosensor against other SARS virus was not evaluated. However, a cross-reactivity with other antibodies against these means that one's serum has antibodies that also recognize S protein, meaning that there is an expected degree of protective immunity conferred by these. Thus, as the main target of the biosensor is to monitor the protective immunity by means of antibodies, an eventual cross-reactivity would not hamper the result of a test provided by this biosensor in POC. Overall, the biosensor provides very low LOD values and can reach very low concentrations of positive sera when testing human sera. Therefore, the biosensor described here has the potential to become a valuable tool for early diagnosis and monitoring of antibody levels during vaccination follow-up. Future work will therefore focus on miniaturization and the use of different nanomaterials as well as an environmentally friendly substrate, as paper. The development of multiplex biosensors covering a variety of different viruses is also foreseeable.

CHAPTER 4

Biographene as a sensing enhancer for electrochemical detection of SARS-CoV-2 spike antibodies

The results presented in this chapter to be submitted. Cardoso, A. R., Alves, J. F., Frasco, M., Fortunato, E., Barquinha, P., Sales, M. G., Biographene as a sensing enhancer for electrochemical detection of SARS-CoV-2 spike antibodies.

4.

BIOGRAPHENE AS A SENSING ENHANCER FOR ELECTROCHEMICAL DETECTION OF SARS-COV-2 SPIKE ANTIBODIES

4.1 Introduction

Graphene-based electrochemical biosensors enable sensitive and cost-effective detection of various biomolecules due to the excellent properties of graphene sheets, which are electrically conductive, have a large surface area and excellent dispersibility, and can be easily functionalized [241], [242]. Graphene can be produced by a variety of methods. Bottom-up strategies rely on the chemical arrangement of carbon atoms to form graphene layers, while top-down strategies use another material as a carbon source to obtain graphene. Mechanical exfoliation of graphite flakes is considered one of the simplest and least expensive methods [243]. These physical and chemical properties, combined with low production costs and reduced environmental impact, make graphene an extremely attractive material for biosensing applications. Moreover, to achieve better compatibility for immobilization of a biological receptor, graphene can be functionalized by covalent or non-covalent bonds with smaller molecules during the graphite exfoliation process. Recent works have already described the production of biographene in the presence of different proteins, which have been shown to facilitate the stabilization of graphene nanosheets after graphite exfoliation [244]–[246].

The daily life of the world population is still under the impact of the 2019 coronavirus pandemic (COVID-19) caused by the highly transmissible and infectious Severe Acute Respiratory Syndrome Coronavirus 2 (SARS-CoV-2) (Billah et al., 2020). COVID-19 is proving to be a highly contagious disease due to the large number of asymptomatic and mildly symptomatic patients, which favor direct and indirect airborne transmission of the pathogenic SARS-CoV-2 [247],

[248]. Similar to other coronaviruses, SARS-CoV-2 consists of four structural proteins: spike (S), membrane (M), envelope (E), and nucleocapsid (N), with the first three being part of the viral envelope and the last protein holding the single positive-stranded RNA genome [249]. Entry of SARS-CoV-2 into host cells occurs via the S protein, making it a useful target for recognition. The S protein consists of S1 and S2 subunits, which enable it to bind to a receptor on the surface of the host cell and fuse viral and host membranes, respectively [250], [251].

Rapid and accurate detection of SARS-CoV-2 proteins as antigens or serological tests to detect antibodies against the virus are critical to understand the biological and epidemiological processes associated with the disease. Virus detection is the most important method for direct diagnosis of infected patients and provides data for competent authorities to develop infection control plans. On the other hand, antibody detection can provide important evidence for the detection of earlier infections (indirect diagnosis) and active infections by complementing negative nucleic acid tests, prompting authorities to monitor the efficiency of the vaccination process, allowing the evaluation of the immune system's response to emerging variants, and assisting in the development of therapeutic antibodies [252]–[258].

All the data obtained by SARS-CoV-2 antibody detection could be massively and rapidly obtained by easy-to-use, accessible, and timely portable tests that are at the same time very accurate, specific, and sensitive [259]. Currently, antibody detection is mostly performed by conventional methods such ELISA or chemiluminescent immunoassay (CLIA), which are expensive and time-consuming. Therefore, lateral flow immunochromatographic assays are more promising detection methods for rapid on-site analysis [260], [261].These tests meet the need for simplicity, speed, and portability, but they only indicate qualitative results, i.e., the presence or absence of antibodies [259].

Due to their excellent ability to discriminate small signal variations, electrochemical biosensors are particularly suitable for quantitative detection of SARS-CoV-2 antibodies [262]–[264]. The material composition and electrode surface properties directly affect the performance of an electrochemical biosensor and determine its conductivity, sensitivity, immobilization capacity, and selectivity [21-23]. Modifying the electrode surface with carbon nanomaterials is a promising strategy to improve the analytical performance of a biosensor [265]–[269].Graphene, a widely used carbon material with the thickness of a single atom, has high mechanical strength, thermal stability (which may positively affect reproducibility), and good surface area (important for immobilization) while improving electron transfer at room temperature [270], [271].

In the present work, the S protein of SARS-CoV-2 is used both to prevent the restacking of graphene sheets obtained by graphite exfoliation by increasing its hydrophilicity and solubility

[272] and to create a biorecognition layer for the highly sensitive detection of antibodies. To the best of knowledge, there are no previous studies on the fabrication of biographene in the presence of S protein. Therefore, the green production of biographene containing SARS-CoV-2 S protein as a stabilizing and recognizing element is reported here (**Figure 4.1**). Considering the advantages of biocompatible graphene materials, the development of a simple and highly sensitive electrochemical biosensor based on the developed biographene was used to detect and quantify antibodies against the S1 subunit of the S protein, and its analytical performance was tested in buffer and serum. Therefore, this work can advance progress toward highly conductive green immobilization matrices and open the door for the development of devices that can readily contribute to epidemiological studies that provide the necessary understanding of the immune response to SARS-CoV-2 infection and vaccination to control the pandemic.

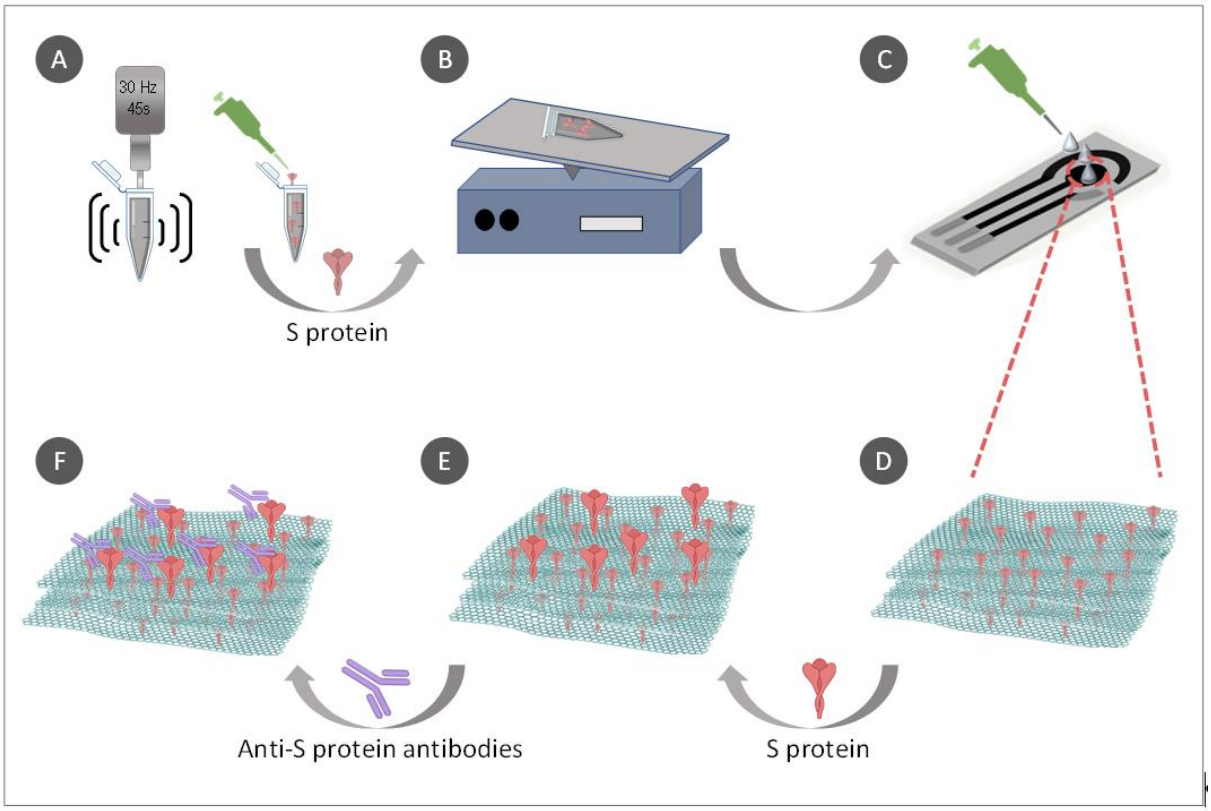

Figure 4.1: Schematic representation of biosensor construction: (A) ultrasonic exfoliation of graphite; (B) biofunctionalization of graphene sheets with spike (S) protein; (C, D) modification of the surface of the WE with the S protein biofunctionalized graphene; (E) addition of S protein as recognition element; (F) detection of antibodies to SARS-CoV-2.

4.2 Experimental Section

4.2.1 Apparatus

The exfoliation of graphite was performed in a VCX 750 ultrasonic processor (Sonics & Materials, Inc, USA) and the stabilization of the obtained graphene nanosheets with spike (S) protein was done in a MB-101 mixing block (Bioer, China). The main electrochemical experiments were performed on screen-printed carbon electrodes (C-SPEs) (DRP-110; Metrohm Dropsens, Spain) containing a WE and an auxiliary electrode made of carbon, and a silver RE. This three-electrode system was connected to a PalmSens4 potentiostat/galvanostat controlled by PSTrace v5.9 software (PalmSens BV, Netherlands). SEM images were collected on a FEI Quanta 400 FEG ESEM equipment.

4.2.2 Reagents and solutions

Potassium hexacyanoferrate (II) 3-hydrate ($K_4[Fe(CN)_6].3H_2O$) was acquired from Panreac and potassium ferricyanide (III) ($K_3[Fe(CN)_6]$) was obtained from Carlo Erba. Potassium chloride (KCl) and isopropanol (70%) were obtained from Fluka/Honeywell. PBS tablets, graphite, and dimethyl sulfoxide (DMSO) were purchased from Sigma-Aldrich. Nafion® (20 wt% in alcohols) was acquired from Quintech. Cormay Serum HN was acquired from PZ Cormay S.A. The recombinant SARS-CoV-2 S protein (S1 subunit derived from E. coli) and the polyclonal Rabbit anti-SARS-CoV-2 S1F antibody were procured from RayBiotech. All chemicals were of analytical grade and ultrapure laboratory grade water was used (conductivity < 0.1 µS/cm).

4.2.3 Production of biofunctionalized graphene

The process of mechanical exfoliation of graphite was performed in a high-energy ultrasonic probe at an amplitude of 30% for 45 s in a solution containing 1 mg of graphite flakes in 1 mL of ultrapure water and DMSO (ratio 2:8). Then, 10 µL of a Nafion® solution diluted in isopropanol (ratio 1:3) was added to better bind the graphene sheets during deposition on the electrode. To the obtained graphene, 2×10^{-6} mol/L of SARS-CoV-2 S protein was added and mixed in a mixing block without temperature for 2 h to obtain the S protein biofunctionalized graphene.

4.2.4 Electrochemical measurements and procedures

All electrochemical measurements were performed at room temperature. First, the surface of the WE was cleaned by an electrochemical CV treatment in which a potential of -1.0 V to +1.0 V was applied with a potential step of 0.01 V and a scan rate of 0.05 V/s in 0.1 M KCl diluted in ultrapure water. A 5 mmol/L ferri/ferrocyanide redox probe solution in 10 mL of PBS (0.01 mol/L, pH 7.4) was used as the electrolyte. EIS was performed in open circuit with a sinusoidal potential perturbation with an amplitude of 0.01 V and 50 data points logarithmically distributed over a frequency range of 0.1-100000 Hz. The SWV method parameters require a sampling potential of −0.3 to + 0.7 V, with a frequency of 2 Hz and a step height of up to 2.5 mV. The EIS and SWV determination of the KCl effect was performed by detecting changes in charge transfer resistance (Rct) and current values compared to the initial unmodified C-SPE, which is due to the ability of the metal halide salt to remove surface impurities and consequently improve electron transfer. Biographene was drop-casted (15 µL) on the WE of the cleaned C-SPE and oven dried at 40 °C for 150 min. Then, the surface of the WE was further incubated with 2×10^{-6} mol/L S protein prepared in PBS buffer at room temperature for 60 min. The electrochemical behavior of the biosensor after modification with graphene biofunctionalized with S protein and after the subsequent reinforcement with S protein were monitored by EIS and SWV. Stabilization of biosensors consisted of EIS readings after buffer incubations until Rct values remained unchanged.

4.2.5 Analytical performance

The analytical performance was first studied in PBS buffer (0.01 mol/L, pH 7.4). The biosensor was incubated in PBS at room temperature for 30 min until it stabilized. Then, the calibration curve was established by incubating the biosensor with increasing concentrations (1 pg/mL, 10 pg/mL, 100 pg/mL, 1 ng/mL, 10 ng/mL, 100 ng/mL) of SARS-CoV-2 S protein antibody prepared in PBS buffer, also at room temperature for 30 min. A similar calibration was tested in C-SPEs modified with nonfunctionalized graphene and with biographene without the additional S protein recognition layer. These served as controls to compare the electrochemical behavior under the different conditions. A more complex matrix was then tested, and the analytical performance of the biosensor was evaluated in 1000-fold diluted human serum. The biosensor was first stabilized with the diluted serum for 30 min at room temperature. Then, the increasing concentrations (1 pg/mL to 100 ng/mL) of SARS-CoV-2 S protein antibody prepared in diluted human serum were also incubated in the biosensor for 30 min at room temperature. Selectivity

assays were performed by testing the response of the biosensor to a solution containing a mixture of anti-S antibody and anti-nucleocapsid antibody, both at a concentration of 10 pg/mL in PBS buffer. Each condition was evaluated after incubation of the biosensor for 30 min at room temperature. All electrochemical measurements were based on EIS by determining the variations in Rct values.

4.3 Results and Discussion

4.3.1 Biosensor assembly and characterization

The assembly of the biosensor included an initial surface treatment with KCl to remove any impurities that might be present in the pristine C-SPEs. Then, ultrasonically exfoliated graphite biofunctionalized with SARS-CoV-2 S protein was drop-casted on the WE. To ensure higher antibody recognition capacity of the system, the amount of SARS-CoV-2 S protein was increased by subsequent addition of S protein on the surface of the WE. The electrochemical response to the different steps of biosensor assembly was monitored by EIS (**Figure 4.2A, Figure 4.2B)** and SWV (**Figure 4.2C**, **Figure 4.2D**).

The electrochemical cleaning procedure with KCl redox cycles resulted in a decrease in Rct values from about 1093 Ω to 419 Ω (**Figure 4.2B**) and an increase in the current from 34.73 µA in the pristine state to 56.09 µA observed by SWV measurements (**Figure 4.2D**). This procedure reduced the potential difference between the peaks of oxidation and reduction, enhancing the conductivity of the surface and decreasing variability between electrodes, which positively and directly affects the reproducibility of this work. The addition of the produced biographene has a double-edged effect, since graphene nanosheets have a very well described ability to increase conductivity in three-electrode systems [268], [269], while the presence of the S protein distributed between its sheets increases substantially the Rct from 419 Ω to 743 Ω (**Figure 4.2B**) and decreases de current from 56.09 µA to 30.77 µA (**Figure 4.2D**). The last phase of biosensor assembly consisted in reinforcing the immobilization of the S protein biorecognition element, with its binding being confirmed by the significant increase in the Rct to 1046 Ω (**Figure 4.2B**) and decrease in current to 18.39 µA (**Figure 4.2D**). The obtained results were expected due to the large recognition protein that hinders electron transfer on the modified surface of the WE.

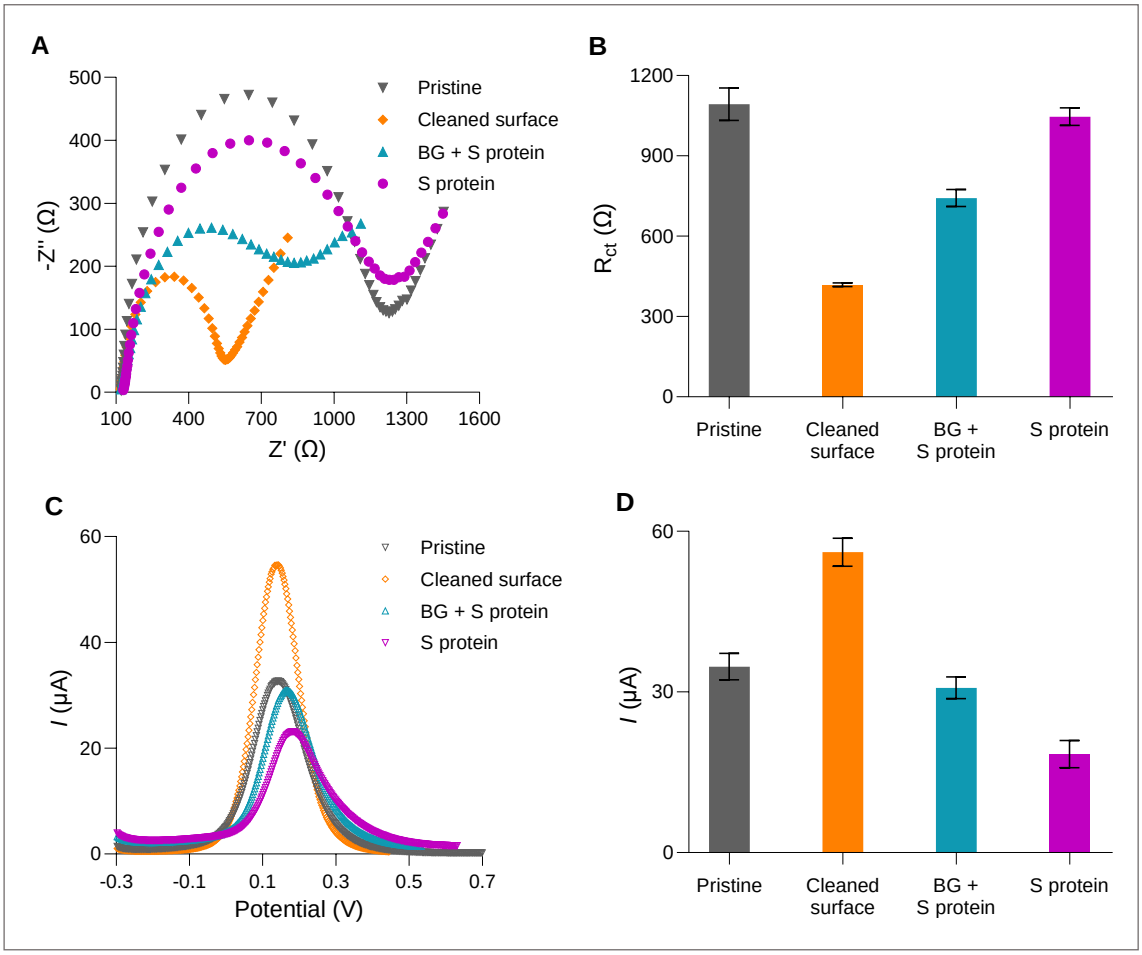

Figure 4.2: Electrochemical data collected during biosensor construction, using EIS (A) Nyquist plot and (B) Rct values, and SWV (C) graphs and (D) current peaks intensities. Data includes pristine C-SPEs, after cleaning, after modification with biographene functionalized with S protein, and after adding S protein as biorecognition element.

The electrode surface containing biofunctionalized graphene deposited was analyzed by SEM (**Figure 4.3**). The SEM images confirmed the presence of graphene sheets spread all over the surface. The presence of the protein was not confirmed by using this technique. The sheets are linked on the surface in a random way improving the overall surface area. This is consistent with the EIS data, considering the decreasing of the Rct when only graphene is added and the increasing the resistance caused by the protein.

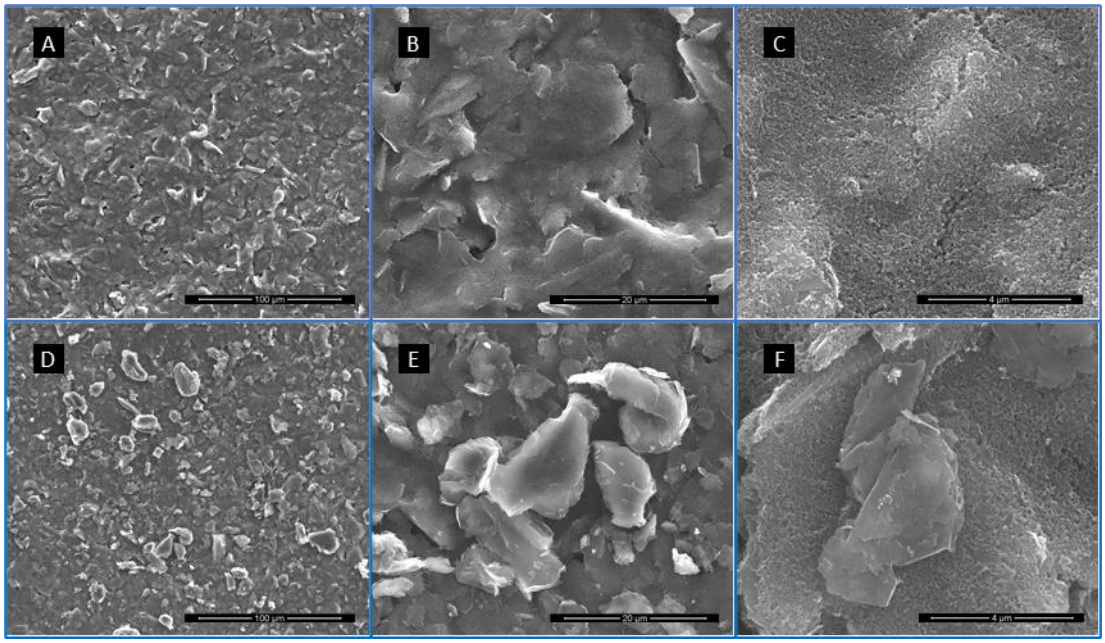

Figure 4.3: Analysis by SEM of the WE of pristine C-SPE (A – C) and of the WE after modification with the biofunctionalized graphene containing S protein (D – F).

4.3.2 Analytical performance of the biosensor

The biosensor responded to a range of increasing concentrations of SARS-CoV-2 S protein antibody diluted in PBS (1 pg/mL to 100 ng/mL), as shown in the Nyquist plots of the EIS measurements (**Figure 4.4A**). This response was evaluated in three replicates, and a linear trend was obtained from 1 pg/mL to 10 ng/mL. Rct values versus the logarithm of antibody concentration showed a slope of 158.07 Ω/decade and a squared correlation coefficient of 0.994 (**Figure 4.4B**). At the concentration of 100 ng/mL, saturation of the sensor saturation may explain the lack of response. The replicates were highly reproducible, with RSD values ranging from 4% (minimum) to 11% (maximum), and a LOD of 0.08 pg/mL was obtained.

To evaluate the response of the electrochemical biosensor in a more realistic situation, diluted human serum was used, which has a complex composition of potentially interfering species. Increasing concentrations (1 pg/mL to 100 ng/mL) of the SARS-CoV-2 S protein antibody diluted in human serum were tested, as shown in the Nyquist plots of the EIS measurements (**Figure 4.4C**). This calibration (three replicates) showed similar behavior to the results obtained in PBS buffer. Here, there was a linear trend for the Rct values against the anti-S protein antibody standards (up to 10 ng/mL) prepared in diluted human serum, with a slope of 242.83 Ω/decade and a squared correlation coefficient of 0.995 (**Figure 4.4D**), and LOD of 0.17 pg/mL. As expected, the LOD was higher in serum than in buffer due to the more complex serum matrix, which presents difficulties in detecting the biomolecule of interest.

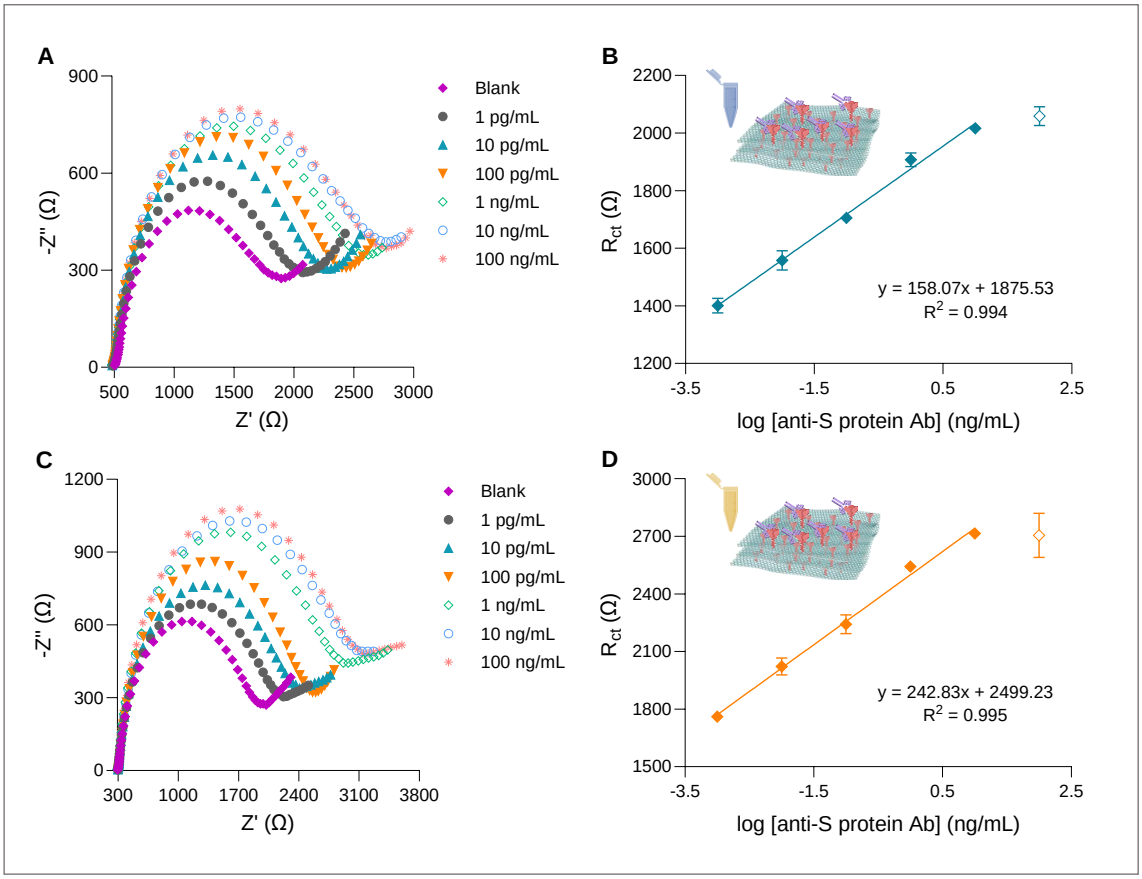

Figure 4.4: EIS measurements of the calibrations with anti-spike (S) protein antibodies (Ab) (1.0 pg/mL – 100 ng/mL), as shown in the Nyquist plots (A, C) and the corresponding calibration curves (B, D), obtained in PBS buffer (A, B) and in diluted human serum (C, D).

The aim of designing the biosensor with an additional S protein layer was to increase the sensitivity. This was confirmed by comparing the performance of the biosensor with C-SPEs prepared with graphene without biofunctionalization and with graphene with biofunctionalization but without the additional S protein layer under the same conditions. The C-SPE whose WE was modified with graphene without biofunctionalization did not show a linear response to increasing concentrations of SARS-CoV-2 S protein antibody diluted in PBS (1 pg/mL to 10 ng/mL) (**Figure 4.5A**, **Figure 4.5B**). Regarding the electrode modified with biographene, the response was linear in the same concentration range (1 pg/mL to 10 ng/mL) (**Figure 4.5C**, **Figure 4.5D**). However, the slope was much lower (68.19 Ω/decade) than the one obtained in the final biosensor when tested in PBS buffer (158.07 Ω/decade). These results suggest that the addition of S protein after biographene on the surface of the WE is a crucial step to guarantee a highly sensitive biosensor.

There are few reports of electrochemical biosensors based on C-SPEs whose surface was modified with carbon nanomaterials to detect anti-S protein antibodies. In one study, a functional

substrate was prepared by electrodeposition of graphene QDs and polyhydroxybutyric acid. The voltametric signal was followed and showed a correlation between 100 ng/mL and 10 µg/mL anti-S antibodies, and a LOD of 100 ng/mL was obtained [273]. In another approach, a carbon electrode was modified with reduced graphene oxide in combination with a specific binding peptide and a LOD of 0.77 µg/mL was determined [274]. Other carbon nanomaterials such as carboxylated SWCNTs have also been investigated for the development of electrochemical biosensors to detect antibodies against SARS-CoV-2 [266]The impedimetric properties of the biosensor followed by EIS displayed a linear response between 1 pg/mL and 10 ng/mL, with a LOD of approximately 0.7 pg/mL [266].Thus, among the studies that have used carbon nanomaterials, the current approach is a simple and straightforward approach, capable of generating accurate data by measuring very low concentrations of SARS-CoV-2 spike antibodies in complex samples, achieving even lower LOD than previous studies in the literature.

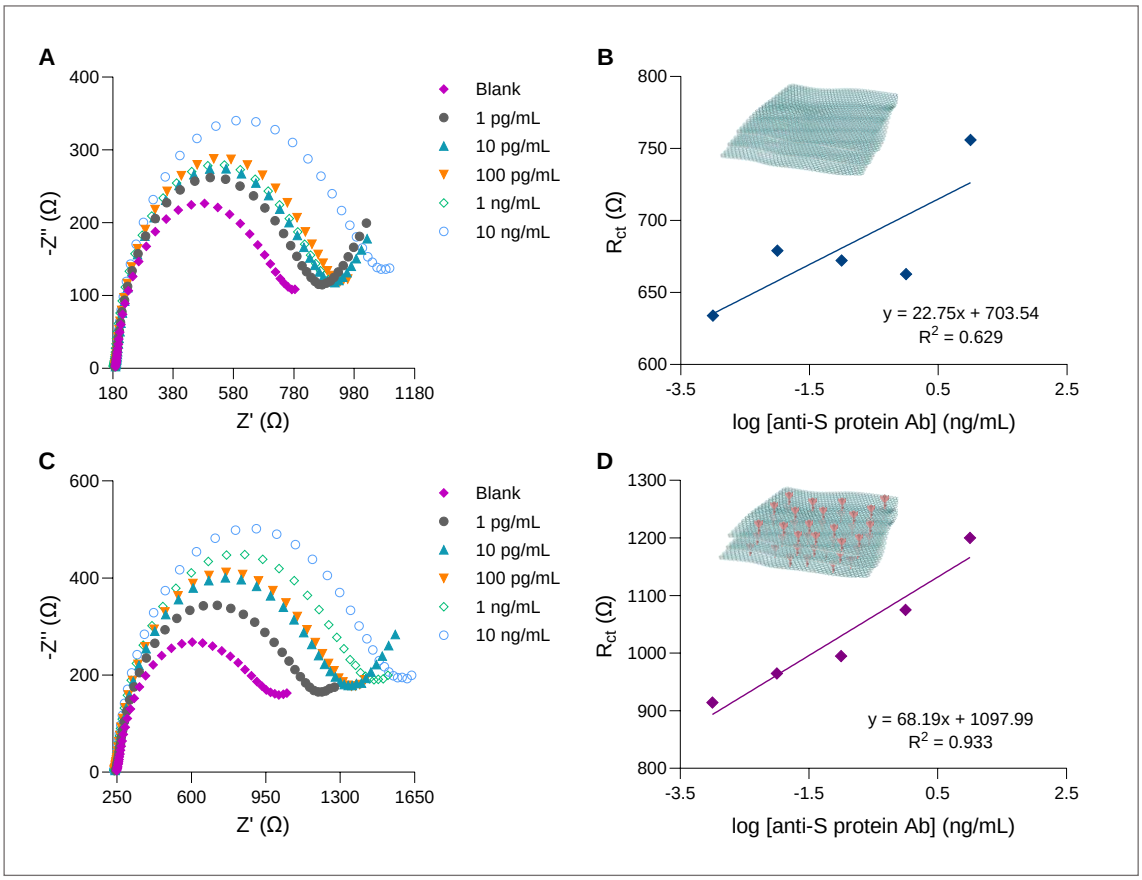

Figure 4.5: EIS analysis of the system with increasing concentrations of anti-spike (S) protein antibodies (Ab) (1.0 pg/mL – 10 ng/mL); (A, C) Nyquist plots and (B, D) Rct values; (A, B) correspond to the biosensor with graphene without biofunctionalization, and (C, D) correspond to graphene with biofunctionalization but without additional biorecognition layer of S protein.

4.3.3 Selectivity assays

To determine the ability of the biosensor to selectivity detect SARS-CoV-2 S protein antibodies in samples containing multiple compounds, it is necessary to evaluate its response to interfering species. SARS-CoV-2 nucleocapsid antibodies, which are commonly found in the serum of SARS-CoV-2 infected patients, were selected to study their effect on biosensor response. To attain this, a concentration (10 pg/mL) of SARS-CoV-2 nucleocapsid antibody and the same concentration of a solution containing a mixture of anti-S and anti-nucleocapsid antibodies were tested. **Figure 4.6A** shows the Nyquist plots of the carbon electrodes modified with biographene, evaluated under these conditions. The average percentage deviation upon the direct readings of anti-S protein antibody produced by anti-N protein antibody was -1.5 % (**Figure 4.6B**). Overall, these results confirmed that anti-N protein antibody had a negligible interfering effect upon the anti-S protein antibody response and that the device was selective in the presence of other antibodies.

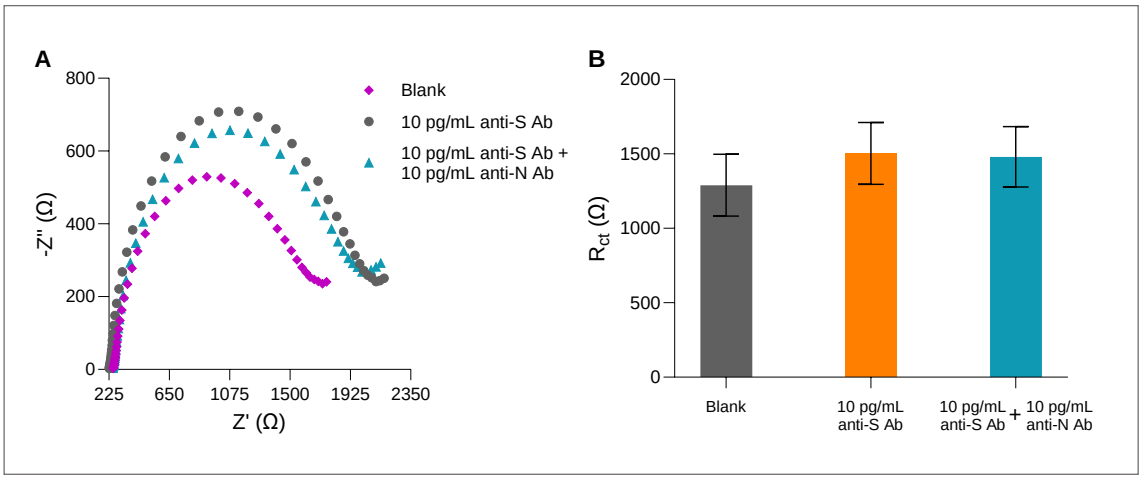

Figure 4.6: Selectivity behaviour of the biosensor for anti-spike (S) protein antibody (10 pg/mL) against anti-nucleocapsid (N) protein antibody (10 pg/mL**).**

4.3.4 Analytical Applications

As a proof-of-concept, the device was applied to the detection of anti-S protein antibody in a sample. The first stage of sample analysis was proceeded by a previous calibration in an independent sensor. As sample and standards should be well-tuned, the standard solutions were prepared in buffer. Comparing to the previous calibrations using standard solutions prepared in electrolyte, it was clear that the use of serum samples had no relevant impact on the biosensor response. Using the calibration curve in the buffer, the concentrations obtained from

spike samples in buffer yielded the errors ranging from 4% to 11% in different concentration levels.

4.4 Conclusions

An innovative, highly sensitive electrochemical biosensor for the detection of antibodies against SARS-CoV-2 was developed. In this work, a cost-effective technology based on mechanical exfoliation of graphite was presented to obtain graphene sheets in the presence of SARS-CoV-2 S protein, making this top-down biographene fabrication strategy simple, fast, and environmentally friendly. In most studies, the electrode surface is modified to improve the performance of the biosensor in terms of conductivity and the ability to immobilize the biorecognition element, thereby enhancing the sensitivity of detection. The presented strategy meets these requirements while being much more cost-effective than using other nanomaterials such as noble metals to modify the surface of the biosensor. Electrochemical characterization showed that the biographene modified electrode, on which an additional layer of S protein was also immobilized, provided the ideal conditions for monitoring the presence of anti-S protein antibodies, in both PBS buffer and diluted human serum samples. With this simple design, a low LOD could be achieved, and the selectivity results are very promising. Overall, the outcomes of the present study revealed an optimized green strategy to produce protein-assisted functional biographene substrates. In addition, the biosensor is easier to manufacture and manipulate than other diagnostic techniques and has the potential to scale its production in a simple and cost-effective manner to effectively control the spread of SARS-CoV-2 and can be adapted for other viruses.

CHAPTER 5

Dual monitoring of glucose by electrochemical and optical signals using a molecularly imprinted polymer with gold nanoparticles

The results presented in this chapter to be submitted. Cardoso, A. R., Frasco, M., Fortunato, E., Sales, M. G., Dual monitoring of glucose by electrochemical and optical signals using MIP with gold nanoparticles.

5.

DUAL MONITORING OF GLUCOSE BY ELECTROCHEMICAL AND OPTICAL SIGNALS USING A MOLECULARLY IMPRINTED POLYMER WITH GOLD NANOPARTICLES

5.1 Introduction

Diabetes Mellitus is a chronic metabolic disease that is a major public health problem and its impact on the global population is expected to increase over time [275]. It is estimated to affect up to 642 million people by 2040 [276]. Mostly, it is caused by the inability of the pancreas to contain the huge fluctuations in glucose levels in the blood, leading to many complications, such as retinopathy leading to blindness, nephropathy leading to kidney failure, peripheral nerve damage with an increased risk of extremity ulcers (foot), amputation, cardiovascular disease, or even cancer [46], [47]. To prevent these complications, blood glucose levels must be controlled, which requires regular/continuous monitoring of blood glucose levels [276]. Since this is a routine daily event, it is imperative that patients do this themselves with a low-cost, easy-to-use, and less invasive procedure.

To this end, a number of glucose biosensors have been developed [277] with the first electrode for monitoring glucose proposed by Clark and Lyons in 1962 [52]. These are mostly based on the selective oxidation of glucose by glucose oxidase to later detect the decrease of a reactant or the appearance of a (side) product (eq. 1). Whether in the form of continuous or discrete monitoring, invasive or non-invasive, the response of enzyme-based detection in common glucose meters used by patients is mainly through electrochemical measurements [56]. However, optical measurements have also been reported in the literature [278] since the first colorimetric

sensor was developed in 1965 [279], based on the detection of hydrogen peroxide formed during the oxidation of glucose by glucose oxidase (GOx).

$$Glucose + O_2 + H_2O \xrightarrow{GOx} \text{Gluconic acid} + H_2O_2 \quad \text{(eq. 1)}$$

Over time, enzyme-based glucose biosensors have become the most important glucose meters on the market and have gone through several generations: 1) the first generation, which uses oxygen as a co-substrate of glucose oxidase and also relies on the formation and release of H_2O_2; 2) the second generation, which replaces oxygen with redox mediators that transfer electrons from the enzymatic reaction; 3) and the third generation, which involves direct transfer of electrons between the enzyme and electrode in the absence of the mediator [280].

However, biosensors based on enzymes have specific drawbacks related to changes in their activity under different conditions, such as temperature, pH, storage, and specific inhibitors [58]. Enzyme-free biosensors can improve reliability by eliminating drift caused by enzymatic degradation [61] These include several studies that use metal catalysts such as Au, Pt, Cu, Ni, or single polycrystalline metals (Au, Pt, and boron-doped diamond) in solution or in the form of NPs [60], also called as nanozymes. Nevertheless, these sensors using only non-biological catalytic materials have the ability to co-oxidise compounds such as ascorbic acid (AA) and uric acid (UA) in addition to glucose [62].

An important approach to mitigate the limitations of enzymes is to combine MIPs [63] with enzyme-free catalytic approaches as nanozymes. The MIP materials provide selectivity for the final analysis by being able to selectively concentrate glucose on the surface of the electrode, while the enzyme-free catalytic approaches provide a sensitive improvement in the analytical response obtained. This sensitivity gain can be even greater if conductive polymers are used to produce the MIP materials when an electrical reading is retrieved from the sensing system. The use of Au NPs to this end offers the additional advantages of advantages like good biocompatibility and unique photoelectron performance [281].

There are several approaches using MIP materials for glucose sensing, some of which include metal nanoparticles as catalytic elements (**Table 5.1**). However, none of these approaches describes the in-situ growth of gold nanoparticles (Au NPs). An additional and very important result of this approach is the possibility of obtaining a dual detection, electrochemical and optical, at the same site, which has never been described before (to our knowledge). This contributes to the accuracy of the measurements. Au NPs formed in situ generate a more ordered distribution of nanoparticles, which allows interrogation of optical measurements in the form of reflection. This in situ generation of Au NPs also provides higher efficiency of the catalytic

process and, due to the straightforward approach, is faster and less expensive, requiring fewer reagents (a few litres) and less time (seconds to a few minutes).

This work describes the preparation of a MIP material for glucose obtained by in situ electropolymerization of pyrrole. This is done on a carbon support of screen-printed electrodes containing Au NPs prepared in situ by suitable reduction of gold salt. The conditions for performing these electrochemical processes were optimized with respect to the presence or not of Au NPs on the electrode surface at the Py-COOH-MIP production. The best device was characterized in terms of its analytical properties, followed by its application in the analysis of human serum.

Table 5.1: List of the sensors for glucose detection using MIP-based sensing systems, along with their main analytical features.

Electrochemical Method	Functional Monomer/ Cross-link	Nanomaterial/Substrate	Linear Range	LOD	Surface Characterization	Cross- Reactivity testing	Ref.
CV	VPBA, MBA	ITO Electrode	Up to 900mg/dl	—	XPS	—	[282]
CV	Silicon Oil on a copper wire	PVA electrodes by MnO_2/CuO on GO NPs	0.5 to 4.4mM	53µM	XRD; FTIR; SEM; EDX;	—	[283]
CV; EIS	MAA, MBA, 4-VP	Porous Ni foam	10 to 55mM	—	Raman; SEM;	DA, FRU, Glucose, AA, AP	[284]
LSV; Chrono-AMP	Nafion, APBA, Polyurethane	CuCo bimetal-coated on SPCE	1.0 µM to 25.0 mM	0.65µM	FE-SEM; EDXS; XRD;	MAN, LAC, UA, AP, DA, AA, Cysteine, GAL, FRU; XYL; SUC, LAA; MAL	[285]
ChronAMP	VPBA, PBA	FET	100 µM to 4 mM	3.0 µM	FTIR; XPS	FRU; SUC	[286]
CV, DPV, EIS	AAM, NNMBA	Au-SPE	0.5 to 50 µg/mL	0.59µg/mL	AFM; SEM-EDS	LAC, SUC	[287]
CV, EIS	AAM	Porous Ni foam	0.8 to 4.0 mM	0.45 mM	SEM; XRD	AA; FRU; AP	[193]
CV, EIS, SWV, UV-Vis	o-PD, Scopoletin	Au NPs	1.25 nM to 2.56 µM	1.25nM	AFM; SEM; QCM; TEM	SUC, DA; starch, BSA	[288]
CV, EIS	pTBA	Au NPs/C-SPE	0.32µM to 1.0 mM	0.19µM	AFM; XPS; QCM	GAL; DA; MAL; FRU, LAC, MAN, XYL; RIB, AP; UA; SUC; AA	[189]
UV-Vis	APBA	Au NPs	2.4 to 30.2 mM	—	TEM; SEM	CHOL, UA	[189]

CV: Cyclic Voltammetry; **VPBA**: 4-vinylphenylboronic acid; **MBA**: Methylene bisacrylamide; **ITO**: Indium Tin Oxide; **XPS**: X-ray Photoelectron Spectroscopy; **PVA**: Polyvinyl acetate; **GO**: Graphene oxide; **FTIR:** Fourier-Transform Infrared Spectroscopy; **SEM**: Scanning Electron Microscopy; **EDX:** Energy-dispersive X-ray spectroscopy; **XRD**: X-Ray Diffraction; **MAA**: Methacrylic acid; MBA - N,N'-Methylene bisacrylamide; **4-VP:** 4-vinyl pyridine; **EIS**: Electrochemical Impedance Spectroscopy; **DA**: Dopamine; **AA:** Ascorbic acid; AP: Acetamidophenol; **APBA**: Aminophenyl Boronic Acid; **UA:** Uric Acid; **FE-SEM**: Field Emission Scanning Electron Microscope; **EDXS**: Energy-dispersive X-ray spectroscopy; **LSV**: Linear Sweep Voltammetry; **DPSV**: Differential Pulse Stripping Voltammetry; **TEM**: Transmission Electron Microscopy; **AFM**: Atomic Force Microscope; **Au NPs**: Gold Nanoparticles; **Au-SPE**: Gold-Screen Printed Electrode; **AAM/NNMBA**: Acrylamide/Bis-Acrylamide; C-SPE: Carbon Screen Printed Electrode; **pTBA**: Benzoic acid-functionalized poly(terthiophene); **GAL**: Galactose; **QCM**: Quartz Crystal Microbalance; **BSA**: Bovine Serum Albumin; **SWV**: Square Wave Voltammetry ; ***o*-PD**: Ortho-phenylenediamine; **FET**: Field-effect transístor; **FRU**: Fructose; **CHOL**: Cholesterol; **NPs**: Nanoparticles; **PBA**: Phenylboronic acid; **Py**: Pyrrole; **DPV**: Differential Pulse Voltammetry; **G**: Graphene; **PSS**: Poly (styrene sulfonate); **TMB**: Tetramethylbenzidine; **EGDMA**: Ethylene glycol dimethacrylate;; **MAN:** Mannose; **LAC**: Lactose; **SUC:** Sucrose; **MAL**: Maltose; **RIB**: ribose; XYL: Xylose; **ChronAMP:** Chronoamperometry.

5.2 Experimental Section

5.2.1 Reagents and Solutions

High purity Milli-Q laboratory grade water (conductivity <0.1μS/cm) was used in this work. Chemical reagents used include Potassium hexacyanoferrate (II) 3-hydrate ($K_4[Fe(CN)_6].3H2O$) was acquired from Panreac and potassium ferricyanide (III) ($K_3[Fe(CN)_6]$) was obtained from Carlo Erba; Phosphate buffer salt solution (PBS), purchased from Riedel-de Haeen; pyrrole (Py) and pyrrole-2-carboxylic acid 99% (Py-COOH), purchased from Alfa Aesar; tetrachloroauric acid ($HAuCl_4.H_2O$), sulfuric acid (H_2SO_4) and glucose, purchased from Sigma Aldrich and urea, purchased from Sigma Aldrich.

All solutions were prepared in ultrapure water. 0.05 M H_2SO_4 was used to electrochemical cleaning of the carbon devices. A 0.1 mg/mL $HAuCl_4$ solution was prepared in ultrapure water. The MIP solution contained 1.0×10^{-3} M of Glucose, 1.0×10^{-3} M of Pyrrol-2-Carboxylic acid (Py-COOH) and 1.0×10^{-3} M Pyrrol (Py) prepared in 0.10M PBS (pH 7.4). The NIP solution contained 1.0×10^{-3} M Py-COOH and 1.0×10^{-3} M of Pyrrole prepared in 0.10M PBS (pH 7.4). The standard solutions of glucose were prepared in 0.10 M PBS (pH 7.4). The changes in the electrical properties other electrode were followed with a solution of 5.0×10^{-3} M $K_3[Fe(CN)_6]$ and 5.0×10^{-3}M $K_4[Fe(CN)_6]$) prepared in 0.10 M PBS.

5.2.2 Apparatus

Electrochemical measurements were performed using a PalmSense4 potentiostat/galvanostat controlled by PSTrace 5.3 software. All electrochemical assays were made in triplicate. C-SPE were purchased from Metrohm/DropSense. All devices were connected in a switch box from PalmSense to perform electrochemical assays. Optical assays were performed using a potentiostat/galvanostat from Metrohm. Optical assays were performed with a reflection fibre probe (fibre diameter of 200 μm, Dropsens), using a deuterium-halogen light source connected to a spectrophotometer (wavelength range of 200–1100 nm, Metrohm, AG). As a reference surface, a diffuse reflectance standard was used, and reflectance was collected at normal incidence. The size and morphology of Au NP nanoparticles were studied by SEM on FEI Quanta 400FEG ESEM/EDAX PEGASUS X4M instruments.

5.2.3 Assembly of the glucose sensor material

Figure 5.1 shows a schematic representation of the glucose biosensor on the carbon working electrode of the C-SPEs. The setup was performed in several steps: (**A**) WE was cleaned by electrochemical treatment (0.05M H_2SO_4), scanning between -0.10V and 1.50V during 5 cycles at a scan rate of 0.05V/s; (**B**) electrochemical fabrication of Au NPs by chronoamperometry at -1.5V for 600s; (**C**) preparation of MIP layer by bulk imprinting in a solution containing glucose, Py and Py-COOH in PBS solution (the NIP only contained Py and Py-COOH in PBS) by CV in the potential range between -0.20V and +0.85V (vs. Ag/AgCl) at a scan rate of 0.10 V/s; (**D**) removal of template, incubation in WE with ultrapure water during 1h. Each modification was followed by electrochemical and optical techniques.

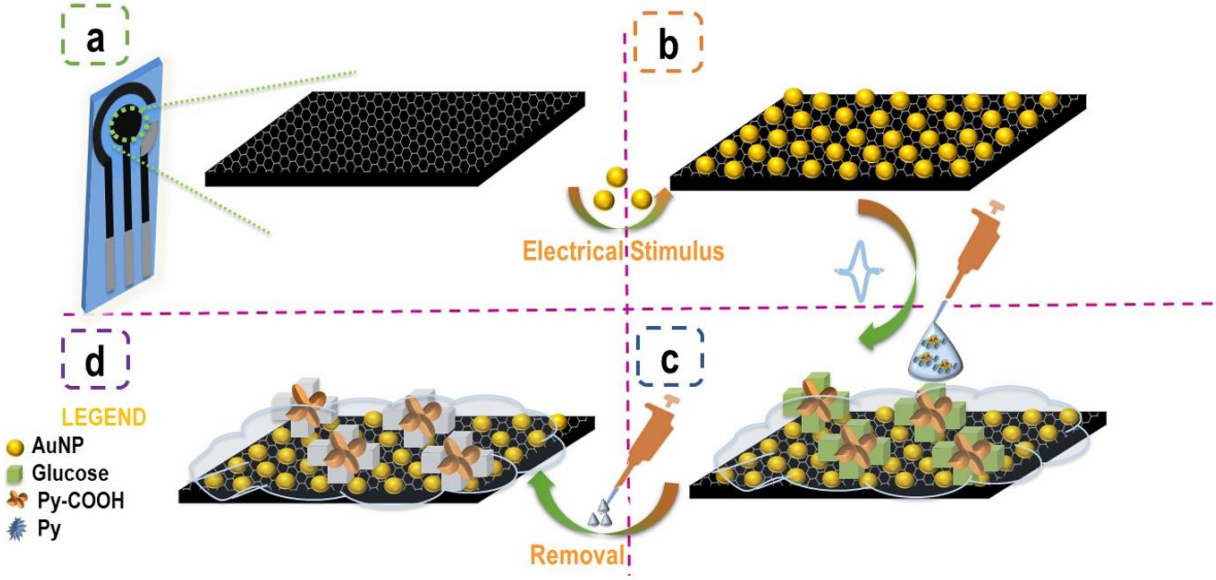

Figure 5.1: Schematic representation of the MIP sensor for glucose detection and different modifications on the working electrode. (A) After Cleaning the surface; (B) Electrodeposition of Au NP; (C) Electropolymerization of MIP sensing layer; (D) Removal of the glucose with water.

5.2.4 Electrochemical Procedures

CV was performed by scanning potentials from -0.3 to +0.7 V at a scan rate of 50 mV/s. EIS measurements were performed using an open-circuit sinusoidal potential perturbation with an amplitude of 0.01 V and 50 data points distributed logarithmically over a frequency range of 10-0.01 Hz. The EIS data were fitted to a Randles equivalent circuit using PalmSens software and analysed using Nyquist plots showing the frequency response of the electrode-electrolyte system and the area plot of the imaginary component (Z'') of the impedance versus the real component (Z'). The diameter of the semicircle obtained in the EIS was considered as the

charge transfer resistance (Rct) [289]. SWV was also used to track the modifications of the MIP assembly by scanning from -0.3 to +0.7 V at a scan rate of 20 mV/s. SWV is a fast and sensitive approach compared to the previous tests and provides large currents, thus increasing the accuracy [290].

Electrochemical measurements of the novel glucose-MIP film were followed by CV, EIS, and SWV measurements using a redox probe solution of 5.0×10^{-3} M $[Fe(CN)_6]^{3-}$ and 5.0×10^{-3} M $[Fe(CN)_6]^{4-}$ in 0.01M PBS (pH 7.4). Calibration curves were followed by EIS with standard solutions of glucose in 0.01M PBS (pH 7.4) ranging from 1×10^{-6} to 1×10^{-3} M. Direct measurements of glucose were made by chronoamperometry at 0.2V/s for 100s for each standard solution. The LOD was calculated as $x+3\sigma$, where x is the average value of EIS blank signals (obtained in the absence of glucose) and σ is the known standard deviation of consecutive EIS blank signal measurements [229].

Selectivity studies used a MIP technology for glucose and various analytes that may be present in serum samples. In these experiments, three independent devices was tested with AA. Direct electrochemical measurements were evaluated to achieve analytical performance with the same concentration range as direct detection of glucose.

5.2.5 Direct Detection for Glucose

All amperometric measurements were performed at room temperature with constant stirring. Increasing concentrations of glucose were obtained by adding 5 to 1500 µL of an aqueous solution of 0.1 mol/L glucose to a 10 mL beaker containing 5 mL of 1.0×10^{-2} mol/L of a suitable buffer of fixed pH and ionic strength. The potentials of the stirred glucose solutions were measured at room temperature by chronoamperometry at +0.2 V for 100 s for each standard solution.

5.3 Results and Discussion

Prior to the preparation of Au NPs on the carbon electrode, the C-SPEs were pre-treated by electrochemical cleaning with H_2SO_4. This pre-treatment step had several advantages, such as reducing electrode variability, increasing the reproducibility of different electrodes from the same commercial batch, and increasing the reproducibility of the resulting biosensors. Before proceeding with each electrode, the stability was confirmed by consecutive incubation and reading of buffer, until a stable signal was achieved.

5.3.1 Production and impact of Au NPs

While there are several chemical methods for producing Au NP that can control size and shape, electrochemical techniques may offer here some advantages [291]. The main advantages include ease of anchoring to the surface, speed, and the fact that no chemical or binding agents are required [292].In addition, the volume of solutions used for electrochemical fabrication of Au NPs is very small, which means that the waste of reagents is low. Therefore, these Au NPs are more environmentally friendly than those produced by chemical techniques. The in-situ electrochemical growth also allows a more homogeneous distribution of the particles on the surface of the electrode.

Au NPs were prepared using a solution of tetrachloric acid in ultrapure water poured onto the 3-electrode system (using stirring and the use of nitrogen improved the reproducibility) by subjecting the working electrode to a constant potential for several minutes. The Au NPs formed in this way were visible to the naked eye as the surface of the working electrode glowed golden (**Figure 5.2 a**, left). The electrochemical data confirmed this by changing the spectra of the original electrode by decreasing the Rct or increasing the current of the standard iron redox probe (**Figure 5.2 b-c,d**). In terms of sensitivity, EIS was the most sensitive method to confirm the presence of gold. The Rct was ~77 times lower than the original value, while the current increase of SWV was ~2 times and the increase of CV currents of oxidation and reduction peaks was ~1 and 1 times, respectively.

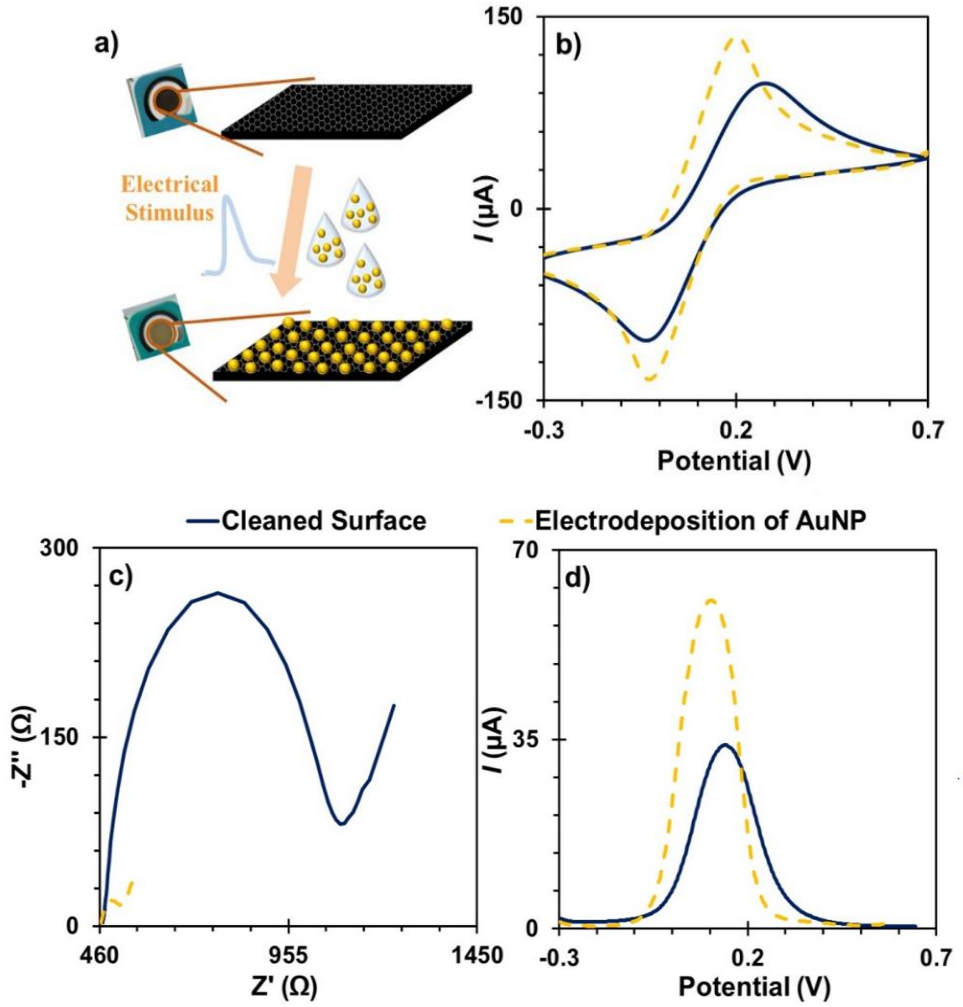

Figure 5.2: Electrochemical data after cleaning and after electrodeposition of Au NPs (a), using CV(b), EIS (c) and SWV (d).

SEM analyses were performed to characterise Au NPs prepared for different deposition times: 100s (**Figure 5.3 B**), 300 (**Figure 5.3 C**), 600s (**Figure 5.3 D**). These were compared to a control, which was the carbon electrode before gold deposition (**Figure 5.3 A**). The Au NPs were identified by the bright spots on the images (which reflected more electrons than the carbon background). These bright spots were not present in the control sample, confirming that they signal the presence of Au NPs (**Figure 5.3 A1, B1, C1, D1**). The number of Au NPs on the surface of the electrode increased with the duration of electrodeposition, as more time was available for nanoparticle production. The nanoparticles were homogeneously distributed on the electrode surface and exhibited small, almost hemispherical Au NPs. Overall, the best condition was the one produced after 600s electrodeposition, since the electrical gains obtained during the electrochemical reaction were relevant.

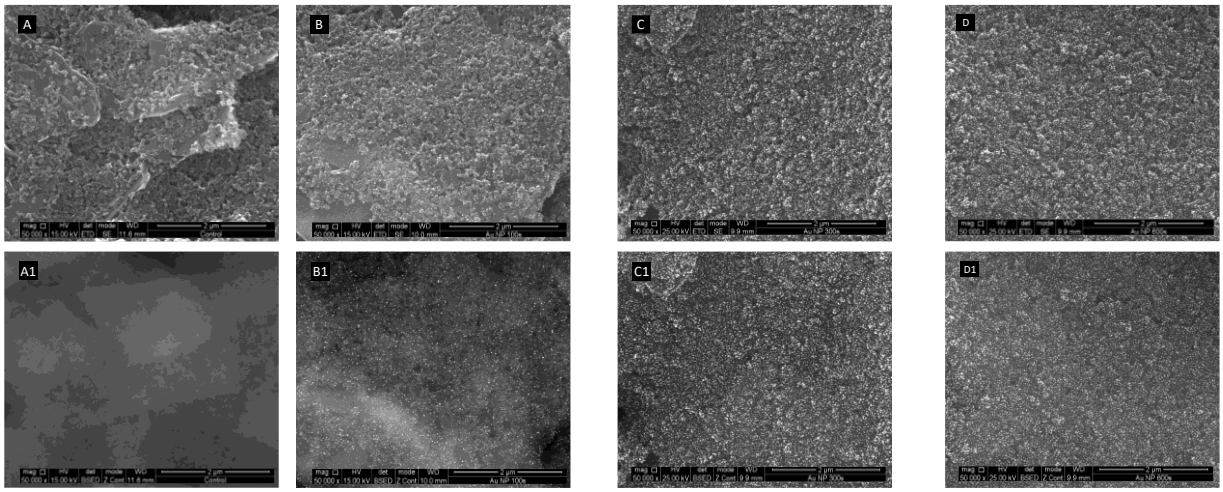

Figure 5.3: SEM images of the C-SPEs having Au NPs generated in situ by means of different electrodeposition times (A) Control (B)100s; (C) 300; (D) 600s; and (A1, B1, C1; D1) SEM figures with Backscattered electrons (BSEs).

Thus, the electrochemical behaviour of individual glucose solutions from -1.0V to 1.0V, in PBS medium, on electrodes with and without Au NPs, was evaluated by CV assays and shown in **Figure 5.4**. Overall, it was clear that glucose was not oxidised when the scan was performed from -1.0 to +1.0 V on carbon electrodes, but an oxidative current was detected after +0.85 V when the carbon electrodes contained Au NPs, indicating that glucose was oxidised in the presence of the Au NPs under milder conditions. Moreover, the current values increased more than 5-fold when the Au NPs were present.

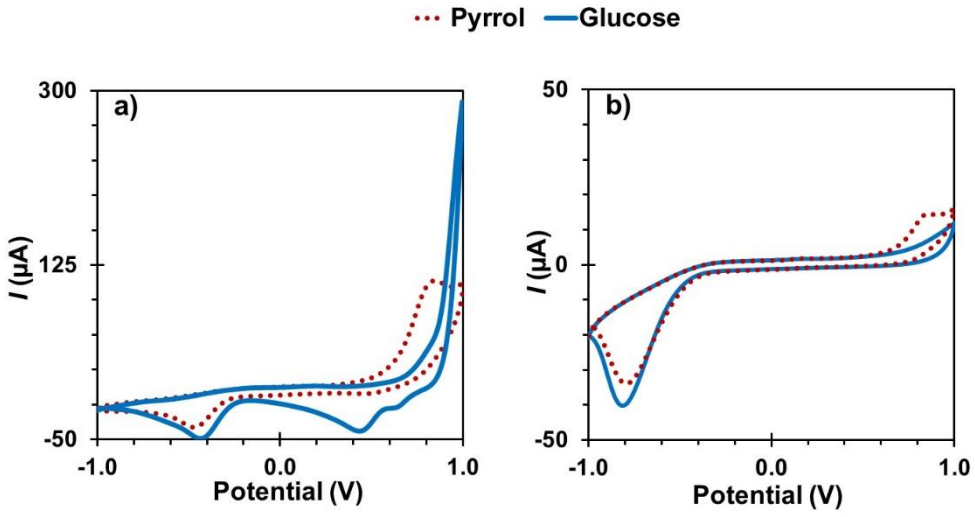

Figure 5.4: Voltammograms of Py and glucose solutions prepared in PBS with (a) and with (b) without Au NPs.

5.3.2 Fabrication of the sensing layer

The MIP production started by selecting the electrochemical conditions that ensured the formation of a suitable polymeric layer using Py and Py-COOH. Py was the main monomer used

to assemble the polymeric network, displaying excellent electrical properties, displaying good conductivity [293], [294]. In addition, poly(Py) has good biocompatibility which is well tuned with the production of MIPs for biological molecules [295], [296]. Moreover, literature data confirms that Poly(Py) has been produced on surfaces containing noble metals, like gold [297]. When present, Py-COOH is added in a smaller amount, together with glucose to form a stable complex, aiming to improve glucose binding by means of hydrogen bridges between glucose and the carboxyl group. This is expected to increase sensitivity and selectivity, as observed before in an approach called SPAM[298]. In terms of polymerization approach, "bulk" imprinting was used by mixing all components and undergoing polymerization at the electrode surface. This is a simple and effective procedure for a small molecule as glucose.

This study was done with electrodes having or not Au NPs, produced as described before, to monitor accurately the impact of these nanoparticles upon the glucose detection by MIP binding (**Figure 5.5**). Accordingly, the potential required to promote the oxidation of Py (and therefore create conditions for the formation of a polymeric network) was lower when Au NPs were present **Figure 5.4**. Still, the potential selected for polymerization of Py in the presence of glucose had to ensure that glucose was not oxidized at the same time, or else it would be irreversibly entrapped in the polymeric network and the imprinting would be technically impossible because glucose would no longer exist (as it would be partially in the form of gluconic acid. The potential range used to produce the polymer was of -0.2V to +0.85V, and this was repeated for 5 cycles, when Au NPs were present. In the absence of Au NPs, the CV was scanned from -0.2 to +0.93 V, for 5 cycles. The effect of the presence of Py-COOH in the polymerization process was also analysed by checking the response with and without this monomer, having the polymerization conducted under the same conditions (as Py, having or not Au NPs). To this end, Py-COOH was mixed with glucose for 2h to allow hydrogen bound formation between glucose and the carboxylate group.

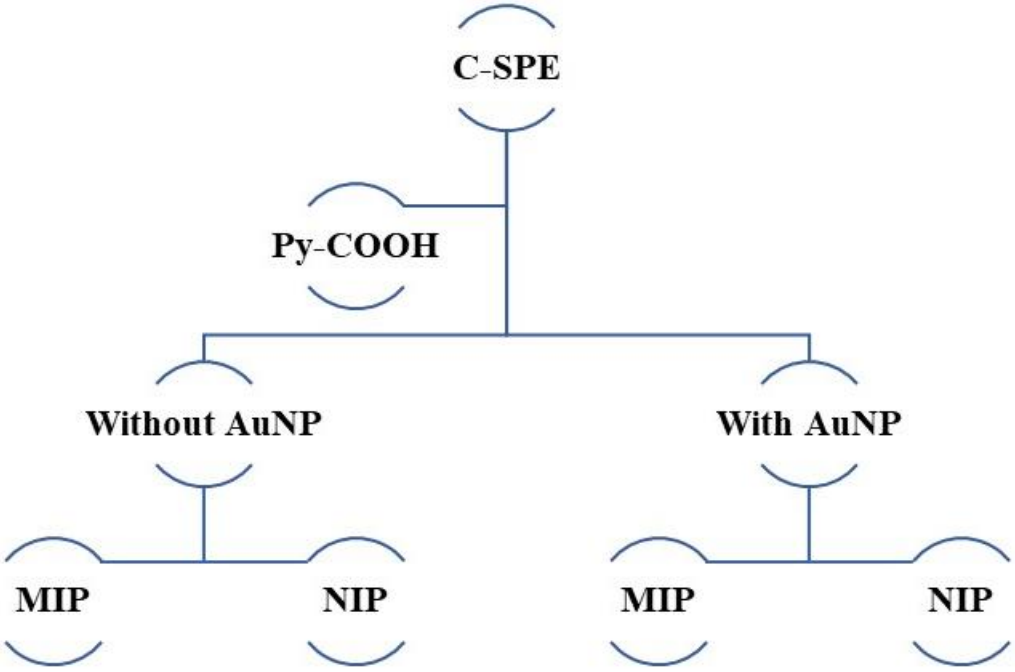

Figure 5.5: Schematic representation the several optimizations.

The final step in all strategies involved removing the template from polymeric film. This was made by incubating ultrapure water in working electrode at 1h, ensuring that glucose would display high solubility on it. In general, each modification on surface was followed with three electrochemical CV, EIS, and SWV features in two MIPs and NIP (with and without gold nano-particles) are compared, also was analyse the analytical performance for both strategies and chose the best condition.

The resulting CV, EIS and SWV data is shown in Figure S5 of C-SPEs/MIP-Py-COOH and C-SPEs/NIP-Py-COOH films without Au NPs. Overall, the CV (**Figure 5.6 a1** and **a2**) profiles given by the iron redox probe of the polymeric film (MIP or NIP) confirmed the presence of a highly blocked surface. The redox peaks of the iron probe at the SPEs had a higher decreasing and higher separation of peak-to-peak potential separation, after growing the polymeric layer. The results in EIS (**Figure 5.6 b1** and **b2**) and SWV (**Figure 5.6 c1** and **c2**) were consistent with these observations.

Comparing MIP and NIP, the Rct increased more evidently in the MIP film. However, in the other electrochemical techniques, CV (**Figure 5.6 a**) and SWV (**Figure 5.6 c**) showed a slightly difference between them. Also, after the removal the template from the polymeric layer. In general, comparing the electrochemical CV, EIS and SWV features of MIPs (**Figure 5.6 - 1**) and NIPs (**Figure 5.6- 2**) before and after glucose removal, presented in NIPs films, has a significantly changes were observed before and after ultrapure water action, also in the MIP material had

higher modification, especially in EIS, decreasing the Rct value. Overall, these results confirmed the ineffective removal of glucose from the MIP films and the instability of the PolyPyrrol film when exposed to ultrapure water incubation. After the assembly of MIP and NIP devices was tested the analytical performance incubating on working electrode, several glucose standard solutions of increasing concentrations by following the EIS electrical features of a standard iron redox probe after each incubation.

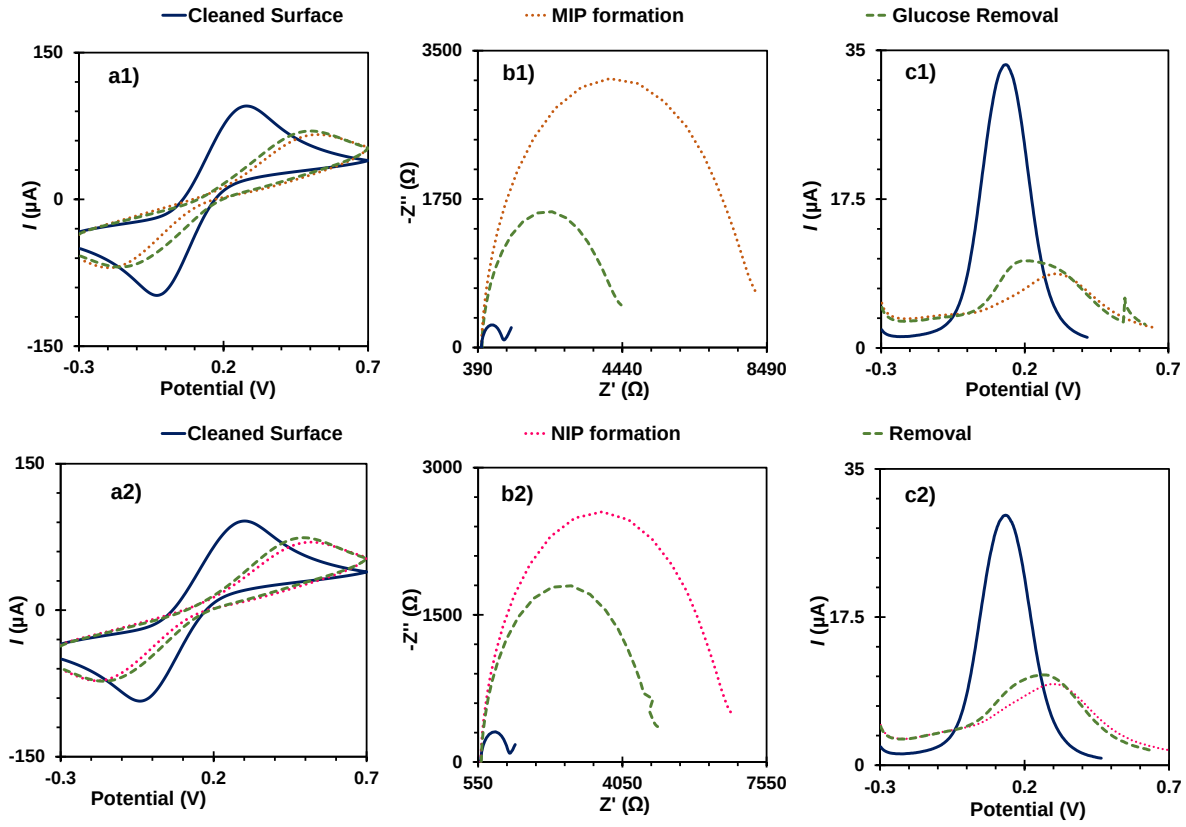

Figure 5.6: Electrochemical measurements of CV (a), EIS (b) and SWV (c) in $5.0x10^{-3}$ M $[Fe(CN)_6]^{3-}$ and $5.0x10^{-3}$ M $[Fe(CN)_6]^{4-}$ solution, prepared in PBS, of the NIP (1) and MIP (2) films (without Au NPs/MIP-Py-COOH), at the several steps of the biosensor assembly.

For this purpose, a drop of glucose standard solution was incubated stand there for a 30-minute rebinding period. The **Figure 5.7** represented the random behaviour on MIP (**Figure 5.7 a**) and NIP (**Figure 5.7 b**) when increasing the concentrations of glucose. The **Figure 5.7 c** and **d** corresponding the calibration curves and showed as well the random and not response to the sensors of Rct against logarithm (glucose concentration).

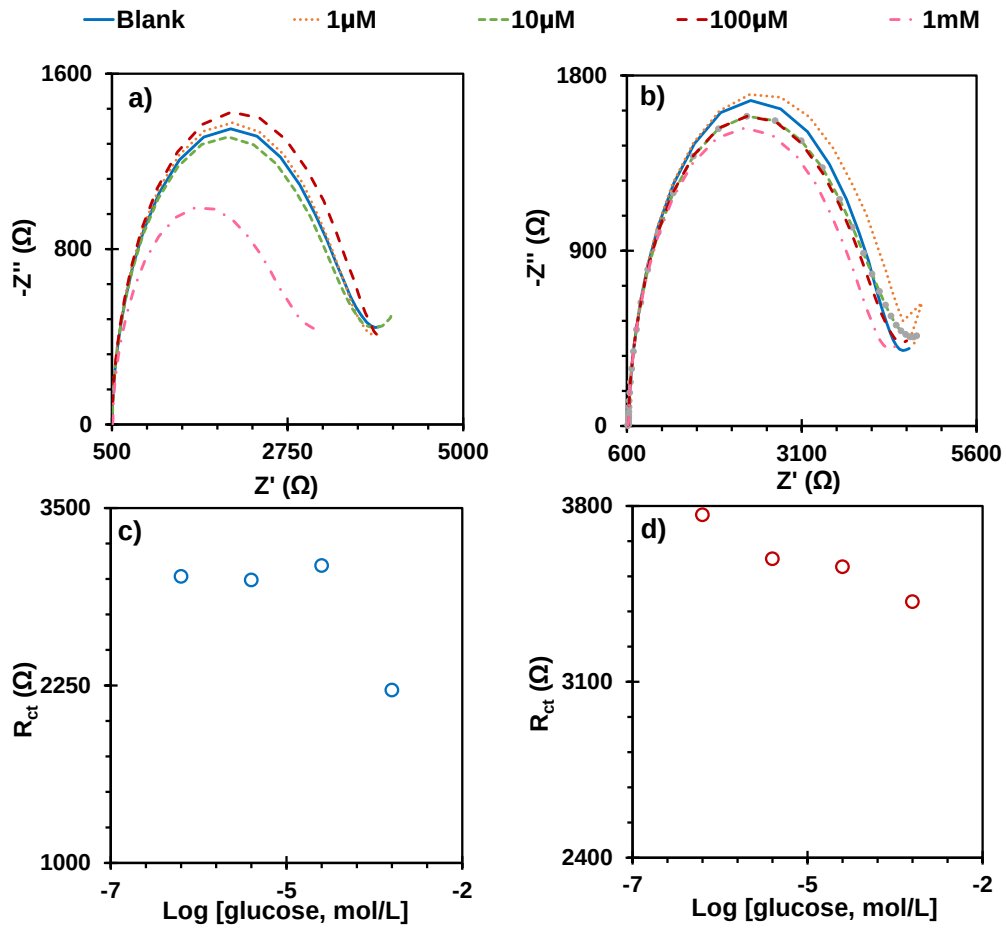

Figure 5.7: Nyquist plots of (a) MIP and (b) in NIP sensors (C-SPEs/without Au NPs/MIP-Py-COOH) in 5.0x10^{-3} M $[Fe(CN)_6]^{3-}$ and 5.0x10^{-3} M $[Fe(CN)_6]^{4-}$, after incubation in standard solutions of glucose of increasing concentrations, prepared in PBS buffer, and the corresponding calibration curves (c and d).

Regarding, the second approach was electrodeposited the gold nanoparticles on top the surface and each modification was followed by CV, EIS and SWV (**Figure 5.8**). After pre-cleaning the surface, was electrodeposition in situ gold nanoparticles. The data showed higher average CV peak current, (**Figure 5.8 a**) attained in the previous cleaning stage. The current of the cathodic peak after cleaning was ~94.38µA lower than after electrodeposition of Au NPs was ~147.83µA (**Figure 5.8 d**). The Rct in EIS (**Figure 5.8 b**) became negligible, thereby confirming the enhanced electrical features of the sensing surface ~12.98Ω. The SWV data was consistent with the previous observations, displaying a current increase and showed ~61.69µA. The next step was producing the MIP film by electropolymerization Pyrrol by CV at –0.2V to +0.85V at 5cycles in presence of template glucose. The negative control (NIP) was shaped similarly, however, in absence of glucose.

Overall, the presence of polymeric film showed a current decreasing in CV (**Figure 5.8 a**) and SWV (**Figure 5.8 c**) measure because poly(pyrrol) signalled the surface are blocked. Besides the pyrrole represent a polymer with a higher conductivity, this property depends of the pH effect and electrolyte [298]. The results in EIS spectra (**Figure 5.8 b**) are consistent with these observations.

The decreasing of current is more evident in the MIP, which signalled the presence of glucose (Figure 3a), hindering the occurrence of redox reaction, which cause this reduction of the current. The current of cathodic peak of MIP device was of~71.6μA, lower than NIP ~82.73μA (Figure 3d), although observe that both materials had a similar CV profile, due the small size of molecule. The Rct in EIS technique (**Figure 5.8 b**), increased more evidently in the MIP device at ~1283Ω compared with NIP at ~860.3Ω (**Figure 5.8 e**) and consistently SWV measurement (**Figure 5.8 f**) the decreasing was more significant in MIP layers at ~23.31 μA than NIP at ~29.23μA.

After the polymerization stage, the electrodes were incubated in ultrapure water for 1h. Ultrapure water was selected because glucose is highly soluble in water, thereby being easily extracted from the polymeric network by simple dissolution. Selecting water also prevent ensured the integrity of the polymer. Overall, in the NIPs films, in terms of CV profile, had few increasing the current at~87.4μA compared with MIP at ~92.34μA (**Figure 5.8 d**), besides that, in EIS spectra, the NIP showed decrease at~625.1Ω than MIP device presented highest decrease at ~ 536.1Ω (**Figure 5.8 e**), and SWV data is consistent with the other measures (**Figure 5.8 f**), in MIP had a highest increase at ~37μA comparing with NIP ~33μA. Overall, these results confirmed the effective removal of glucose from the MIP films and the stability of the poly(Py) film when exposed to ultrapure water, when used the Au NPs, increasing the superficial area, increasing the sensibility.

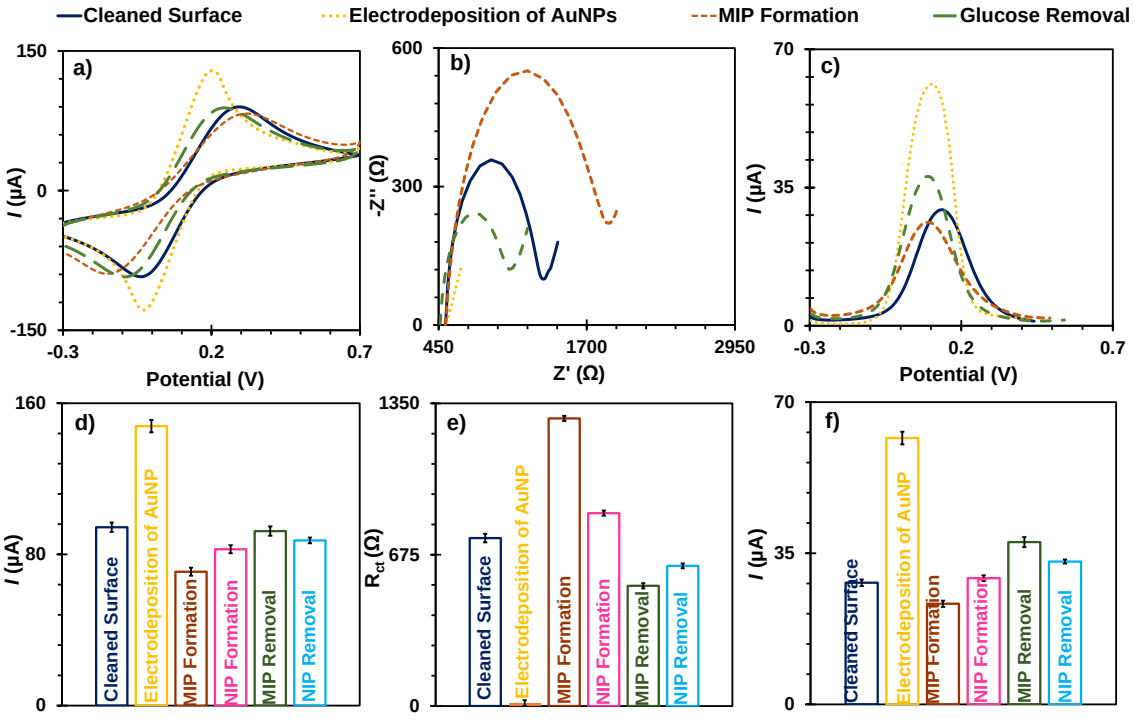

Figure 5.8: Electrochemical data upon the biosensor construction, using CV (a), EIS (b) and SWV (c) measurements. Data includes after cleaning the surface, after electrodeposition of Au NPs, Electropolymerization of MIP film (with Py and Py-COOH) and removal of the template. Graphics (d) and (f) show the current peak's intensity, and graphic (e) presents the Rct values with the respective error bars, highlighting the reproducibility of three independent devices.

5.3.3 Electrochemical analytical performance

The analytical performance of the device was evaluated by incubating a standard glucose solution on the MIP for 30 minutes, then washing it out and replacing it with the standard iron redox probe to extract the corresponding Nyquist plot (**Figure 5.9 b**). This procedure was repeated sequentially for increasing concentrations of glucose after doing so with buffer the required number of times until the signal was stable.

The linear response was observed from 1.0 µM to 1.0 mM (0.02 to 18.02 mg/dL), plotting Rct against logarithm (glucose concentration). The average slope of 3-independent readings was 73.9 Ω/decade (**Figure 5.9 d**), with a maximum standard deviation of 3.4% and an LOD of 0.15 µM (3 µg/dL). The calibration curves showed squared correlation coefficients >0.99, confirming the excellent quality of the linear response. The reproducibility was also excellent, considering that the RSD values ranged from 1.37% (minimum) to 3.2% (maximum) within the linear response range.

The same approach of calibration was used for the NIP to understand the ability of the imprinted sites on the electrode surface to bind glucose (**Figure 5.9 a**). The random response of the NIP against increasing glucose concentrations confirmed that the electrochemical response of the MIP was being dominated by the imprinted binding sites and that non-specific binding to the poly(Py) was negligible (**Figure 5.9 c**).

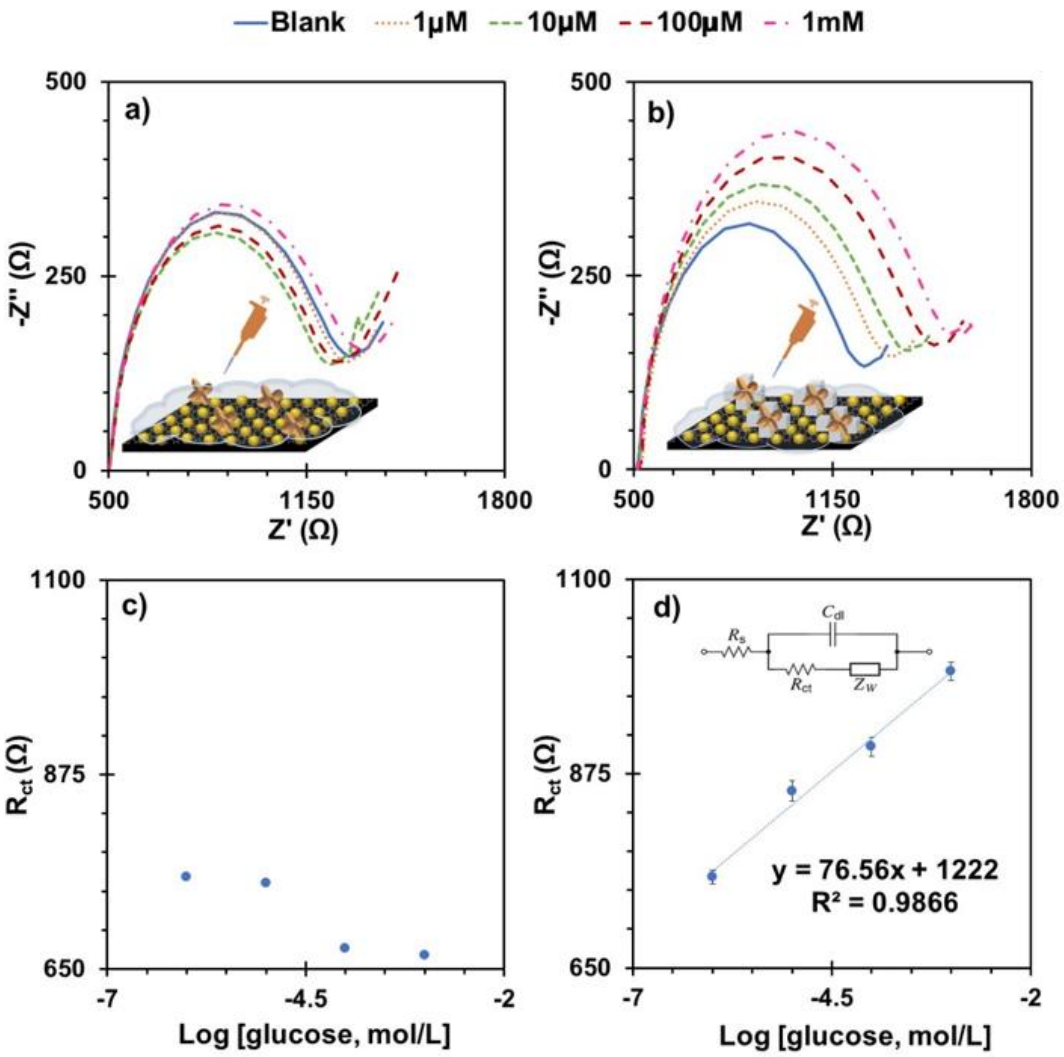

Figure 5.9: Calibration curves of the biosensors C-SPEs/Au NPs/MIP-NIP-Py-COOH, with EIS measurements of NIP devices and (c) the corresponding calibration curves; (b) EIS measurements of MIP devices and the corresponding calibration curves (d), obtained in 5.0×10^{-3} M $[Fe(CN)_6]^{3-}$ and 5.0×10^{-3} M $[Fe(CN)_6]^{4-}$ solution prepared in PBS buffer.

5.3.4 Optical analytical performance

The ability of the biosensor to provide quantitative data in terms of optical response was also investigated, taking into account the presence of AuNPs on the surface and the possibility of producing an organized reflection on the surface that can be altered by the presence of glucose [299].

To understand the feasibility of this approach, the reflectance spectra were collected for each step of the biosensor construction (**Figure 5.10**). As expected, the presence of the Au NPs significantly increased the total surface reflectance compared to the carbon substrate. The presence of the polymer on this substrate (C-SPE/Au NPs/MIP-glucose and C-SPE/Au NPs/NIP) reversed this tendency and decreased the observed reflectance. The reduction was more pronounced with MIP, suggesting that the presence of glucose affects surface reflectance. This was confirmed when the extraction of glucose from the imprinted polymer to produce the C-SPE/AuNPs/MIP sensing partially restored the reflectance values of the C-SPE/Au NPs (**Figure 5.10 a**). The effect of glucose on the reflectance signal was also demonstrated by the C-SPE/AuNPs/NIP control conditions, whose reflectance value did not change significantly after the final template removal step (**Figure 5.10 b**).

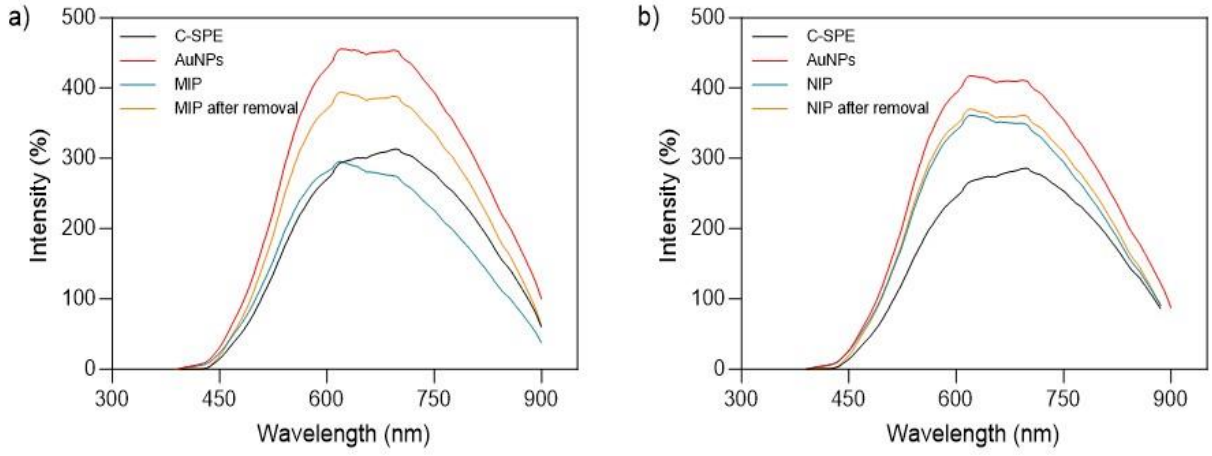

Figure 5.10: Reflectance spectra collected at each step of modification of the C-SPEs to produce C-SPEs/AuNPs/MIP-Py-COOH (a) and C-SPEs/Au NPs/NIP-Py-COOH (b) films.

To verify the concept, analytical performance was evaluated by successively incubating glucose standard solutions with increasing concentration and checking the obtained reflectance spectra (**Figure 5.11 a**). The reflectance signal decreased with increasing glucose concentration. The spectra were analysed using the area under the curve of the measured signals and a linear trend as a function of glucose concentration was obtained (**Figure 5.11 b**). This was already expected considering the results of the biosensor assembly. Glucose may contribute to block

both the radiation hitting the AuNPs at the underlying surface and the radiation that could be reflected from the nanoparticles.

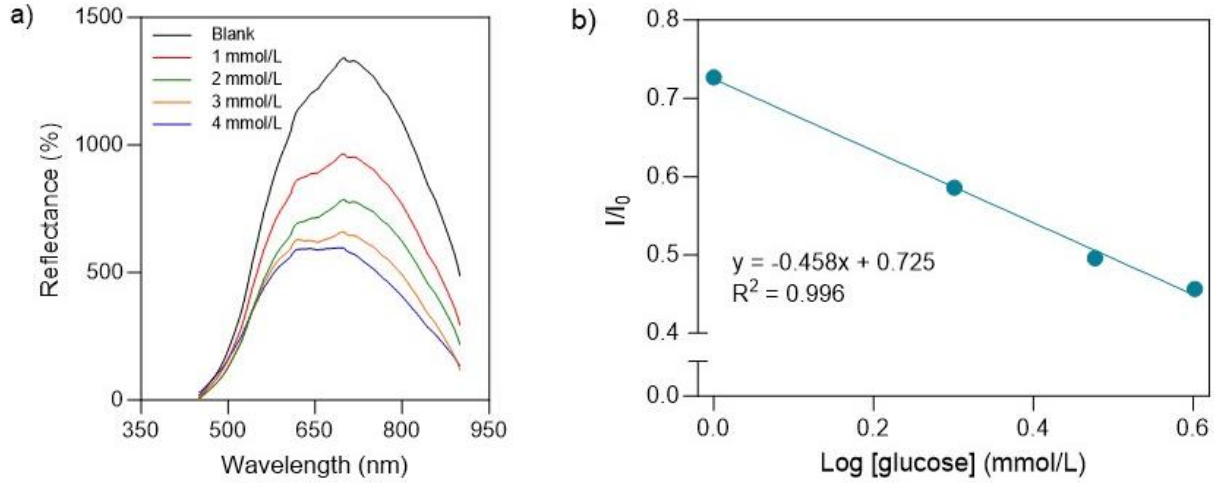

Figure 5.11: Reflectance spectra obtained from C-SPEs/Au NPs/MIP-Py-COOH after incubation with glucose standard solutions of increasing concentration prepared in PBS buffer (a) and the corresponding calibration curve (b).

5.3.5 Direct electrochemical readings of glucose

The direct reading of glucose was tried out by chronoamperometry, aiming to avoid the need to add a redox probe when conducting quantitative measures with the devices C-SPs/Au NPs/MIP. Chronoamperometry was conducted at +0.2V, because Au NPs were present at the surface. They catalysed the oxidation of glucose, thereby decreasing the required potential to undergo this oxidation (without Au NPs no current signals would be generated in this potential, as may be seen in **Figure 5.12**.

The typical data obtained is shown in **Figure 5.13** in specific time t=20s.The calibration curves showed a higher sensitivity using a MIP technology in different times points in chronoamperometry in **Figure 5.13b**.

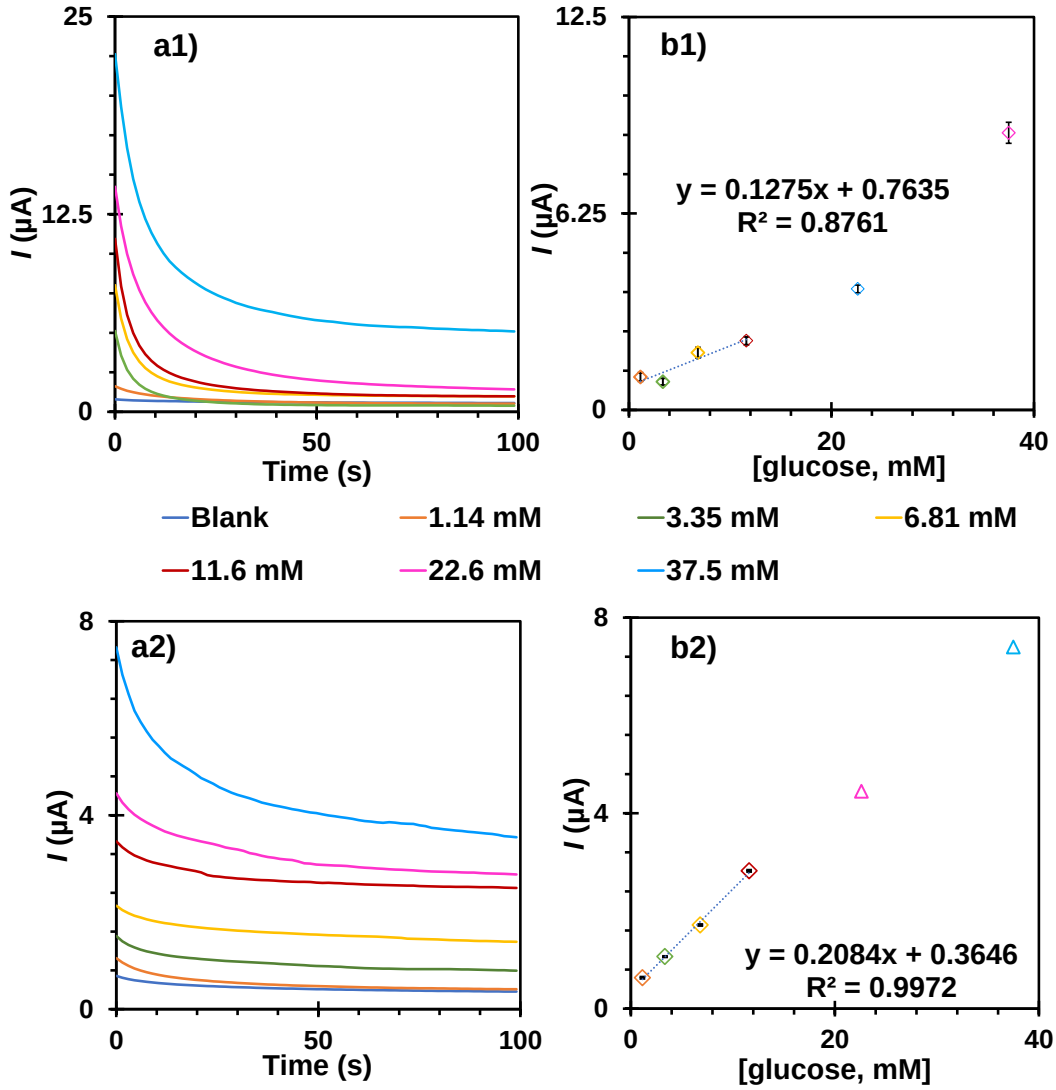

Figure 5.12: Chronoamperometric data (a) of direct readings of glucose (1) on the C-SPEs/MIP-Py-COOH film and (2) on the C-SPEs/Au NPs/MIP-Py-COOH film, along with the corresponding representative calibration curves in t=20s (b).

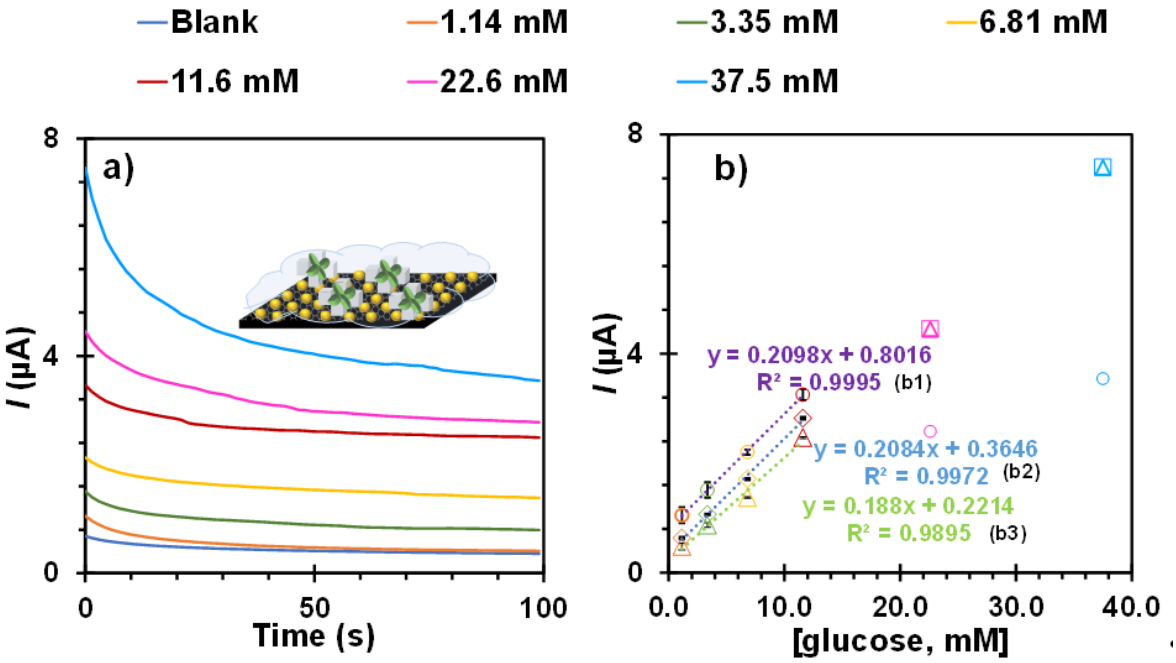

Figure 5.13: Chronoamperometric data (a) of direct readings of glucose on the C-SPEs/MIP-Py-COOH film with the corresponding representative calibration curves (b) in different time points: 0s (b1); 20s (b2) and 100s (b3).

The importance of the presence of the MIP upon the electrochemical readings was confirmed by checking the response of glucose directly on a substrate without MIP (C-SPEs/Au NPs). As may be seen in **Figure 5.13 a**, the maximum current intensity observed was ~3× greater than in a device containing the MIP, because the conductivity of the sensing area was being blocked by the polymer. Yet, one must consider that there is no discrimination for a selective glucose oxidation under the selected potential, as other compounds being able to undergo an oxidation at the same potential would be also producing current signals.

Thus, the capacity of the MIP to selectively discriminate glucose from other compounds was checked by evaluating the response of the C-SPEs/Au NPs/MIP against AA standard solutions, because AA is well-known interfering compound in glucose readings. In this study, AA solutions were prepared in the same concentrations as those assessed for glucose, ranging from 1.14 to 37.5 mM. The results obtained are shown in **Figure 5.14**, which evidence a random response. The maximum initial current levels were also ~4× less than those in a direct glucose reading, meaning that AA is being excluded from the polymeric network, becoming too distant from the Au NPs to be efficiently oxidized. It is important to note that the AA levels in serum normally range 0.4 to 1.7 mg/dL (22 to 85 µM), which is much lower than the concentration tested, meaning that the interference of AA in real serum analysis is negligible.

Overall, the analytical data generated by chronoamperometry indicates a linear trend of current against concentration, from 1 to ~40 mM for a direct glucose reading. This makes clear that

the use of a redox probe enhances the capacity of the same electrode in terms of detection ability and sensitivity. With using EIS and a redox probe, the C-SPEs/Au NPs/MIP is able to reach ~1000× less glucose, over a wider concentration range, as linear responses ranged 1 to 1000 μM. Having in mind that a sample dilution is always conducted to ensure that the sample contains similar electrolyte content in terms of pH and ionic strength, the use of a redox probe seems more adequate. The normal fasting blood glucose level range between 70 mg/dL (3.9 mM) and 100 mg/dL (5.6 mM), meaning that the levels of sample dilution permitted by this reading approach are much higher.

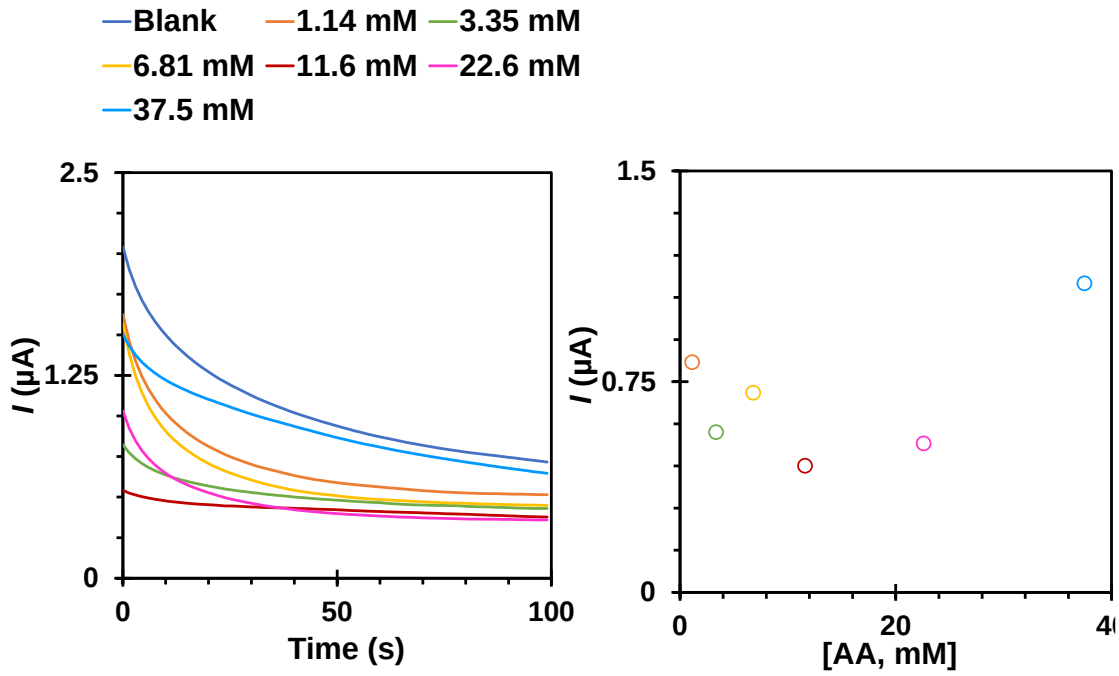

Figure 5.14: Chronoamperometric data (a) of direct readings of (1) AA on the C-SPEs/Au NPs/MIP-Py-COOH film along with the corresponding representative calibration curves in t=20s (b).

5.3.6 Analytical Performance in human sera

The electrode C-SPEs/Au NPs/MIP was evaluated in glucose standard solutions prepared in buffer and diluted human sera (1:1000), to assess the capacity of the system to undergo accurate analysis of real samples. All assays were evaluated in triplicate and a typical Nyquist plot so obtained is represented in **Figure 5.15**. Considering the sensitivity of the signals obtained, it is apparent that the slope is greater when diluted human serum solutions were used, compared to buffered solutions, however relative data shows otherwise.

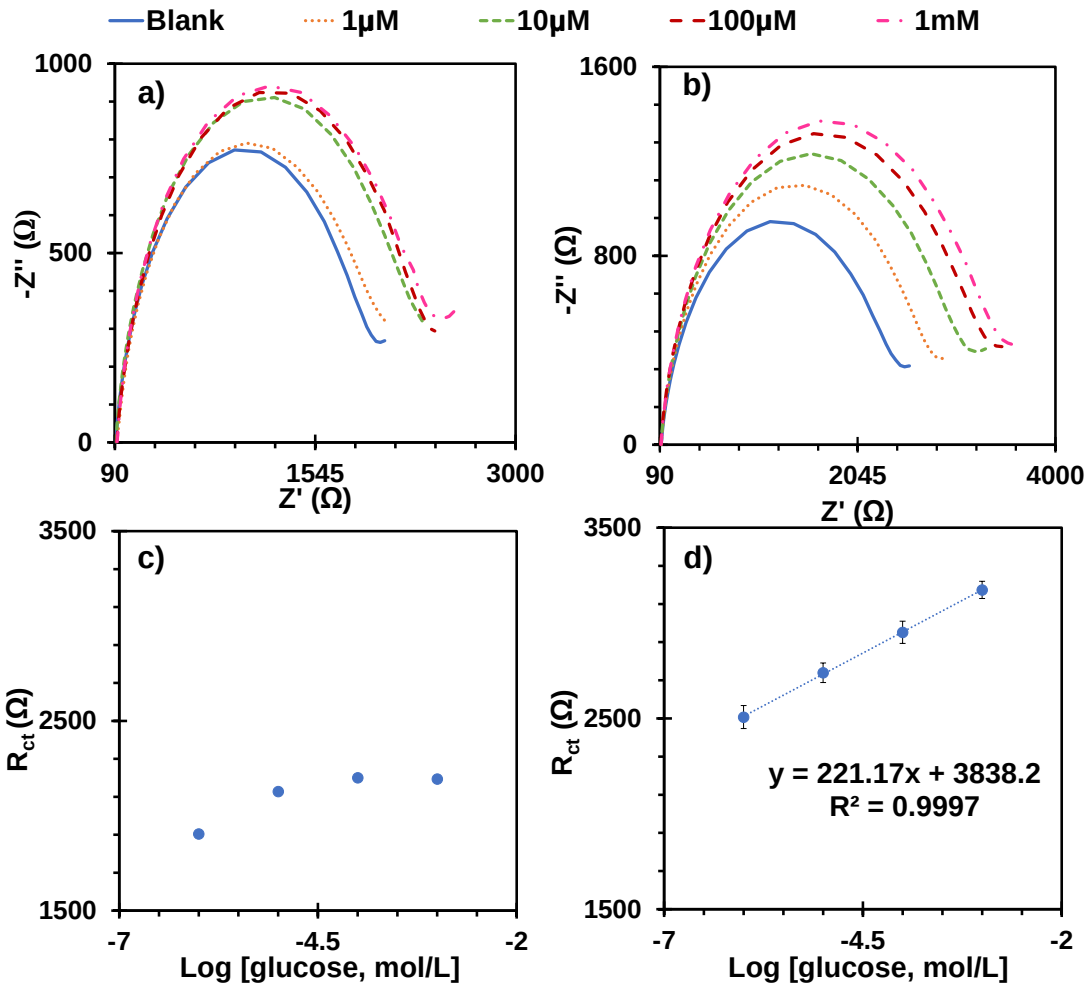

Figure 5.15: Calibration curves of the biosensors C-SPEs/Au NPs/MIP-NIP-Py-COOH, with (a) EIS measurements of NIP devices and (c) the corresponding calibration curves; (b) EIS measurements of MIP devices and the corresponding calibration curves (d) in serum 1000x diluted. Readings obtained in 5.0×10^{-3} M $[Fe(CN)_6]^{3-}$ and 5.0×10^{-3} M $[Fe(CN)_6]^{4-}$ solution prepared in PBS buffer, after incubation in increasing concentrations of glucose standard solutions.

Calibrations plotting the ratio 'standard solution Rct/blank Rct' have similar trend in buffered standard solutions and buffered standard solutions containing diluted serum, meaning that the analytical sensitivity was similar (**Figure 5.16**). The limit of detection (LOD) calculated upon the Nyquist plots obtained was 0.11µM, and the linear trend indicates that the biosensor can be used to analyse human sera from 1000µM to 1000 mM. As control purposes, the response of the NIP to this diluted serum solutions was also evaluated, and a random response was observed, thereby confirming the critical role of the MIP on the working electrode.

As there is glucose in the original human serum used to dilute the buffered standard solutions, the blank sample is always generating a high background signal, according to the concentration present in this diluted serum solution.

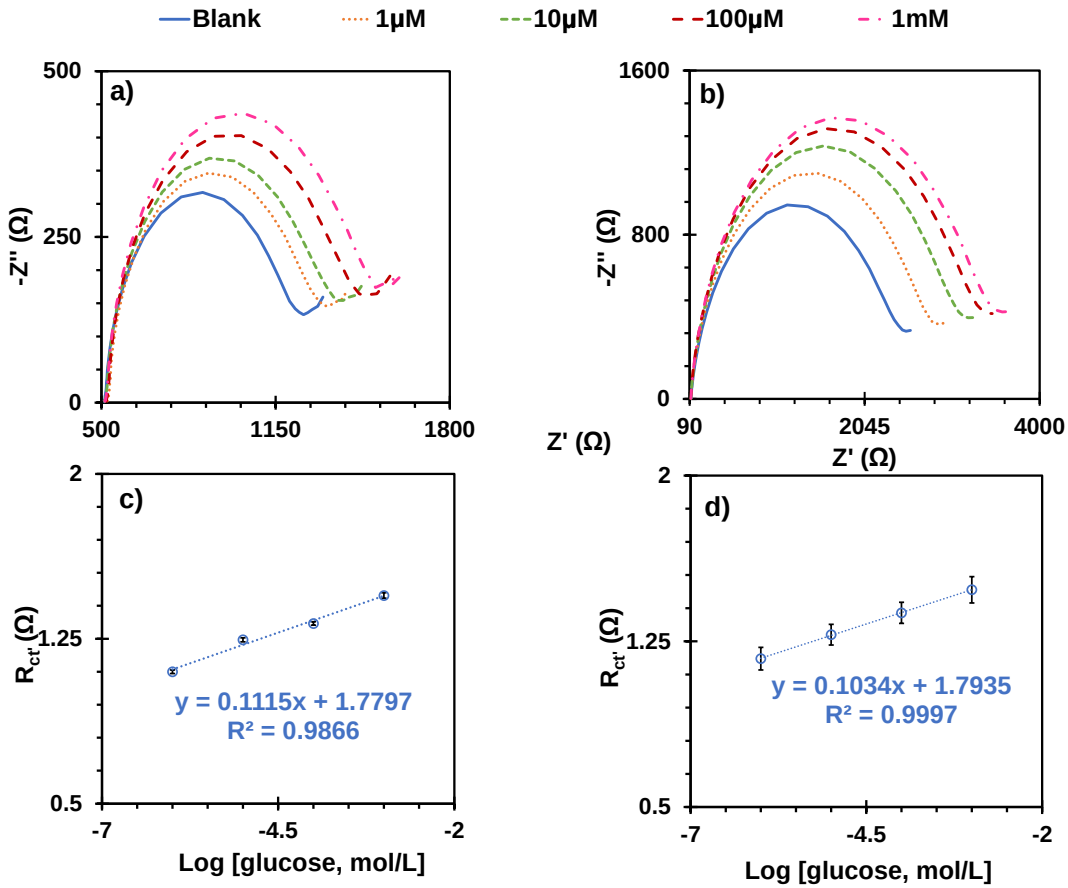

Figure 5.16: Calibration curves of the biosensors C-SPEs/Au NPs/MIP-NIP-Py-COOH, with EIS measurements in buffer (a) and serum (b) and the corresponding calibration curves with relative values (c) in buffer and (d) serum 1000x diluted. Readings obtained in 5.0 × 10^{-3} M $[Fe(CN)_6]^{3-}$ and 5.0 × 10^{-3} M $[Fe(CN)_6]^{4-}$ solution prepared in PBS buffer, after incubation in increasing concentrations of glucose standard solutions in different medium (buffer and serum).

5.4 Conclusions

This work demonstrates the successful development of a simple, innovative, highly sensitive and selective MIP material for the detection of glucose on a carbon substrate modified with Au NPs. This simple construction involves all stages assembled in-situ, with great advantages in terms of the catalytic effect of the Au NPs upon the oxidation of glucose. This was confirmed and optimized by selecting the best conditions to generate in-situ the nanoparticles, improving the sensibility and the MIP technology improves the selectivity of the sensor. The impact of nanomaterial electrodeposited on the sensor performance was proved by studying without this metal and could not detect glucose with linear trend. The C-SPE/Au NPs/MIP/Py-COOH sensor showed a selectivity toward the target molecule.

Overall, this electrochemical biosensor can be used with dual detection optical and electrochemistry with a good sensitivity.

CHAPTER 6

Catalytic MIP

6.

CATALYTIC MIP

6.1 Introduction

Recently, the combination of NANOZYMES and MIP technology has evidenced several advantages for increasing the selectivity of the analytical response. A MIP sensing material is a valuable approach for the spatial recognition involved in the enzyme interaction with the substrate. These materials are host-tailored polymers, where a given target analyte acts as a mould when a polymeric network forms around it, as mentioned in the **Chapter 2.** The exit of the analyte from this matrix reveals imprinted positions that display complementary shape to the moulded compound. The target analyte may therefore rebind to such positions later, as a natural antibody binds to its target compound, allowing both electrical or optical readout of this rebinding event [300]–[303]. MIP materials are typically produced by radical polymerization, from which electrochemically driven polymerizations have been found attractive [304]. Electropolymerization allows a greater control over the growing polymer while also being suitable for scaling-up processes.

Thus, this specific work aims to generate novel artificial enzymatic materials combining catalytic activity and spatial recognition abilities by merging MIP with nanozyme technologies. Such artificial enzyme materials make use of (i) the ability of MIP materials to establish a spatial recognition of the substrate, as in natural enzymes, and combine this with (ii) nanozymes, introducing catalytic properties at the "active site" where recognition takes place. The idea is applied as proof of concept to generate innovative enzyme-free sensing devices for diabetes. The innovative enzyme-free sensor is tailored for glucose sensing, as a worldwide need in diabetes control. This includes (i) preparing an artificial material acting like GOx; (ii) applying it to prepare a suitable electrochemical sensor (competitive with the current commercial glucose meters).

The catalytic-MIP material is set-up on a conductive material, using carbon SPEs. SPEs are similar to glucose-strips, allowing the use of a small sample drop (~15-microL). Its production requires a three-stage development, as selecting amino acids to which the key biomarkers hold great affinity; selecting suitable catalytic materials for the electron transfer; and selecting a suitable MIP composition.

Natural enzymes display great affinity for a given target compound, due to specific amino acids strategically placed at the active site. The sidechains of these amino acids are greatly responsible for such affinity. Thus, the first assays shall identify the sidechains that need to be introduced at the synthetic process for assembling the MIP. These must be part of an aromatic-based compound, as common electropolymerization processes involve aromatic-rings.

Regarding glucose, a synthetic GOx material is meant. GOx catalyses D-glucose oxidation, leading to gluconic acid[305]. The redox-active site of the enzyme contains three main residues, His516/His559/Glu412[306] (**Figure 6.1**), close to Flavin Adenine Dinucleotide (FAD).

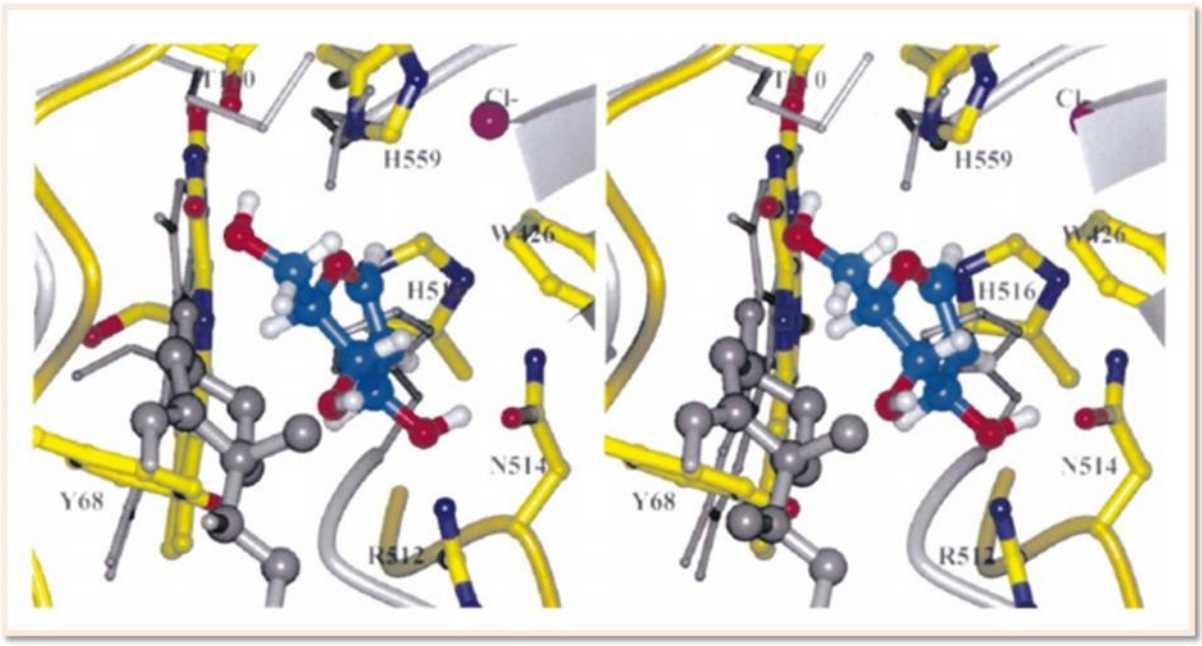

Figure 6.1 The three main residues of active site of the enzyme.

Thus, affinity tests are made between glucose and different aromatic-based compounds containing the sidechains of the amino acids present at the active site of the enzyme. The most suitable combination for each side chain (Glutamic acid and Histidine) is defined by monitoring the direct affinity of glucose to the resulting electropolymerised material on the SPEs with carbon-supports. Regarding the catalytic materials involved in the electron transfer, metal

nanoparticles and/or FAD derivatives are included within the artificial rebinding site. FAD derivatives contain Flavin/Isoalloxazin ring, which is the chemical part of the co-factor responsible for electron transfer [307].

The assembly of the MIP material for glucose is made with aromatic-based monomeric materials capable of electropolymerizing under mild conditions and low potentials (**Figure 6.2**). The monomers used for this purpose were tested in MIP assembly, showing excellent features in terms of stability [308], [309]. The best conditions of electrical-based polymerization are optimized for each monomer (p.e., chronoamperometry or CV; scan-rate and/or potential-range; medium composition, its pH and ionic strength). The rebinding of glucose is checked under optimum conditions. The final assembly is characterized in terms of analytical performance. This includes linear working range, LOD, sensitivity, cross-reactivity (with competitive assays of concurrent compounds in serum/blood), repeatability and reproducibility, long term stability and storage requirements.

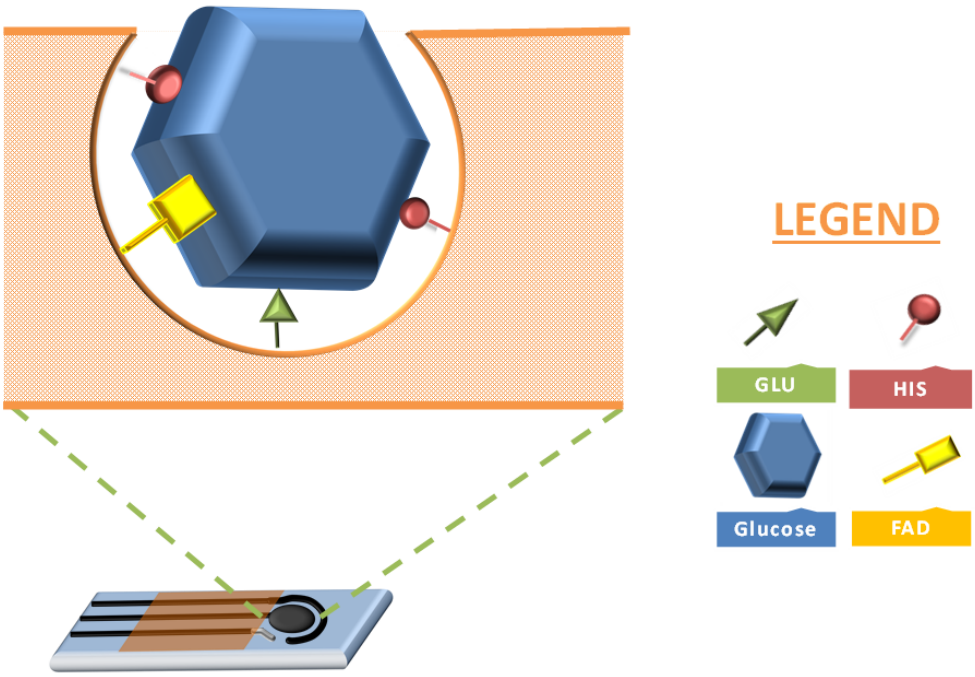

Figure 6.2: Scheme for assembly of the Catalytic MIP for glucose.

6.2 Experimental Section

Monomers used for this purpose are those tested in MIP assemblies and monomers used in MIP for glucose (previously mentioned in **Chapter 5**). This work is ongoing.

6.2.1 Reagents and Solutions

All chemicals were of analytical grade and ultrapure Milli-Q water laboratory grade (conductivity <0.1 μS/cm) was used in this work. Chemical reagents used include potassium hexacyanoferrate III ($K_3[Fe(CN)_6]$) from Carlo Erba; potassium hexacyanoferrate II ($K_4[Fe(CN)_6]$) trihydrate from Panreac; PBS, 0.01 mol/L, pH 7.4), glucose, *N*-(4-Aminobenzoyl)-L-glutamic acid and Benzoyl-*l*-histidine monohydrate were purchased from Sigma-Aldrich; Pyrrole (Py) purchased from Alfa Aesar; FAD was purchased from ThermoFisher Scientific. Potassium Chloride (KCl) was purchased from Honeywell Fluka. All solutions were prepared in ultrapure water. 0.1M KCl was used to electrochemical cleaning of the surface. The MIP solution contained 100mM of glucose, 5mM of Benzoyl-*l*-histidine monohydrate, 5mM of *N*-(4-Aminobenzoyl)-L-glutamic acid, 10 mM of FAD and 1mM of Py prepared in 10 mM PBS (pH 7.4). The NIP solution contained 5 mM of Benzoyl-*l*-histidine monohydrate, 5mM of *N*-(4-Aminobenzoyl)-L-glutamic acid, 10 mM of FAD and 1 mM of pyrrole prepared in 10 mM PBS (pH 7.4). The standard solutions of glucose were prepared in 10 mM PBS (pH 7.4). The electrical changes after cleaning process on the electrode were followed with a solution of 5.0×10^{-3}M K_3 $[Fe(CN)_6]$ and 5.0×10^{-3}M K_4 $[Fe(CN)_6]$) prepared in 10 mM PBS.

6.2.2 Apparatus

Electrochemical measurements were performed using a PalmSens4 potentiostat/galvanostat controlled by PSTrace 5.8 software. Commercial carbon SPEs (C-SPEs) from Metrohm DropSens (DRP-110) were used. These contain a three-electrode system, including: (a) a carbon counter electrode, (b) a silver RE, and (c) a 4 mm diameter carbon WE. The C-SPEs were connected to a PalmSens switch box that allows connection to the potentiostat.

6.2.3 Electrochemical measurements

The analytical performance of the novel glucose-MIP was followed by CV -0.2 to +0.8V with a scan-rate 0.05V/s and Chronoamperometry applied a potential deposition at -0.7V during 20s in pre-settings and then in the measurement was applied +0.4V during 100s.

6.2.4 Preparation of Carbon biosensor

The approach used to build the current biosensor is described in **Figure 6.2** and was inspired by our previous work described in 2.1.3. The setup was performed in several steps (**Figure 6.3**):

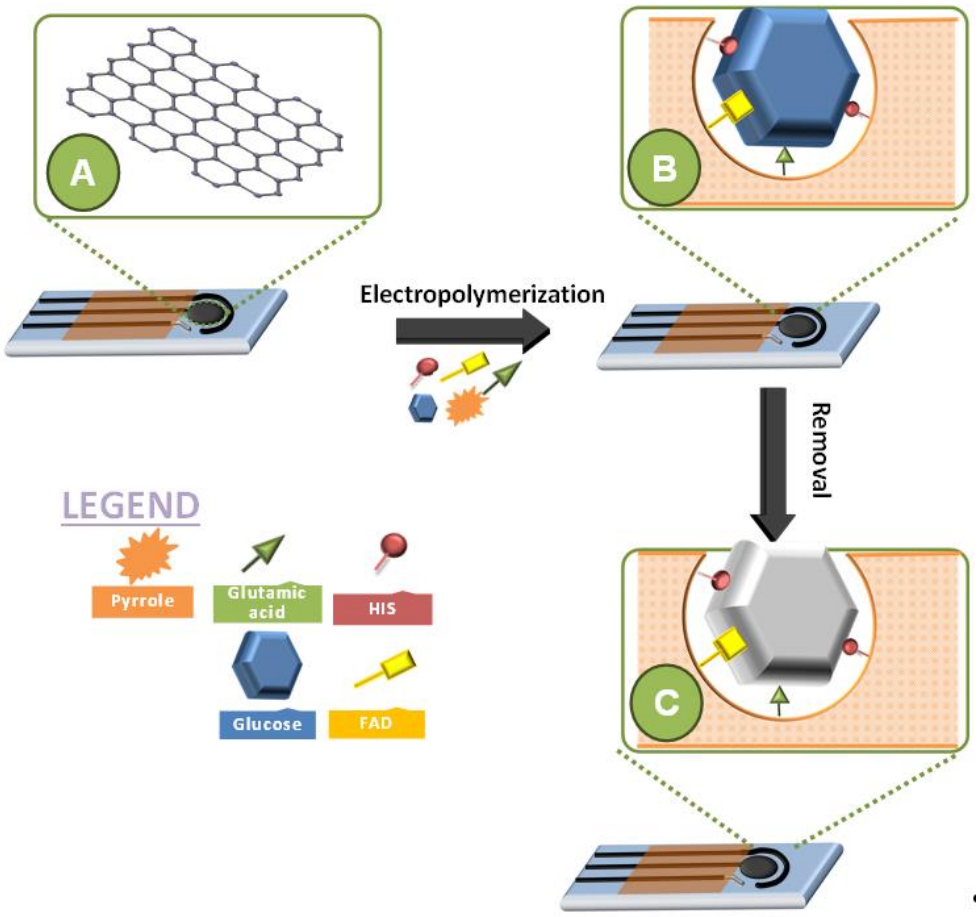

Figure 6.3: Several steps for assembly the Catalytic MIP. (A) Cleaning the surface; (B) Electropolymerization of MIP and NIP; (C) Removal Process.

In this, **(A)** the WE was cleaned by electrochemical treatment (0.1M KCl), scanning between -1.0V and+1.0V during 1 cycle with a scan rate of 0.05V/s; (**B**) preparation of MIP layer by bulk imprinting in a solution containing glucose, benzoyl-l-histidine monohydrate, *N*-(4-aminobenzoyl)-L-glutamic acid, FAD, pyrrole in PBS solution (the NIP only contained Benzoyl-l-histidine monohydrate, *N*-(4-aminobenzoyl)-L-glutamic acid, FAD, pyrrole in PBS) by CV in the potential range between -0.20V and +0.95V (vs. Ag/AgCl) with a scan rate of 0.10 V/s; (**C**) removal of template by CV measurement (-0.20V to+0.95V) during 10 cycles with a scan rate of 0.10 V/s and the final step was test the analytical performance of MIP and NIP device with several concentrations of glucose and by CV and chronoamperometry.

All compounds of the MIP (glucose, benzoyl-*l*-histidine monohydrate, *N*-(4-aminobenzoyl)-L-glutamic acid, FAD) and NIP devices (Benzoyl-*l*-histidine monohydrate, *N*-(4-aminobenzoyl)-L-glutamic acid, FAD) were mixed for 2h and then was added the monomer, pyrrole, for polymerization. All solutions were deoxygenated by bubbling nitrogen gas for 5 minutes.

6.3 Preliminary Results

Several assays were performed to test different parameters to measure the catalytic activity in the presence of glucose, using positive and negative potentials in chronoamperometry and CV measurements promoting oxidation/reduction of FAD. The first assay to confirm this activity fixed the positive potential at +0.4V in chronoamperometry, using pre-settings with a negative potential, and then tested the sensor's analytical performance using different glucose concentrations (**Figure 6.4**). The results showed a promising response in the presence of glucose (MIP), however, with little sensitivity, around 0.016Ω/decade, for a linear response range between 5 mM to 100 mM (**Figure 6.4B**). The current values increased with increasing the concentrations of glucose, due the oxidation of glucose and FAD received the electrons. The current values increased with increasing the concentrations of glucose, due the oxidation of glucose and FAD received the electrons. In contrast, in the absence of glucose, the non-imprinted polymer (NIP) shows a random response (**Figure 6.4D**). These preliminary results prove that MIP for Glucose had a catalytic activity. However, another experimental assay needs to be performed to confirm this evidence and should have a better sensitivity, optimizing several conditions in the assembly of the sensor.

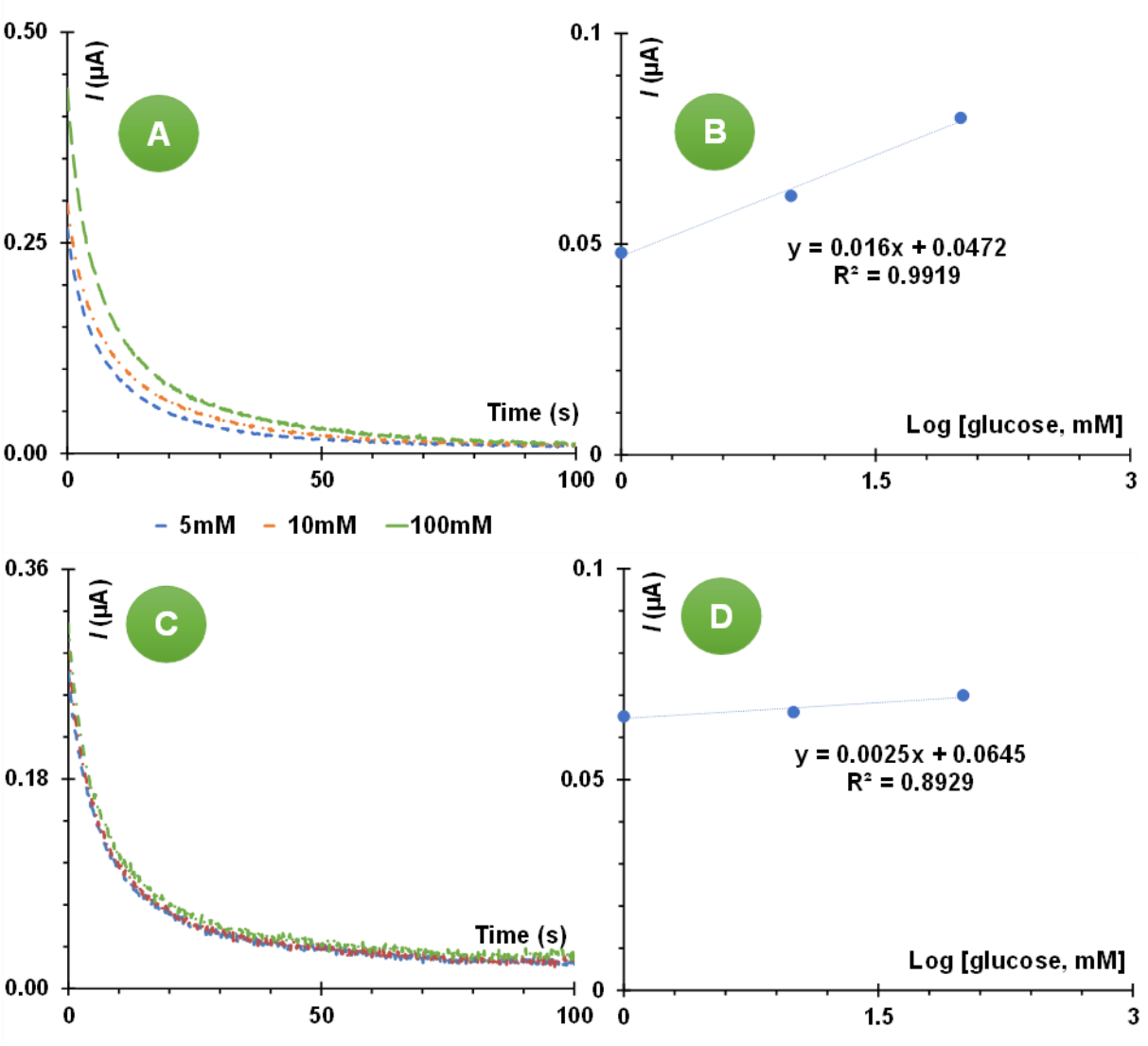

Figure 6.4: Current plots within time for glucose concentrations between 5 mM and 100 mM, obtained in the MIP (A) and NIP (C) biosensors, respectively, and the corresponding calibration curves (B and D). The potential was set to +0.4V.

The second assay measured the electroactivity properties toward FAD reduction, using CV readings under a negative potential range. FAD is involved in biological processes and can be considered as a relevant redox-active biomolecule in biosensor field. The electrochemical detection of interaction FAD/glucose may be very challenging [310]–[312]. **Figure 6.5** shows the so obtained voltammograms, down to -0.8 V. In general, the reduction of FAD decreased as the concentration of glucose increased because the FAD present in the polymeric network had been partially involved in the oxidation of glucose, being therefore already in its reduced form. Overall, there was a good analytical performance in the presence of different concentrations of glucose, although with little sensitivity, around -3.33Ω/decade, and showed a linear range between 0.5 mM to 100 mM. As explained, the results showed a negative correlation between

the decrease the current and the successive increase in glucose concentrations, thereby confirming the existence of a spontaneous FAD reduction in the presence of glucose.

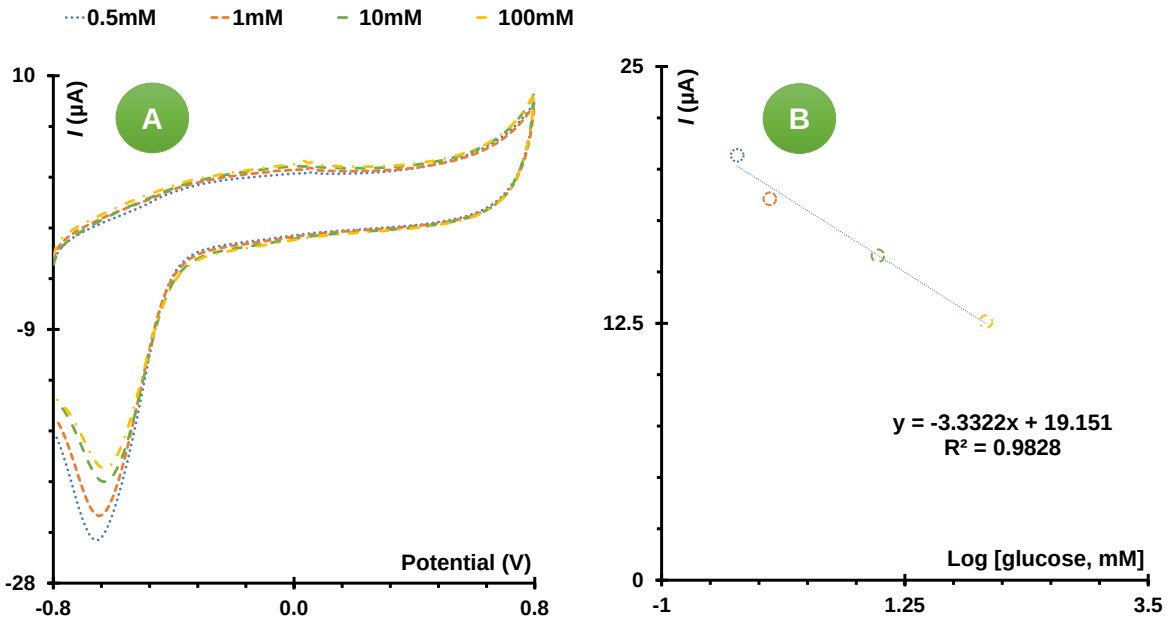

Figure 6.5: Cyclic voltammograms obtained as the concentration of glucose increases in MIP (A) using negative potentials of FAD with different glucose concentrations and calibration Curve (B) respectively. The measurements were done at 50 mV s^{-1}.

This work is proceeding further, with overall optimization procedures until the MIP-catalytic biosensor is found useful for a practical application to the determination of glucose in serum.

6.4 Conclusions

A simple method to fabricate a nanozyme based on MIP technology was developed.

This novel biosensor showed a promising result and confirmed that was possible to measure and mimic the activity of GOx using MIP technology.

However, this biosensor needs to be optimized further to perform with a wider range, good sensitivity, and selectivity. Even though. additional assays are require this approach opens a new field to search for developing alternative biosensing systems that are enzyme free.

CHAPTER 7

General Conclusions and Future Work

7.

General Conclusions and Future Work

Overall, the design of the electrochemical sensors developed for this work has been shown to achieve the same standards as current methods, namely sensitivity, reproducibility, and selectivity, combined with the advantages of using different nanomaterials with a low-cost analysis suitable for POC screening. Although some limitations in the operation of some devices were identified throughout the research, the use of nanomaterials and biomimetic films enabled the required performance standards to be achieved for these novel biosensor systems. In the future, it is essential to remember that sensitivity is also controlled by the type and nature of the transducer.

Herein, the electrochemical behaviour of the chosen material may affect the LOD of the sensor planned for the detection of antibodies against SARS-CoV-2. Specifically, a comparison of all sensing devices constructed during this thesis revealed that using carbon nanomaterials and metal NPs achieved lower LOD values. Comparing the preparation of carbon nanomaterials, two different approaches are tested. These included either more steps to enable the detection the lowest concentrations of antibodies anti-S Protein published by that time and enabling the analysis of real serum samples, or a simple and low-cost method to fabricate graphene sheets to be casted on carbon-SPE for outstanding interfacial properties. This last method consisted of a direct mechanical exfoliation process of graphite using an ultrasonic method and mixing with proteins of SARS-CoV-2 and then testing the binding with antibodies against the S protein. This biosensor showed a lower LOD and could be applied in real contexts as well. In addition to the constructions, characterization and application of each of the electrochemical sensors developed herein for detecting antibodies anti-S protein, important complementary techniques, such as Raman spectroscopy and SEM, were employed to confirm the formation

of the various nanomaterials. As a result, from a point of view of biosensor application in typical situations, quick and practical devices of great valued.

The assembly of a catalytic-MIP for glucose was also found possible. The work developed included a novel sensor with dual detection for glucose using metal NPs (as gold nanoparticles), produced in situ based on MIP technology, offering selectivity and improving the sensitivity of the sensor. One of the most critical factors influencing the electrochemical performance of MIP-based sensing materials was the fabrication of very thin films, which was required because the recognition event should take place as close to the electronic transduction surface as possible. As for the biomimetic polymer synthesis strategy, electropolymerization was identified as the most suitable method because it allowed for high adherence to the transducer substrate, allowed easy control of film thickness and growth, and worked under mild conditions, such as aqueous solutions and ambient temperature. Furthermore, pyrrole was a promising material for the fabrication of the polymeric matrix forming the recognition sites, because of its excellent stability and specific affinity to the target molecules. The Au NPs were characterized by SEM to confirm the production in situ of these nanostructures on the surface of the electrode. Within this work, it is possible to detect directly different glucose concentrations with higher selectivity and great sensitivity.

Looking towards the future, the catalytic MIP was developed to mimic the GOx activity and measure the electroactivity of the interaction of FAD and glucose based on MIP technology, introducing the specific amino acids to help in the spatial orientation of glucose. To better understand and follow the electroactivity, chronoamperometry and CV measurements were performed. These electrochemical techniques allow measuring the current formation due to the reduction or oxidation of FAD in the presence of different glucose concentrations.

In summary, the electrochemical performance of the developed sensors was thoroughly explored. Another possibility would be to incorporate Au NPs into the surface to create a facile optical strategy. Besides, the use of different nanomaterials in the field of biosensors improves the sensitivity and rapid diagnosis in real contexts by using other biomarkers. The main advantage of this nanomaterial is that it is the first electrochemical biosensor with the potential to become a portable and low-cost diagnostic tool for different targets detection.

CHAPTER 8

Scientific outputs

This chapter shows the scientific outputs during the thesis period, detailing the publications in peer-review periodicals and invited chapter books, oral and poster communications, research activities, and master thesis guidance.

8.

SCIENTIFIC OUTPUTS

8.1 Publications

The publications of the candidate from which results are present in this dissertation document are listed below:

8.1.1 Peer-reviewed publications

- **Cardoso, A. R*.,** Frasco, M*., Serrano, V*., Fortunato, E., Sales, M. G. Molecular Imprinting on Nanozymes for Sensing Applications. Biosensors **2021**, 11, 152. https://doi.org/10.3390/bios11050152

*Equal first authors

- Pinheiro, T *., **Cardoso, A. R*.,** Sousa, C. E. A., Marques, A. C., Tavares, A. P. M., Matos, A. M., Cruz, M. T., Moreira, F.T.C., Martins, R., Fortunato, E., Sales, M. G., Paper-Based Biosensors for COVID-19: A Review of Innovative Tools for Controlling the Pandemic. ACS Omega **2021**, 6, 44. https://doi.org/10.1021/acsomega.1c04012

*Equal first authors

- **Cardoso, A. R.;** Alves, J.F., Frasco, M., Piloto, A. M., Serrano, V., Mateus, D., Sebastião, A. I., Matos, A. M., Carmo, A., Cruz, M.T., Fortunato, E., Sales, M. G. An ultra-sensitive electrochemical biosensor using the Spike protein for capturing antibodies against SARS-CoV-2 in point-of-care. Materials Today Bio **2022**, 16100354. https://doi.org/10.1016/j.mtbio.2022.100354.

8.1.2 Invited chapter books:

- Marques, A. C*., Pinheiro, T*., Martins, G*. V., **Cardoso, A. R***.; Martins, R., Sales, M. G., Fortunato, E. Non-Enzymatic Lab-on-Paper Devices for Biosensing Application. In Comprehensive Analytical Chemistry, Elsevier, **2020**, Vol. 89, pp 189–237.

*Equal first authors

The publications of the candidate, during the thesis period, from which results are not present in this dissertation are listed below:

- •**Cardoso A.R.,** Tavares A.P.M, Sales M.G.F, In-situ generated molecularly imprinted material for chloramphenicol electrochemical sensing in waters down to the nanomolar level. Sensors and Actuators B: Chemical, **2018,** 256. (https://doi.org/10.1016/j.snb.2017.10.114)

- Cabral-Miranda*, G., **Cardoso, A.R***., Ferreira, L.C.S., Sales, M.G.F., Bachmann, M.F, Biosensor-based selective detection of Zika virus specific antibodies in infected individuals. Biosensors and Bioelectronics, **2018,** .113. (https://doi.org/10.1016/j.bios.2018.04.058)

*. Equal first author

- **Cardoso, A.R**.*, Marques, A.C.*, Santos, L., Carvalho F. A., Costa M. F., Martins R., Sales, M.G.F., Fortunato, E. Molecularly-imprinted chloramphenicol sensor with laser-induced graphene electrodes. Biosensors and Bioelectronics, **2019,** 124–125, 167–175. (https://doi.org/10.1016/j.bios.2018.10.01)

*. Equal first author

** To whom correspondence

- **Cardoso, A.R.,** de Sá, M.H., Sales, M.G.F, An impedimetric molecularly-imprinted biosensor for Interleukin-1 β determination, prepared by *in-situ* electropolymerization on carbon screen-printed electrodes. Bioelectrochemistry, **2019**, 130. (https://doi.org/10.1016/j.bioelechem.2019.04.017)

- Marques, A.C.*, **Cardoso, A.R**.*, Martins, R., Sales, M.G.F., Fortunato, E., Laser-Induced Graphene-Based Platforms for Dual Biorecognition of Molecules. ACS Applied Nano Materials, **2020,** 3(3), 2795–2803. (https://dx.doi.org/10.1021/acsanm.0c00117)

*. Equal first author

- Serrano, V.M., **Cardoso, A.R.,** Diniz, M., Sales, M.G.F., In-situ production of Histamine-imprinted polymeric materials for electrochemical monitoring of fish. Sensors and Actuators, B: Chemical, **2020**, 311. (https://doi.org/10.1016/j.snb.2020.127902)
- **Cardoso, A.R.,** Carneiro, L.P.T., Cabral-Miranda, G., Bachmann, M.F., Sales, M.G.F., Employing bacteria machinery for antibiotic detection: Using DNA gyrase for ciprofloxacin detection. Chemical Engineering Journal, **2021**, 409. (https://doi.org/10.1016/j.cej.2020.128135)

- Serrano, V.M., Silva, I.S.P., **Cardoso, A.R**., Sales, M.G.F., Carbon Electrodes with Gold Nanoparticles for the Electrochemical Detection of miRNA 21-5p. Chemosensors, **2022,** 10(5), 189**.** (https://doi.org/10.3390/chemosensors10050189)

- Vaz, R., Serrano, V.M., Castaño-Guerrero, Y., **Cardoso, A.R**., Frasco, M.F., Sales, M.G.F, Breaking the classics: Next-generation biosensors for the isolation, profiling and detection of extracellular vesicles. Biosensors and Bioelectronics: X, **2022**, 10. (https://doi.org/10.1016/j.biosx.2022.100115)

8.2 Oral and poster presentations

8.2.1 Oral presentations

- **Cardoso, A. R.;** Alves, J.F., Frasco, M.F., Sales, M.G.F, Biographene for electrochemical applications, XXV Meeting of the Portuguese Electrochemical Society, Coimbra University. 30 August-01 September 2023, Coimbra, Portugal.

8.2.2 Poster presentations

- Ana Rita A. Cardoso, Elvira Fortunato, M. Goreti F. Sales. Driving nanozymes towards stereochemical recognition: application to biomolecules of interest in health. Poster presentation. Encontro Ciência FCT 2021-online. 16-18 May 2021, Lisbon, Portugal.

- Verónica Serrano, Ana Rita Cardoso, M. G. F. Sales. Electrochemical detection of anti-SARS-CoV-2. Poster presentation at the 31st Anniversary World Congress on Biosensors, on-line (2021). 5-9 June 2021, Busan, Korea.

8.3 Participation in international and national research projects

As part of the PhD activities, opportunities to participate in several projects to develop different biosensors for miRNA detection and develop a MIP for alpha-synuclein in Parkinson's Disease. Besides, testing biosensors at microgravity were taken in different activities.

- April 2019 To March 2024 MindGAP (Bridging the gap between Mind and Body)

Development of an electrochemical biosensor composed of complementary miRNA sequences for specific miRNA detection.
(https://mindgap-fet-open.eu/home)

- February 2021 To March 2024 OligoFiT

Development a MIP for alpha -synuclein in Parkinson's Disease.
(https://www.fct.pt/apoios/cooptrans/eranets/jpco_fund/index.phtml.en

- Lab on paper at micro-G

Development of the unmanned automated experiment for testing microfluidic paper-based biosensor in 12 minutes of microgravity. European Low Gravity Association Grant.
(https://www.elgra.org/?p=1493).

- July 2020 to November 2021 TecniCOV

Development of rapid tests for monitoring of antibodies in serum and saliva, COMPETE2020, Lisboa 2020, nº 69745.

8.4 Master thesis guidance

- Rita Monteiro, Development of a Molecularly-Imprinted Polymer based electrochemical biosensor for the detection of Spike Protein in SARS-CoV-2, 2022, Coimbra University (Supervisor: Goreti Sales; Co-Supervisor: **Rita Cardoso**);

- Ederlino Ramos, Development of a redox-free electrochemical biosensor for glucose detection., 2023, Coimbra University (Supervisor: Goreti Sales; Co-Supervisor Akmaral Suleimenova and **Rita Cardoso**);

- Abigail Dias, Development a novel and sustainable substrate to miRNA detection2024, Coimbra University (Supervisor Goreti Sales; Co-Supervisor: Akmaral and **Rita Cardoso**)

- Miguel Godinho, Development an electrochemical biosensor for miRNA26a-5p in real samples 2024, Coimbra University (Supervisor Goreti Sales; Co-Supervisor **Rita Cardoso**)

REFERENCES

[1] " Global Burden of Disease Collaborative Network. Global Burden of Disease Study 2019. Results. Institute for Health Metrics and Evaluation ."

[2] In Grand View Research (No. 978-1-68038-739–1), "Glucose Biosensors Market Size, Share & Trends Analysis Report By Type (Electrochemical, Optical, Others), By End Use (Hospitals, Homecare, Diagnostic centers), By Region, And Segment Forecasts."

[3] O. Pashchenko, T. Shelby, T. Banerjee, and S. Santra, "A Comparison of Optical, Electrochemical, Magnetic, and Colorimetric Point-of-Care Biosensors for Infectious Disease Diagnosis," *ACS Infectious Diseases*, vol. 4, no. 8. American Chemical Society, pp. 1162–1178, Aug. 10, 2018. doi: 10.1021/acsinfecdis.8b00023.

[4] Global Market Insights, "Biosensors Market - By Type (Wearable, Non-wearable), By Technology (Electrochemical, Optical, Thermal, Piezoelectric), By Medical Application (Blood Glucose Testing, Cholesterol Testing, Blood Gas Analysis, Pregnancy Testing), By End-use & Forecast, 2023-2032."

[5] S. Liu, W. Su, and X. Ding, "A review on microfluidic paper-based analytical devices for glucose detection," *Sensors (Switzerland)*, vol. 16, no. 12. MDPI AG, pp. 1–17, Dec. 01, 2016. doi: 10.3390/s16122086.

[6] X. Wang, Y. Hu, and H. Wei, "Nanozymes in bionanotechnology: From sensing to therapeutics and beyond," *Inorg Chem Front*, vol. 3, no. 1, pp. 41–60, Jan. 2016, doi: 10.1039/c5qi00240k.

[7] K. Sode, Y. Takahashi, S. Ohta, W. Tsugawa, and T. Yamazaki, "A new concept for the construction of an artificial dehydrogenase for fructosylamine compounds and its application for an amperometric fructosylamine sensor," 2001.

[8] G. Wulff, "Enzyme-like catalysis by molecularly imprinted polymers," *Chem Rev*, vol. 102, no. 1, pp. 1–27, Jan. 2002, doi: 10.1021/cr980039a.

[9] F. T. C. Moreira, S. Sharma, R. a. F. Dutra, J. P. C. Noronha, A. E. G. Cass, and M. G. F. Sales, "Smart plastic antibody material (SPAM) tailored on disposable screen printed electrodes for protein recognition: Application to myoglobin detection," *Biosens Bioelectron*, vol. 45, no. 1, pp. 237–244, 2013, doi: 10.1016/j.bios.2013.02.012.

[10] L. a a N. a Truta, N. S. Ferreira, and M. G. F. Sales, "Graphene-based biomimetic materials targeting urine metabolite as potential cancer biomarker: Application over different conductive materials for potentiometric transduction," *Electrochim Acta*, vol. 150, pp. 99–107, 2014, doi: 10.1016/j.electacta.2014.10.136.

[11] A. C. Carpenter, I. T. Paulsen, and T. C. Williams, "and Applications," 2018, doi: 10.3390/genes9080375.

[12] D. Grieshaber, R. MacKenzie, J. Vörös, and E. Reimhult, "Electrochemical Biosensors - Sensor Principles and Architectures," *Sensors*, vol. 8, no. 3, pp. 1400–1458, 2008, doi: 10.3390/s8031400.

[13] B. Bohunicky and S. a. Mousa, "Biosensors: The new wave in cancer diagnosis," *Nanotechnol Sci Appl*, vol. 4, no. 1, pp. 1–10, 2011, doi: 10.2147/NSA.S13465.

[14] A. C. Marques, "Office Paper Platform for Bioelectrochromic Detection of Electrochemically Active Bacteria using," *Tungsten Trioxide Nanoprobes*, vol. 3, no. 5, pp. 1–7, 2015, doi: 10.1038/srep09910.

[15] K. Yamada, T. G. Henares, K. Suzuki, and D. Citterio, "Distance-Based Tear Lactoferrin Assay on Microfluidic Paper Device Using Interfacial Interactions on Surface-Modified Cellulose," *ACS Appl Mater Interfaces*, vol. 7, no. 44, pp. 24864–24875, Nov. 2015, doi: 10.1021/acsami.5b08124.

[16] S. Kumar, P. Bhushan, and S. Bhattacharya, "Positively charged silver nanoparticles as labels for paper-based colorimetric detection of heparin," in *IFMBE Proceedings*, Springer Verlag, 2018, pp. 235–240. doi: 10.1007/978-981-10-7554-4_41.

[17] W. Dungchai, O. Chailapakul, and C. S. Henry, "Use of multiple colorimetric indicators for paper-based microfluidic devices," *Anal Chim Acta*, vol. 674, no. 2, pp. 227–233, Aug. 2010, doi: 10.1016/j.aca.2010.06.019.

[18] D. Mabey, R. W. Peeling, A. Ustianowski, and M. D. Perkins, "Diagnostics for the developing world," *Nature Reviews Microbiology*, vol. 2, no. 3. pp. 231–240, Mar. 2004. doi: 10.1038/nrmicro841.

[19] A. C. Marques *et al.*, "Non-enzymatic lab-on-paper devices for biosensing applications," in *Comprehensive Analytical Chemistry*, vol. 89, Elsevier B.V., 2020, pp. 189–237. doi: 10.1016/bs.coac.2020.05.001.

[20] G. G. Morbioli, T. Mazzu-Nascimento, A. M. Stockton, and E. Carrilho, "Technical aspects and challenges of colorimetric detection with microfluidic paper-based analytical devices (μPADs) - A review," *Analytica Chimica Acta*, vol. 970. Elsevier B.V., pp. 1–22, Jun. 01, 2017. doi: 10.1016/j.aca.2017.03.037.

[21] Z. Li, M. You, Y. Bai, Y. Gong, and F. Xu, "Equipment-Free Quantitative Readout in Paper-Based Point-of-Care Testing," *Small Methods*, vol. 4, no. 4. John Wiley and Sons Inc., Apr. 01, 2020. doi: 10.1002/smtd.201900459.

[22] V. Gaudin, "Receptor-based electrochemical biosensors for the detection of contaminants in food products," in *Electrochemical Biosensors*, Elsevier, 2019, pp. 307–365. doi: 10.1016/B978-0-12-816491-4.00011-5.

[23] Y. Huang, J. Xu, J. Liu, X. Wang, and B. Chen, "Disease-Related Detection with Electrochemical Biosensors : A Review," pp. 1–29, 2017, doi: 10.3390/s17102375.

[24] K. Yamanaka, M. C. Vestergaard, and E. Tamiya, "Printable electrochemical biosensors: A focus on screen-printed electrodes and their application," *Sensors (Switzerland)*, vol. 16, no. 10, pp. 1–16, 2016, doi: 10.3390/s16101761.

[25] N. J. Ronkainen, H. Brian, and W. R. Heineman, "Electrochemical biosensors," pp. 1747–1763, 2010, doi: 10.1039/b714449k.

[26] J. G. Pacheco, M. F. Barroso, H. P. A. Nouws, S. Morais, and C. Delerue-Matos, "Biosensors," in *Current Developments in Biotechnology and Bioengineering: Bioprocesses, Bioreactors and Controls*, Elsevier Inc., 2017, pp. 627–648. doi: 10.1016/B978-0-444-63663-8.00021-5.

[27] F. Bettazzi, G. Marrazza, M. Minunni, I. Palchetti, and S. Scarano, "Biosensors and Related Bioanalytical Tools," *Comprehensive Analytical Chemistry*, vol. 77, pp. 1–33, 2017, doi: 10.1016/bs.coac.2017.05.003.

[28] I. H. Cho, D. H. Kim, and S. Park, "Electrochemical biosensors: Perspective on functional nanomaterials for on-site analysis," *Biomaterials Research*, vol. 24, no. 1. BioMed Central Ltd., Feb. 04, 2020. doi: 10.1186/s40824-019-0181-y.

[29] G. Maduraiveeran and W. Jin, "Nanomaterials based electrochemical sensor and biosensor platforms for environmental applications," *Trends in Environmental Analytical Chemistry*, vol. 13. Elsevier B.V., pp. 10–23, Jan. 01, 2017. doi: 10.1016/j.teac.2017.02.001.

[30] M. Pohanka and P. Skládal, "Electrochemical biosensors-principles and applications".

[31] S. Mao, K. Yu, J. Chang, D. A. Steeber, L. E. Ocola, and J. Chen, "Direct growth of vertically-oriented graphene for field-effect transistor biosensor," *Sci Rep*, vol. 3, 2013, doi: 10.1038/srep01696.

[32] J. Ding and W. Qin, "Recent advances in potentiometric biosensors," *TrAC - Trends in Analytical Chemistry*, vol. 124. Elsevier B.V., Mar. 01, 2020. doi: 10.1016/j.trac.2019.115803.

[33] N. J. Ronkainen, H. B. Halsall, and W. R. Heineman, "Electrochemical biosensors," *Chem Soc Rev*, vol. 39, no. 5, pp. 1747–1763, Apr. 2010, doi: 10.1039/b714449k.

[34] D. Grieshaber, R. Mackenzie, J. Vörös, and E. Reimhult, "Electrochemical Biosensors-Sensor Principles and Architectures," *Sensors*, vol. 8, pp. 1400–1458, 2008, [Online]. Available: www.mdpi.org/sensors

[35] C. Karunakaran, R. Rajkumar, and K. Bhargava, *Biosensors and Bioelectronics*. Elsevier, 2015. doi: 10.1016/C2014-0-03790-2.

[36] M. Labib, E. H. Sargent, and S. O. Kelley, "Electrochemical Methods for the Analysis of Clinically Relevant Biomolecules," *Chemical Reviews*, vol. 116, no. 16. American Chemical Society, pp. 9001–9090, Aug. 24, 2016. doi: 10.1021/acs.chemrev.6b00220.

[37] E. B. Bahadir and M. K. Sezgintürk, "A review on impedimetric biosensors," *Artificial Cells, Nanomedicine and Biotechnology*, vol. 44, no. 1. Taylor and Francis Ltd., pp. 248–262, Jan. 01, 2016. doi: 10.3109/21691401.2014.942456.

[38] J. A. Lee, S. Hwang, J. Kwak, S. Il Park, S. S. Lee, and K. C. Lee, "An electrochemical impedance biosensor with aptamer-modified pyrolyzed carbon electrode for label-free protein detection," *Sens Actuators B Chem*, vol. 129, no. 1, pp. 372–379, Jan. 2008, doi: 10.1016/j.snb.2007.08.034.

[39] Y. Wang, Z. Ye, and Y. Ying, "New trends in impedimetric biosensors for the detection of foodborne pathogenic bacteria," *Sensors*, vol. 12, no. 3. pp. 3449–3471, Mar. 2012. doi: 10.3390/s120303449.

[40] J. Muñoz, R. Montes, and M. Baeza, "Trends in electrochemical impedance spectroscopy involving nanocomposite transducers: Characterization, architecture surface and biosensing," *TrAC - Trends in Analytical Chemistry*, vol. 97. Elsevier B.V., pp. 201–215, Dec. 01, 2017. doi: 10.1016/j.trac.2017.08.012.

[41] C. M. A. Brett, "Electrochemical Impedance Spectroscopy in the Characterisation and Application of Modified Electrodes for Electrochemical Sensors and Biosensors," *Molecules*, vol. 27, no. 5, Mar. 2022, doi: 10.3390/molecules27051497.

[42] H. Pratikno and H. S. Titah, "Bio-corrosion on Aluminium 6063 by Escherichia coli in Marine Environment," 2017.

[43] M. Sharifirad, F. Kiani, and F. Koohyar, "Glassy carbon electrode modified by Poly(m-aminobenzoic acid)/ nano SiO 2 film and electrical and electrochemical properties," *European Online Journal of Natural and Social Sciences*, vol. 2, no. 3, pp. 366–378, 2013, [Online]. Available: www.european-science.com

[44] R. A. Hackett and A. Steptoe, "Psychosocial Factors in Diabetes and Cardiovascular Risk," *Current Cardiology Reports*, vol. 18, no. 10. Current Medicine Group LLC 1, Oct. 01, 2016. doi: 10.1007/s11886-016-0771-4.

[45] S. Jang and C. Xu, "Review of emerging approaches in non- or minimally invasive glucose monitoring and their application to physiological human body fluids," vol. 4, no. 1, pp. 6–10, 2018, doi: 10.15406/ijbsbe.2018.04.00087.

[46] D. Bruen, C. Delaney, L. Florea, and D. Diamond, "Glucose Sensing for Diabetes Monitoring : Recent Developments," pp. 1–21, 2017, doi: 10.3390/s17081866.

[47] M. Gusev *et al.*, "Review Article Noninvasive Glucose Measurement Using Machine Learning and Neural Network Methods and Correlation with Heart Rate Variability," vol. 2020, 2020.

[48] M. Z. Banday, A. S. Sameer, and S. Nissar, "Pathophysiology of diabetes: An overview," *Avicenna J Med*, vol. 10, no. 04, pp. 174–188, Oct. 2020, doi: 10.4103/ajm.ajm_53_20.

[49] J. Wang, "Electrochemical glucose biosensors," *Chemical Reviews*, vol. 108, no. 2. pp. 814–825, Feb. 2008. doi: 10.1021/cr068123a.

[50] S. Vigneshvar, C. C. Sudhakumari, B. Senthilkumaran, and H. Prakash, "Recent Advances in Biosensor Technology for Potential Applications – An Overview," vol. 4, no. February, pp. 1–9, 2016, doi: 10.3389/fbioe.2016.00011.

[51] M. Taguchi, A. Ptitsyn, E. S. Mclamore, J. C. Claussen, and J. C. Claussen, "Monitoring Glucose," 2014, doi: 10.1177/1932296814522799.

[52] L. C. Clark and C. Lyons, "ELECTRODE SYSTEMS FOR CONTINUOUS MONITORING IN CARDIOVASCULAR SURGERY," *Annals New York Academy of Sciences*, 1962.

[53] E.-H. Yoo and S.-Y. Lee, "Glucose biosensors: an overview of use in clinical practice.," *Sensors (Basel)*, vol. 10, no. 5, pp. 4558–76, 2010, doi: 10.3390/s100504558.

[54] H. Lee, Y. J. Hong, S. Baik, T. Hyeon, and D. Kim, "Enzyme-Based Glucose Sensor : From Invasive to Wearable Device," vol. 1701150, pp. 1–14, 2018, doi: 10.1002/adhm.201701150.

[55] D. Tankasala and J. C. Linnes, "Noninvasive glucose detection in exhaled," *Translational Research*, vol. 213, pp. 1–22, 2019, doi: 10.1016/j.trsl.2019.05.006.

[56] W. V. Gonzales, A. T. Mobashsher, and A. Abbosh, "The Progress of Glucose Monitoring—A Review of Invasive to Minimally and Non-Invasive Techniques, Devices and Sensors," *Sensors*, vol. 19, no. 800, pp. 1–45, 2019, doi: 10.3390/s19040800.

[57] S. J. Updike and G. P. Hicks, "The enzyme electrode," *Nature*, vol. 214, no. 5092, pp. 986–988, 1967.

[58] N. Asghar, G. Mustafa, M. Yasinzai, and Y. A. Al-soud, "Real-Time and Online Monitoring of Glucose Contents by Using Molecular Imprinted Polymer-Based IDEs Sensor," pp. 1156–1166, 2019.

[59] T.-T. Wang, X.-F. Huang, H. Huang, P. Luo, and L.-S. Qing, "Nanomaterial-based optical- and electrochemical-biosensors for urine glucose detection: A comprehensive review," *Advanced Sensor and Energy Materials*, vol. 1, no. 3, p. 100016, Sep. 2022, doi: 10.1016/j.asems.2022.100016.

[60] S. Je, H. Noh, M. Won, C. Cho, and K. Bok, "Biosensors and Bioelectronics A selective glucose sensor based on direct oxidation on a bimetal catalyst with a molecular im-printed polymer," *Biosensors and Bioelectronic*, vol. 99, no. August 2017, pp. 471–478, 2018, doi: 10.1016/j.bios.2017.08.022.

[61] H. H. Nguyen, S. H. Lee, U. J. Lee, C. D. Fermin, and M. Kim, "Immobilized Enzymes in Biosensor Applications," *Materials*, vol. 12, no. 121, pp. 1–34, 2019, doi: 10.3390/ma12010121.

[62] B. J. van Enter and E. Von Hauff, "Challenges and perspectives in continuous," pp. 5032–5045, 2018, doi: 10.1039/c8cc01678j.

[63] J. J. Belbruno, "Molecularly Imprinted Polymers," *Chem Rev*, vol. 119, pp. 94–119, 2018, doi: 10.1021/acs.chemrev.8b00171.

[64] World Health Organization, "WHO Coronavirus (COVID-19) Dashboard | WHO Corona-virus (COVID-19) Dashboard With Vaccination Data."

[65] V. M. Corman *et al.*, "Detection of 2019 novel coronavirus (2019-nCoV) by real-time RT-PCR," *Eurosurveillance*, vol. 25, no. 3, Jan. 2020, doi: 10.2807/1560-7917.ES.2020.25.3.2000045.

[66] G. M. Bwire, M. V. Majigo, B. J. Njiro, and A. Mawazo, "Detection profile of SARS-CoV-2 using RT-PCR in different types of clinical specimens: A systematic review and meta-analysis," *Journal of Medical Virology*, vol. 93, no. 2. John Wiley and Sons Inc, pp. 719–725, Feb. 01, 2021. doi: 10.1002/jmv.26349.

[67] M. P. Cheng *et al.*, "Diagnostic testing for severe acute respiratory syndrome–related coronavirus 2: A narrative review," *Annals of Internal Medicine*, vol. 172, no. 11. American College of Physicians, pp. 726–734, Jun. 02, 2020. doi: 10.7326/M20-1301.

[68] M. Shen *et al.*, "Recent advances and perspectives of nucleic acid detection for corona-virus," *Journal of Pharmaceutical Analysis*, vol. 10, no. 2. Xi'an Jiaotong University, pp. 97–101, Apr. 01, 2020. doi: 10.1016/j.jpha.2020.02.010.

[69] W. Feng *et al.*, "Molecular Diagnosis of COVID-19: Challenges and Research Needs," *Analytical Chemistry*, vol. 92, no. 15. American Chemical Society, pp. 10196–10209, Aug. 04, 2020. doi: 10.1021/acs.analchem.0c02060.

[70] E. Morales-Narváez and C. Dincer, "The impact of biosensing in a pandemic outbreak: COVID-19," *Biosens Bioelectron*, vol. 163, Sep. 2020, doi: 10.1016/j.bios.2020.112274.

[71] C. K. C. Lai and W. Lam, "Laboratory testing for the diagnosis of COVID-19," *Biochem Biophys Res Commun*, vol. 538, pp. 226–230, Jan. 2021, doi: 10.1016/j.bbrc.2020.10.069.

[72] B. Giri, S. Pandey, R. Shrestha, K. Pokharel, F. S. Ligler, and B. B. Neupane, "Review of analytical performance of COVID-19 detection methods", doi: 10.1007/s00216-020-02889-x/Published.

[73] A. Hosseini *et al.*, "Roadmap to the Bioanalytical Testing of COVID-19: From Sample Collection to Disease Surveillance," *ACS Sensors*, vol. 5, no. 11. American Chemical Society, pp. 3328–3345, Nov. 25, 2020. doi: 10.1021/acssensors.0c01377.

[74] Q. Song *et al.*, "Point-of-care testing detection methods for COVID-19," *Lab on a Chip*, vol. 21, no. 9. Royal Society of Chemistry, pp. 1634–1660, May 07, 2021. doi: 10.1039/d0lc01156h.

[75] J. R. Choi, "Development of Point-of-Care Biosensors for COVID-19," *Frontiers in Chemistry*, vol. 8. Frontiers Media S.A., May 27, 2020. doi: 10.3389/fchem.2020.00517.

[76] A. K. Azkur *et al.*, "Immune response to SARS-CoV-2 and mechanisms of immunopathological changes in COVID-19," *Allergy: European Journal of Allergy and Clinical Immunology*, vol. 75, no. 7. Blackwell Publishing Ltd, pp. 1564–1581, Jul. 01, 2020. doi: 10.1111/all.14364.

[77] V. K. Shah, P. Firmal, A. Alam, D. Ganguly, and S. Chattopadhyay, "Overview of Immune Response During SARS-CoV-2 Infection: Lessons From the Past," *Frontiers in Immunology*, vol. 11. Frontiers Media S.A., Aug. 07, 2020. doi: 10.3389/fimmu.2020.01949.

[78] Y. Jin *et al.*, "Diagnostic value and dynamic variance of serum antibody in coronavirus disease 2019," *International Journal of Infectious Diseases*, vol. 94, pp. 49–52, May 2020, doi: 10.1016/j.ijid.2020.03.065.

[79] W. Zhang *et al.*, "Molecular and serological investigation of 2019-nCoV infected patients: implication of multiple shedding routes," *Emerg Microbes Infect*, vol. 9, no. 1, pp. 386–389, Jan. 2020, doi: 10.1080/22221751.2020.1729071.

[80] B. Sun *et al.*, "Kinetics of SARS-CoV-2 specific IgM and IgG responses in COVID-19 patients," *Emerg Microbes Infect*, vol. 9, no. 1, pp. 940–948, Jan. 2020, doi: 10.1080/22221751.2020.1762515.

[81] K. K. W. To *et al.*, "Temporal profiles of viral load in posterior oropharyngeal saliva samples and serum antibody responses during infection by SARS-CoV-2: an observational cohort study," *Lancet Infect Dis*, vol. 20, no. 5, pp. 565–574, May 2020, doi: 10.1016/S1473-3099(20)30196-1.

[82] T. Pinheiro *et al.*, "Paper-Based Biosensors for COVID-19: A Review of Innovative Tools for Controlling the Pandemic," *ACS Omega*, vol. 6, no. 44. American Chemical Society, pp. 29268–29290, Nov. 09, 2021. doi: 10.1021/acsomega.1c04012.

[83] C. Jiang, X. Mu, B. Du, and Z. Tong, "A review of electrochemical biosensor application in the detection of the SARS-COV-2," *Micro and Nano Letters*, vol. 17, no. 3. John Wiley and Sons Inc, pp. 49–58, Mar. 01, 2022. doi: 10.1049/mna2.12101.

[84] M. S. Andrianova, O. S. Panova, A. A. Titov, N. V. Komarova, and A. E. Kuznetsov, "Electrochemical Biosensors for SARS-CoV-2 Detection," *Moscow University Chemistry Bulletin*, vol. 78, no. 5, pp. 231–254, Oct. 2023, doi: 10.3103/S0027131423050048.

[85] M. M. Rahman, "Progress in Electrochemical Biosensing of SARS-CoV-2 Virus for COVID-19 Management," *Chemosensors*, vol. 10, no. 7. MDPI, Jul. 01, 2022. doi: 10.3390/chemosensors10070287.

[86] O. Sadak *et al.*, "Electrochemical Biosensing and Deep Learning-Based Approaches in the Diagnosis of COVID-19: A Review," *IEEE Access*, vol. 10. Institute of Electrical and Electronics Engineers Inc., pp. 98633–98648, 2022. doi: 10.1109/ACCESS.2022.3207207.

[87] S. Mao, L. Fu, C. Yin, X. Liu, and H. Karimi-Maleh, "The role of electrochemical biosensors in SARS-CoV-2 detection: a bibliometrics-based analysis and review," *RSC Advances*, vol. 12, no. 35. Royal Society of Chemistry, pp. 22592–22607, Aug. 12, 2022. doi: 10.1039/d2ra04162f.

[88] O. Ramstriim, I. A. Nicholls, and K. Mosbach', "Synthetic Peptide Receptor Mimics: Highly Stereoselective Recognition in Non-Covalent Molecularly Imprinted Polymers."

[89] D. Refaat *et al.*, "Strategies for molecular imprinting and the evolution of MIP nanoparticles as plastic antibodies—synthesis and applications," *International Journal of Molecular Sciences*, vol. 20, no. 24. MDPI AG, Dec. 02, 2019. doi: 10.3390/ijms20246304.

[90] L. Ye and K. Mosbach, "Molecularly imprinted microspheres as antibody binding mimics," *React Funct Polym*, vol. 48, pp. 149–157, 2001.

[91] C. Dong, H. Shi, Y. Han, Y. Yang, R. Wang, and J. Men, "Molecularly imprinted polymers by the surface imprinting technique," *European Polymer Journal*, vol. 145. Elsevier Ltd, Feb. 15, 2021. doi: 10.1016/j.eurpolymj.2020.110231.

[92] K. Mosbach and O. Ramström, "The Emerging Technique of Molecular Imprinting and Its Future on Biotechnology," *Nature Biotechnology* , vol. 14, pp. 163–170, 1996.

[93] M. J. Whitcombe *et al.*, "The rational development of molecularly imprinted polymer-based sensors for protein detection," *Chem Soc Rev*, vol. 40, no. 3, pp. 1547–1571, Feb. 2011, doi: 10.1039/c0cs00049c.

[94] T. Cowen, K. Karim, and S. Piletsky, "Computational approaches in the design of synthetic receptors – A review," *Analytica Chimica Acta*, vol. 936. Elsevier B.V., pp. 62–74, Sep. 14, 2016. doi: 10.1016/j.aca.2016.07.027.

[95] J. J. Belbruno, "Molecularly Imprinted Polymers," *Chemical Reviews*, vol. 119, no. 1. American Chemical Society, pp. 94–119, Jan. 09, 2019. doi: 10.1021/acs.chemrev.8b00171.

[96] H. R. Culver and N. A. Peppas, "Protein-Imprinted Polymers: The Shape of Things to Come?," *Chemistry of Materials*, vol. 29, no. 14, pp. 5753–5761, Jul. 2017, doi: 10.1021/acs.chemmater.7b01936.

[97] V. D. Salian and M. E. Byrne, "Living Radical Polymerization and Molecular Imprinting : Improving Polymer Morphology in Imprinted Polymers," *Macromol. Mater. Eng.*, vol. 298, pp. 379–390, 2013, doi: 10.1002/mame.201200191.

[98] F. T. C. Moreira, A. P. Moreira-Tavares, M. Goreti, and F. Sales, "Sol-Gel-Based Biosensing Applied to Medicinal Science," 2015.

[99] L. Chen, X. Wang, W. Lu, X. Wu, and J. Li, "Molecular imprinting: Perspectives and applications," *Chemical Society Reviews*, vol. 45, no. 8. Royal Society of Chemistry, pp. 2137–2211, Apr. 21, 2016. doi: 10.1039/c6cs00061d.

[100] M. F. Frasco, L. A. A. N. A. Truta, M. G. F. Sales, and F. T. C. Moreira, "Imprinting Technology in Electrochemical Biomimetic Sensors," *Sensors*, vol. 17, no. 523, pp. 1–29, 2017, doi: 10.3390/s17030523.

[101] A. R. Cardoso *et al.*, "Molecularly-imprinted chloramphenicol sensor with laser-induced graphene electrodes," *Biosensors and Bioelectronic*, vol. 124–125, pp. 167–175, 2019, doi: 10.1016/j.bios.2018.10.015.

[102] A. P. M. Tavares, M. H. De Sá, and M. G. F. Sales, "Innovative screen-printed electrodes on cork composite substrates applied to sulfadiazine electrochemical sensing," *Journal of Electroanalytical Chemistry*, vol. 880, p. 114922, 2021, doi: 10.1016/j.jelechem.2020.114922.

[103] G. V Martins, A. C. Marques, E. Fortunato, and M. G. F. Sales, "Wax-printed paper-based device for direct electrochemical detection of 3-nitrotyrosine," *Electrochim Acta*, vol. 284, pp. 60–68, 2018, doi: 10.1016/j.electacta.2018.07.150.

[104] R. D. Crapnell, N. C. Dempsey-hibbert, M. Peeters, A. Tridente, and C. E. Banks, "Talanta Open Molecularly imprinted polymer based electrochemical biosensors : Overcoming the challenges of detecting vital biomarkers and speeding up diagnosis," *Talanta Open*, vol. 2, p. 100018, 2020, doi: 10.1016/j.talo.2020.100018.

[105] C. Dong, H. Shi, Y. Han, Y. Yang, R. Wang, and J. Men, "Molecularly imprinted polymers by the surface imprinting technique," *Eur Polym J*, vol. 145, p. 110231, 2021, doi: 10.1016/j.eurpolymj.2020.110231.

[106] S. Piletsky, F. Canfarotta, A. Poma, A. M. Bossi, and S. Piletsky, "Molecularly Imprinted Polymers for Cell Recognition," *Trends Biotechnol*, vol. 38, no. 4, pp. 368–387, doi: 10.1016/j.tibtech.2019.10.002.

[107] T. Vaneckova, J. Bezdekova, G. Han, V. Adam, and M. Vaculovicova, "Application of molecularly imprinted polymers as artificial receptors for imaging," *Acta Biomater*, vol. 101, pp. 444–458, 2020, doi: 10.1016/j.actbio.2019.11.007.

[108] J. Xu, H. Miao, J. Wang, and G. Pan, "Molecularly Imprinted Synthetic Antibodies : From Chemical Design to Biomedical Applications," *Small*, vol. 1906644, pp. 1–21, 2020, doi: 10.1002/smll.201906644.

[109] S. Bhogal, K. Kaur, A. Kumar, C. Sonne, S. Soo, and K. Kim, "Core-shell structured molecularly imprinted materials for sensing applications," *Trends in Analytical Chemistry*, vol. 133, p. 116043, 2020, doi: 10.1016/j.trac.2020.116043.

[110] Z. El-Schich *et al.*, "Review Molecularly imprinted polymers in biological applications," *Biotechniques*, vol. 69, no. 6, pp. 407–420, 2020.

[111] A. Leonhardt and K. Mosbach, "Enzyme-Mimicking Polymers Exhibiting Specific Substrate Binding and Catalytic Functions," *Reactive Polymers*, vol. 6, pp. 285–290, 1987.

[112] D. K. Robinson and K. Mosbach, "Molecular Imprinting of a Transition State Analogue Leads to a Polymer Exhibiting Esterolytic Activity," *J Chem Soc Chem Commun*, no. 1, pp. 969–970, 1989.

[113] B. Sellergren, R. N. Karmalkar, and K. J. Shea, "Enantioselective Ester Hydrolysis Catalyzed by Imprinted," *J. Org. Chem.*, no. 9, pp. 4009–4027, 2000.

[114] G. Wulff and L. Junqiu, "Design of Biomimetic Catalysts by Molecular Imprinting in Synthetic Polymers : The Role of," *Acc Chem Res*, vol. 45, no. 2, pp. 239–247, 2012.

[115] D. Mathew, B. Thomas, and K. S. Devaky, "Geometrical effect of 3D-memory cavity on the imprinting efficiency of transition-state analogue-built artificial hydrolases," *Polymer Bulletin*, vol. 75, pp. 3883–3896, 2018, doi: 10.1007/s00289-017-2237-2.

[116] M. Resmini, "Molecularly imprinted polymers as biomimetic catalysts," *Anal Bioanal Chem*, vol. 402, pp. 3021–3026, 2012, doi: 10.1007/s00216-011-5671-2.

[117] O. Ramström and K. Mosbach, "Synthesis and catalysis by molecularly imprinted materials," *Curr Opin Chem Biol*, pp. 759–764, 1999.

[118] D. Mathew, B. Thomas, K. S. Devaky, D. Mathew, B. Thomas, and K. S. D. Transition, "Transition state analogue imprinted polymers as artificial amidases for amino acid p -nitroanilides : morphological effects of polymer network on catalytic efficiency," *Artif Cells Nanomed Biotechnol*, vol. 46, no. 8, pp. 1830–1837, 2018, doi: 10.1080/21691401.2017.1394871.

[119] J. Pan *et al.*, "Rapid hydrolysis of nerve agent simulants by molecularly imprinted porous crosslinked polymer incorporating mononuclear zinc (II) - picolinamine-amidoxime module," *J Catal*, vol. 380, pp. 83–90, 2019, doi: 10.1016/j.jcat.2019.10.023.

[120] M. Stepanova, O. Solomakha, D. Ten, T. Tennikova, and E. Korzhikova-Vlakh, "Flow-Through Macroporous Polymer Monoliths Containing Artificial Catalytic Centers Mimicking Chymotrypsin Active Site," *catalysts*, vol. 10, no. 1395, pp. 1–19, 2020.

[121] T. Monteiro and M. G. Almeida, "Electrochemical Enzyme Biosensors Revisited: Old Solutions for New Problems," *Critical Reviews in Analytical Chemistry*, vol. 49, no. 1. Taylor and Francis Ltd., pp. 44–66, Jan. 02, 2019. doi: 10.1080/10408347.2018.1461552.

[122] M. Hamid and Khalil-ur-Rehman, "Potential applications of peroxidases," *Food Chemistry*, vol. 115, no. 4. pp. 1177–1186, Aug. 15, 2009. doi: 10.1016/j.foodchem.2009.02.035.

[123] M. Ali *et al.*, "Paper-based selective and quantitative detection of uric acid using citrate-capped Pt nanoparticles (PtNPs) as a colorimetric sensing probe through a simple and remote-based device," *New Journal of Chemistry*, vol. 43, no. 20, pp. 7636–7645, 2019, doi: 10.1039/c9nj01257e.

[124] P. Si, Y. Huang, T. Wang, and J. Ma, "Nanomaterials for electrochemical non-enzymatic glucose biosensors," *RSC Advances*, vol. 3, no. 11. Royal Society of Chemistry, pp. 3487–3502, Mar. 21, 2013. doi: 10.1039/c2ra22360k.

[125] X. Tao, X. Wang, B. Liu, and J. Liu, "Conjugation of antibodies and aptamers on nanozymes for developing biosensors," *Biosens Bioelectron*, vol. 168, Nov. 2020, doi: 10.1016/j.bios.2020.112537.

[126] Y. Lin, J. Ren, and X. Qu, "Catalytically active nanomaterials: A promising candidate for artificial enzymes," *Acc Chem Res*, vol. 47, no. 4, pp. 1097–1105, Apr. 2014, doi: 10.1021/ar400250z.

[127] M. Resmini, "Molecularly imprinted polymers as biomimetic catalysts," *Anal Bioanal Chem*, vol. 402, no. 10, pp. 3021–3026, Apr. 2012, doi: 10.1007/s00216-011-5671-2.

[128] H. Wei and E. Wang, "Nanomaterials with enzyme-like characteristics (nanozymes): Next-generation artificial enzymes," *Chem Soc Rev*, vol. 42, no. 14, pp. 6060–6093, Jun. 2013, doi: 10.1039/c3cs35486e.

[129] C. Revathi and R. T. Rajendra Kumar, "Enzymatic and nonenzymatic electrochemical biosensors," in *Fundamentals and Sensing Applications of 2D Materials*, Elsevier, 2019, pp. 259–300. doi: 10.1016/B978-0-08-102577-2.00007-5.

[130] M. Nasir, M. H. Nawaz, U. Latif, M. Yaqub, A. Hayat, and A. Rahim, "An overview on enzyme-mimicking nanomaterials for use in electrochemical and optical assays," *Microchimica Acta*, vol. 184, no. 2. Springer-Verlag Wien, pp. 323–342, Feb. 01, 2017. doi: 10.1007/s00604-016-2036-8.

[131] L. Gao *et al.*, "Intrinsic peroxidase-like activity of ferromagnetic nanoparticles," *Nat Nanotechnol*, vol. 2, no. 9, pp. 577–583, 2007, doi: 10.1038/nnano.2007.260.

[132] Y. Huang, J. Ren, and X. Qu, "Nanozymes: Classification, Catalytic Mechanisms, Activity Regulation, and Applications," *Chemical Reviews*, vol. 119, no. 6. American Chemical Society, pp. 4357–4412, Mar. 27, 2019. doi: 10.1021/acs.chemrev.8b00672.

[133] H. Dong, Y. Fan, W. Zhang, N. Gu, and Y. Zhang, "Catalytic mechanisms of nanozymes and their applications in biomedicine," *Bioconjugate Chemistry*, vol. 30, no. 5. American Chemical Society, pp. 1273–1296, May 15, 2019. doi: 10.1021/acs.bioconjchem.9b00171.

[134] H. Dong, Y. Fan, W. Zhang, N. Gu, and Y. Zhang, "Catalytic mechanisms of nanozymes and their applications in biomedicine," *Bioconjugate Chemistry*, vol. 30, no. 5. American Chemical Society, pp. 1273–1296, May 15, 2019. doi: 10.1021/acs.bioconjchem.9b00171.

[135] R. G. Mahmudunnabi, F. Z. Farhana, N. Kashaninejad, S. H. Firoz, Y. B. Shim, and M. J. A. Shiddiky, "Nanozyme-based electrochemical biosensors for disease biomarker detection," *Analyst*, vol. 145, no. 13. Royal Society of Chemistry, pp. 4398–4420, Jul. 07, 2020. doi: 10.1039/d0an00558d.

[136] A. R. Cardoso, M. F. Frasco, V. Serrano, E. Fortunato, and M. G. F. Sales, "Molecular imprinting on nanozymes for sensing applications," *Biosensors*, vol. 11, no. 5. MDPI, 2021. doi: 10.3390/bios11050152.

[137] J. Wu *et al.*, "Nanomaterials with enzyme-like characteristics (nanozymes): Next-generation artificial enzymes (II)," *Chemical Society Reviews*, vol. 48, no. 4. Royal Society of Chemistry, pp. 1004–1076, Feb. 21, 2019. doi: 10.1039/c8cs00457a.

[138] F. Manea, F. B. Houillon, L. Pasquato, and P. Scrimin, "Nanozymes: Gold-nanoparticle-based transphosphorylation catalysts," *Angewandte Chemie - International Edition*, vol. 43, no. 45, pp. 6165–6169, Nov. 2004, doi: 10.1002/anie.200460649.

[139] H. Shu, L. Cao, G. Chang, H. He, Y. Zhang, and Y. He, "Direct electrodeposition of gold nanostructures onto glassy carbon electrodes for non-enzymatic detection of glucose," *Electrochim Acta*, vol. 132, pp. 524–532, Jun. 2014, doi: 10.1016/j.electacta.2014.04.031.

[140] C. Yang, M. E. Denno, P. Pyakurel, and B. J. Venton, "Recent trends in carbon nanomaterial-based electrochemical sensors for biomolecules: A review," *Analytica Chimica Acta*, vol. 887. Elsevier B.V., pp. 17–37, Aug. 05, 2015. doi: 10.1016/j.aca.2015.05.049.

[141] H. Zhu, L. Li, W. Zhou, Z. Shao, and X. Chen, "Advances in non-enzymatic glucose sensors based on metal oxides," *Journal of Materials Chemistry B*, vol. 4, no. 46. Royal Society of Chemistry, pp. 7333–7349, 2016. doi: 10.1039/C6TB02037B.

[142] M. Liang and X. Yan, "Nanozymes: From New Concepts, Mechanisms, and Standards to Applications," *Acc Chem Res*, vol. 52, no. 8, pp. 2190–2200, Aug. 2019, doi: 10.1021/acs.accounts.9b00140.

[143] D. Jiang, D. Ni, Z. T. Rosenkrans, P. Huang, X. Yan, and W. Cai, "Nanozyme: New horizons for responsive biomedical applications," *Chemical Society Reviews*, vol. 48, no. 14. Royal Society of Chemistry, pp. 3683–3704, Jul. 21, 2019. doi: 10.1039/c8cs00718g.

[144] Y. Lin, J. Ren, and X. Qu, "Nano-gold as artificial enzymes: Hidden talents," *Advanced Materials*, vol. 26, no. 25, pp. 4200–4217, Jul. 2014, doi: 10.1002/adma.201400238.

[145] H. Zhang, L. Lu, Y. Cao, S. Du, Z. Cheng, and S. Zhang, "Fabrication of catalytically active Au/Pt/Pd trimetallic nanoparticles by rapid injection of NaBH4," *Mater Res Bull*, vol. 49, no. 1, pp. 393–398, 2014, doi: 10.1016/j.materresbull.2013.09.025.

[146] P. Zhang *et al.*, "Modified carbon nitride nanozyme as bifunctional glucose oxidase-peroxidase for metal-free bioinspired cascade photocatalysis," *Nat Commun*, vol. 10, no. 1, Dec. 2019, doi: 10.1038/s41467-019-08731-y.

[147] P. Li *et al.*, "Group IV nanodots: Newly emerging properties and application in biomarkers sensing," *TrAC - Trends in Analytical Chemistry*, vol. 131. Elsevier B.V., Oct. 01, 2020. doi: 10.1016/j.trac.2020.116007.

[148] A. R. Cardoso, M. F. Frasco, V. Serrano, E. Fortunato, and M. G. F. Sales, "Molecular imprinting on nanozymes for sensing applications," *Biosensors*, vol. 11, no. 5. MDPI, 2021. doi: 10.3390/bios11050152.

[149] H. Liang *et al.*, "Multicopper laccase mimicking nanozymes with nucleotides as ligands," *ACS Appl Mater Interfaces*, vol. 9, no. 2, pp. 1352–1360, Jan. 2017, doi: 10.1021/acsami.6b15124.

[150] J. Chen, W. Wu, L. Huang, Q. Ma, and S. Dong, "Self-Indicative Gold Nanozyme for H2O2 and Glucose Sensing," *Chemistry - A European Journal*, vol. 25, no. 51, pp. 11940–11944, Sep. 2019, doi: 10.1002/chem.201902288.

[151] X. Liu, Y. Zhou, J. Liu, and H. Xia, "The intrinsic enzyme mimetic activity of platinum oxide for biosensing of glucose," *Spectrochim Acta A Mol Biomol Spectrosc*, vol. 248, Mar. 2021, doi: 10.1016/j.saa.2020.119280.

[152] H. Y. Shin, T. J. Park, and M. Il Kim, "Recent Research Trends and Future Prospects in Nanozymes," *J Nanomater*, vol. 2015, 2015, doi: 10.1155/2015/756278.

[153] X. Liu, J. Yang, J. Cheng, Y. Xu, W. Chen, and Y. Li, "Facile preparation of four-in-one nanozyme catalytic platform and the application in selective detection of catechol and hydroquinone," *Sens Actuators B Chem*, vol. 337, Jun. 2021, doi: 10.1016/j.snb.2021.129763.

[154] H. Wei and E. Wang, "Fe3O4 magnetic nanoparticles as peroxidase mimetics and their applications in H2O2 and glucose detection," *Anal Chem*, vol. 80, no. 6, pp. 2250–2254, Mar. 2008, doi: 10.1021/ac702203f.

[155] F. Cui, Q. Deng, and L. Sun, "Prussian blue modified metal-organic framework MIL-101(Fe) with intrinsic peroxidase-like catalytic activity as a colorimetric biosensing platform," *RSC Adv*, vol. 5, no. 119, pp. 98215–98221, 2015, doi: 10.1039/c5ra18589k.

[156] B. Jiang *et al.*, "Standardized assays for determining the catalytic activity and kinetics of peroxidase-like nanozymes," *Nat Protoc*, vol. 13, no. 7, pp. 1506–1520, Jul. 2018, doi: 10.1038/s41596-018-0001-1.

[157] C. W. Lien, C. C. Huang, and H. T. Chang, "Peroxidase-mimic bismuth-gold nanoparticles for determining the activity of thrombin and drug screening," *Chemical Communications*, vol. 48, no. 64, pp. 7952–7954, Jul. 2012, doi: 10.1039/c2cc32833j.

[158] C. Lien, C. Huang, and H. Chang, "Peroxidase-mimic bismuth–gold nanoparticles for determining the activity of thrombin and drug screening," *Chem. Commun*, vol. 48, pp. 7952–7954, 2012, doi: 10.1039/c2cc32833j.

[159] Q. Wang, H. Wei, Z. Zhang, E. Wang, and S. Dong, "Nanozyme: An emerging alternative to natural enzyme for biosensing and immunoassay," *TrAC - Trends in Analytical Chemistry*, vol. 105. Elsevier B.V., pp. 218–224, Aug. 01, 2018. doi: 10.1016/j.trac.2018.05.012.

[160] Y. Zhou, Y. Wei, J. Ren, and X. Qu, "A chiral covalent organic framework (COF) nanozyme with ultrahigh enzymatic activity," *Mater Horiz*, vol. 7, no. 12, pp. 3291–3297, Dec. 2020, doi: 10.1039/d0mh01535k.

[161] C. Korsvik, S. Patil, S. Seal, and W. T. Self, "Superoxide dismutase mimetic properties exhibited by vacancy engineered ceria nanoparticles," *Chemical Communications*, no. 10, pp. 1056–1058, 2007, doi: 10.1039/b615134e.

[162] T. Pirmohamed *et al.*, "Nanoceria exhibit redox state-dependent catalase mimetic activity," *Chemical Communications*, vol. 46, no. 16, pp. 2736–2738, 2010, doi: 10.1039/b922024k.

[163] G. L. Wang, L. Y. Jin, X. M. Wu, Y. M. Dong, and Z. J. Li, "Label-free colorimetric sensor for mercury(II) and DNA on the basis of mercury(II) switched-on the oxidase-mimicking activity of silver nanoclusters," *Anal Chim Acta*, vol. 871, pp. 1–8, Apr. 2015, doi: 10.1016/j.aca.2015.02.027.

[164] G. Wang, L. Jin, X. Wu, Y. Dong, and Z. Li, "Label-free colorimetric sensor for mercury(II) and DNA on the basis of mercury(II) switched-on the oxidase-mimicking activity of silver nanoclusters," *Anal Chim Acta*, vol. 871, pp. 1–8, 2015, doi: 10.1016/j.aca.2015.02.027.

[165] Y. Zhang, Q. Su, D. Song, J. Fan, and Z. Xu, "Label-free detection of exosomes based on ssDNA-modulated oxidase-mimicking activity of CuCo2O4 nanorods," *Anal Chim Acta*, vol. 1145, pp. 9–16, Feb. 2021, doi: 10.1016/j.aca.2020.12.018.

[166] W. He *et al.*, "Intrinsic catalytic activity of Au nanoparticles with respect to hydrogen peroxide decomposition and superoxide scavenging," *Biomaterials*, vol. 34, no. 3, pp. 765–773, Jan. 2013, doi: 10.1016/j.biomaterials.2012.10.010.

[167] Y. Zhang, Y. Jin, H. Cui, X. Yan, and K. Fan, "Nanozyme-based catalytic theranostics," *RSC Advances*, vol. 10, no. 1. Royal Society of Chemistry, pp. 10–20, 2019. doi: 10.1039/c9ra09021e.

[168] S. Khan, M. Sharifi, S. H. Bloukh, Z. Edis, R. Siddique, and M. Falahati, "In vivo guiding inorganic nanozymes for biosensing and therapeutic potential in cancer, inflammation and microbial infections," *Talanta*, vol. 224. Elsevier B.V., Mar. 01, 2021. doi: 10.1016/j.talanta.2020.121805.

[169] X. Zhang *et al.*, "Recent progress in the construction of nanozyme-based biosensors and their applications to food safety assay," *TrAC - Trends in Analytical Chemistry*, vol. 121. Elsevier B.V., Dec. 01, 2019. doi: 10.1016/j.trac.2019.115668.

[170] S. Campuzano, M. Pedrero, P. Yáñez-Sedeño, and J. M. Pingarrón, "Nanozymes in electrochemical affinity biosensing", doi: 10.1007/s00604-020-04390-9/Published.

[171] S. S. Menon, S. V. Chandran, A. Koyappayil, and S. Berchmans, "Copper- Based Metal-Organic Frameworks as Peroxidase Mimics Leading to Sensitive H2O2 and Glucose Detection," *ChemistrySelect*, vol. 3, no. 28, pp. 8319–8324, Jul. 2018, doi: 10.1002/slct.201800667.

[172] Y. Li and J. Liu, "Nanozyme's catching up: activity, specificity, reaction conditions and reaction types," *Mater Horiz*, 2020, doi: 10.1039/d0mh01393e.

[173] H. Dong, Y. Fan, W. Zhang, N. Gu, and Y. Zhang, "Catalytic mechanisms of nanozymes and their applications in biomedicine," *Bioconjugate Chemistry*, vol. 30, no. 5. American Chemical Society, pp. 1273–1296, May 15, 2019. doi: 10.1021/acs.bioconjchem.9b00171.

[174] Y. Huang, J. Ren, and X. Qu, "Nanozymes: Classification, Catalytic Mechanisms, Activity Regulation, and Applications," *Chemical Reviews*, vol. 119, no. 6. American Chemical Society, pp. 4357–4412, Mar. 27, 2019. doi: 10.1021/acs.chemrev.8b00672.

[175] J. Wu *et al.*, "Nanomaterials with enzyme-like characteristics (nanozymes): Next-generation artificial enzymes (II)," *Chemical Society Reviews*, vol. 48, no. 4. Royal Society of Chemistry, pp. 1004–1076, Feb. 21, 2019. doi: 10.1039/c8cs00457a.

[176] O. Ramström and K. Mosbach, "Synthesis and catalysis by molecularly materials," *Curr Opin Chem Biol*, vol. 3, pp. 759–764, 1999.

[177] T. Vaneckova, J. Bezdekova, G. Han, V. Adam, and M. Vaculovicova, "Application of molecularly imprinted polymers as artificial receptors for imaging," *Acta Biomater*, vol. 101, pp. 444–458, Jan. 2020, doi: 10.1016/j.actbio.2019.11.007.

[178] M. F. Frasco, L. A. A. N. A. Truta, M. G. F. Sales, and F. T. C. Moreira, "Imprinting technology in electrochemical biomimetic sensors," *Sensors (Switzerland)*, vol. 17, no. 3. MDPI AG, Mar. 06, 2017. doi: 10.3390/s17030523.

[179] K. Haupt, P. X. Medina Rangel, and B. T. S. Bui, "Molecularly imprinted polymers: Antibody mimics for bioimaging and therapy," *Chemical Reviews*, vol. 120, no. 17. American Chemical Society, pp. 9554–9582, Sep. 09, 2020. doi: 10.1021/acs.chemrev.0c00428.

[180] J. Xu, H. Miao, J. Wang, and G. Pan, "Molecularly Imprinted Synthetic Antibodies: From Chemical Design to Biomedical Applications," *Small*, vol. 16, no. 27. Wiley-VCH Verlag, Jul. 01, 2020. doi: 10.1002/smll.201906644.

[181] M. S. Silva, A. P. M. Tavares, H. D. de Faria, M. G. F. Sales, and E. C. Figueiredo, "Molecularly Imprinted Solid Phase Extraction Aiding the Analysis of Disease Biomarkers," *Critical Reviews in Analytical Chemistry*, vol. 52, no. 5. Taylor and Francis Ltd., pp. 933–948, 2022. doi: 10.1080/10408347.2020.1843131.

[182] L. Hu and Y. Zhao, "Cross-Linked Micelles with Enzyme-Like Active Sites for Biomimetic Hydrolysis of Activated Esters," *Helv. Chim. Acta*, vol. 100, no. e1700147, pp. 1–10, 2017, doi: 10.1002/hlca.201700147.

[183] L. Hu, M. Arifuzzaman, and Y. Zhao, "Controlling Product Inhibition through Substrate-Specific Active Sites in Nanoparticle-Based Phosphodiesterase and Esterase," *ACS Catal*, vol. 9, pp. 5019–5024, 2019, doi: 10.1021/acscatal.9b00630.

[184] Z. Chen, B. Sellergren, and X. Shen, "Synergistic Catalysis by ' Polymeric Microzymes and Inorganic Nanozymes ': The 1 + 1 > 2 Effect for Intramolecular Cyclization of Peptides," *Front Chem*, vol. 5, no. 60, pp. 1–7, 2017, doi: 10.3389/fchem.2017.00060.

[185] Z. Zhang, X. Zhang, B. Liu, and J. Liu, "Molecular Imprinting on Inorganic Nanozymes for Hundred-fold Enzyme Speci fi city," *J. Am. Chem. Soc.*, vol. 139, p. 5412−5419, 2017, doi: 10.1021/jacs.7b00601.

[186] X. Wang, L. Qin, M. Zhou, Z. Lou, and H. Wei, "Nanozyme Sensor Arrays for Detecting Versatile Analytes from Small Molecules to Proteins and Cells," *Anal. Chem.*, vol. 90, p. 11696−11702, 2018, doi: 10.1021/acs.analchem.8b03374.

[187] Z. Zhang, Y. Li, X. Zhang, and J. Liu, "Molecularly imprinted nanozymes with faster catalytic activity and better specificity," *Nanoscale*, vol. 11, pp. 4854–4863, 2019, doi: 10.1039/c8nr09816f.

[188] Y. Hu, J. Liu, H. Xing, H. Zhou, and M. Wu, "Fabrication and Application of Magnetically Catalytic Imprinting Nanozymes," *Chemistry Select*, vol. 5, pp. 8284–8288, 2020, doi: 10.1002/slct.202000900.

[189] L. Fan *et al.*, "A Novel AuNP-Based Glucose Oxidase Mimic with Enhanced Activity and Selectivity Constructed by Molecular Imprinting and O 2 -Containing Nanoemulsion Embedding," *Adv. Mater. Interfaces*, vol. 5, no. 1801070, pp. 1–9, 2018, doi: 10.1002/admi.201801070.

[190] F. Lin, L. Doudou, W. Haoan, C. Yan, G. Ning, and Z. Yu, "Catalytic Gold-Platinum Alloy Nanoparticles and a Novel Glucose Oxidase Mimic with Enhanced Activity and Selectivity Constructed by Molecular Imprinting," *Analytical Methods*, pp. 1–8, 2019, doi: 10.1039/C9AY01308C.

[191] C. Fan *et al.*, "Molecular imprinting on PtPd nanoflowers for selective recognition and determination of hydrogen peroxide and glucose," *RSC Adv*, pp. 33678–33683, 2019, doi: 10.1039/c9ra05677g.

[192] L. Guo, H. Zheng, C. Zhang, L. Qu, and L. Yu, "A novel molecularly imprinted sensor based on PtCu bimetallic nanoparticle deposited on PSS functionalized graphene with

peroxidase-like activity for selective determination of puerarin," *Talanta*, vol. 210, no. 120621, 2020, doi: 10.1016/j.talanta.2019.120621.

[193] Y. Wu, Q. Chen, S. Liu, H. Xiao, M. Zhang, and X. Zhang, "Surface molecular imprinting on g-C 3 N 4 photooxidative nanozyme for improved colorimetric biosensing," *Chinese Chemical Letters*, vol. 30, no. 12, pp. 2186–2190, 2019, doi: 10.1016/j.cclet.2019.08.014.

[194] S. Li *et al.*, "Biosensors and Bioelectronics Novel chloramphenicol sensor based on aggregation-induced electrochemiluminescence and nanozyme amplification," *Biosens Bioelectron*, vol. 176, p. 112944, 2021, doi: 10.1016/j.bios.2020.112944.

[195] M. Yan *et al.*, "Sensitive and Simple Competitive Biomimetic Nanozyme-Linked Immunosorbent Assay for Colorimetric and Surface-Enhanced Raman Scattering Sensing of Triazophos," *J. Agric. Food Chem*, vol. 67, p. 9658−9666, 2019, doi: 10.1021/acs.jafc.9b03401.

[196] J. He, G. Liu, M. Jiang, L. Xu, F. Kong, and Z. Xu, "Development of novel biomimetic enzyme- linked immunosorbent assay method based on Au @ SiO 2 nanozyme labelling for the detection of sulfadiazine," *Food Agric Immunol*, vol. 31, no. 1, pp. 341–351, 2020, doi: 10.1080/09540105.2020.1728234.

[197] J. He, L. Zhang, L. Xu, F. Kong, and Z. Xu, "Development of Nanozyme-Labeled Biomimetic Immunoassay for Determination of Sulfadiazine Residue in Foods," *Advances in Polymer Technology*, vol. 2020, pp. 1–8, 2020.

[198] X. Wang, X. Song, L. Si, L. Xu, and Z. Xu, "A novel biomimetic immunoassay method based on Pt nanozyme and molecularly imprinted polymer for the detection of histamine in foods nanozyme and molecularly imprinted polymer for the," *Food Agric Immunol*, vol. 31, no. 1, pp. 1036–1050, 2020, doi: 10.1080/09540105.2020.1807916.

[199] Z. Zhang, Y. Liu, X. Zhang, and J. Liu, "A Cell-Mimicking Structure Converting Analog Volume Changes to Digital Colorimetric Output with Molecular Selectivity," *Nano Lett*, vol. 17, p. 7926−7931, 2017, doi: 10.1021/acs.nanolett.7b04298.

[200] A. G. P. Ross, S. M. Crow, and M. W. Tyndal, "Planning for the Next Global Pandemic," *International Journal of Infectious Diseases*, vol. 38, pp. 89–94, 2015, doi: 10.1016/j.ijid.2015.07.016.

[201] P. Zhou *et al.*, "A pneumonia outbreak associated with a new coronavirus of probable bat origin," *Nature*, vol. 579, no. 7798, pp. 270–273, 2020, doi: 10.1038/s41586-020-2012-7.

[202] D. K. W. Chu *et al.*, "Molecular Diagnosis of a Novel Coronavirus (2019-nCoV) Causing an Outbreak of Pneumonia," *Clin Chem*, vol. 66, no. 4, pp. 549–555, 2020, doi: 10.1093/clinchem/hvaa029.

[203] H. Nishiura *et al.*, "Estimation of the asymptomatic ratio of novel coronavirus infections (COVID-19)," *International Journal of Infectious Diseases*, vol. 94, pp. 154–155, 2020, doi: 10.1016/j.ijid.2020.03.020.

[204] B. Sun *et al.*, "Kinetics of SARS-CoV-2 specific IgM and IgG responses in COVID-19 patients," *Emerg Microbes Infect*, vol. 9, pp. 940–948, 2020, doi: 10.1080/22221751.2020.1762515.

[205] K. K.-W. To *et al.*, "Temporal profiles of viral load in posterior oropharyngeal saliva samples and serum antibody responses during infection by SARS-CoV-2 : an observational cohort study," *Lancet Infect Dis*, vol. 20, pp. 565–574, 2020, doi: 10.1016/S1473-3099(20)30196-1.

[206] J. D. Whitman *et al.*, "Evaluation of SARS-CoV-2 serology assays reveals a range of test performance," *Nat Biotechnol*, vol. 38, pp. 1174–1183, 2020, doi: 10.1038/s41587-020-0659-0.

[207] M. A. Macmullan *et al.*, "ELISA detection of SARS - CoV - 2 antibodies in saliva," *Sci Rep*, vol. 10, no. 20818, pp. 1–8, 2020, doi: 10.1038/s41598-020-77555-4.

[208] N. Koerber *et al.*, "Dynamics of spike-and nucleocapsid speci fi c immunity during long-term follow-up and vaccination of SARS-CoV-2 convalescents," *Nat Commun*, vol. 13, no. 153, pp. 1–14, 2022, doi: 10.1038/s41467-021-27649-y.

[209] N. Kumar, N. P. Shetti, S. Jagannath, and T. M. Aminabhavi, "Electrochemical sensors for the detection of SARS-CoV-2 virus," *Chemical Engineering Journal*, vol. 430, no. 132966, pp. 1–15, 2022, doi: 10.1016/j.cej.2021.132966.

[210] A. Yakoh, U. Pimpitak, S. Rengpipat, N. Hirankarn, O. Chailapakul, and S. Chaiyo, "Paper-based electrochemical biosensor for diagnosing COVID-19: Detection of SARS-CoV-2 antibodies and antigen," *Biosens Bioelectron*, vol. 176, no. 112912, pp. 1–8, 2021, doi: 10.1016/j.bios.2020.112912.

[211] S. K. Elledge *et al.*, "Engineering luminescent biosensors for point-of-care SARS-CoV-2 antibody detection," *Nat Biotechnol*, vol. 39, pp. 928–935, 2021, doi: 10.1038/s41587-021-00878-8.

[212] O. Calvo-lozano *et al.*, "Label-free plasmonic biosensor for rapid , quantitative , and highly sensitive COVID-19 serology : implementation and clinical validation," *Anal Chem*, 2021.

[213] A. Ali *et al.*, "Sensing of COVID-19 Antibodies in Seconds via Aerosol Jet Nanoprinted Reduced-Graphene-Oxide-Coated 3D Electrodes," *Advanced Materials*, vol. 33, no. 2006647, pp. 1–15, 2021, doi: 10.1002/adma.202006647.

[214] X. Bin, E. H. Sargent, and S. O. Kelley, "Nanostructuring of sensors determines the efficiency of biomolecular capture," *Anal Chem*, vol. 82, no. 14, pp. 5928–5931, 2010, doi: 10.1021/ac101164n.

[215] L. Soleymani, Z. Fang, E. H. Sargent, and S. O. Kelley, "Programming the detection limits of biosensors through controlled nanostructuring," *Nat Nanotechnol*, vol. 4, no. 12, pp. 844–848, 2009, doi: 10.1038/nnano.2009.276.

[216] Z. Wang and Z. Dai, "Carbon nanomaterial-based electrochemical biosensors: An overview," *Nanoscale*, vol. 7, no. 15, pp. 6420–6431, 2015, doi: 10.1039/c5nr00585j.

[217] M. Pagán, D. Suazo, N. del Toro, and K. Griebenow, "A comparative study of different protein immobilization methods for the construction of an efficient nano-structured lactate oxidase-SWCNT-biosensor," *Biosens Bioelectron*, vol. 64, pp. 138–146, 2015, doi: 10.1016/j.bios.2014.08.072.

[218] N. Etminan, M. Yoosefian, H. Raissi, and M. Hakimi, "Solvent effects on the stability and the electronic properties of histidine/Pd-doped single-walled carbon nanotube biosensor," *J Mol Liq*, vol. 214, pp. 313–318, 2016, doi: 10.1016/j.molliq.2015.12.009.

[219] H. Ashiba *et al.*, "Detection of norovirus virus-like particles using a surface plasmon resonance-assisted fluoroimmunosensor optimized for quantum dot fluorescent labels," *Biosens Bioelectron*, vol. 93, pp. 260–266, 2017, doi: 10.1016/j.bios.2016.08.099.

[220] Z. Deng, Y. Zhang, J. Yue, F. Tang, and Q. Wei, "Green and orange CdTe quantum dots as effective pH-sensitive fluorescent probes for dual simultaneous and independent detection of viruses," *Journal of Physical Chemistry B*, vol. 111, no. 41, pp. 12024–12031, 2007, doi: 10.1021/jp074609z.

[221] A. M. Piloto, D. S. M. Ribeiro, S. S. M. Rodrigues, C. Santos, J. L. M. Santos, and M. G. F. Sales, "Plastic antibodies tailored on quantum dots for an optical detection of myoglobin down to the femtomolar range," *Sci Rep*, vol. 8, pp. 1–11, 2018, doi: 10.1038/s41598-018-23271-z.

[222] Q. Liu, X. Lu, J. Li, X. Yao, and J. Li, "Direct electrochemistry of glucose oxidase and electrochemical biosensing of glucose on quantum dots / carbon nanotubes electrodes," *Biosens Bioelectron*, vol. 22, pp. 3203–3209, 2007, doi: 10.1016/j.bios.2007.02.013.

[223] M. A. Macdonald and H. A. Andreas, "Method for equivalent circuit determination for electrochemical impedance spectroscopy data of protein adsorption on solid surfaces," *Electrochim Acta*, vol. 129, pp. 290–299, 2014, doi: 10.1016/j.electacta.2014.02.046.

[224] E. B. Bahadır and M. K. Sezgintürk, "A review on impedimetric biosensors A review on impedimetric biosensors," vol. 1401, 2016, doi: 10.3109/21691401.2014.942456.

[225] F. Lisdat and D. Schäfer, "The use of electrochemical impedance spectroscopy for biosensing," *Anal Bioanal Chem*, vol. 391, no. 5, pp. 1555–1567, 2008, doi: 10.1007/s00216-008-1970-7.

[226] N. O. Laschuk, E. B. Easton, and O. V. Zenkina, "Reducing the resistance for the use of electrochemical impedance spectroscopy analysis in materials chemistry," *RSC Adv*, vol. 11, no. 45, pp. 27925–27936, 2021, doi: 10.1039/d1ra03785d.

[227] G. Cabral-Miranda, A. R. Cardoso, L. C. S. Ferreira, M. G. F. Sales, and M. F. Bachmann, "Biosensor-based selective detection of Zika virus specific antibodies in infected individuals," *Biosens Bioelectron*, vol. 113, no. May, pp. 101–107, 2018, doi: 10.1016/j.bios.2018.04.058.

[228] A. R. Cardoso, G. Cabral-miranda, A. Reyes-sandoval, M. F. Bachmann, and M. G. F. Sales, "Detecting circulating antibodies by controlled surface modi fi cation with speci fi c target proteins : Application to malaria," *Biosens Bioelectron*, vol. 91, pp. 833–841, 2017, doi: 10.1016/j.bios.2017.01.031.

[229] D. Harvey, "Modern Analytic Chemistry," in *Modern Analytical Chemistry*, 1st ed., K. Kane, Ed., McGraw-Hill Higher Education, 2000, p. 797.

[230] N. Renard *et al.*, "Performance Characteristics of the Vidas SARS-CoV-2 IgM and IgG Serological Assays," *J Clin Microbiol*, vol. 59, no. 4, pp. 1–14, 2021.

[231] M. Bubonja-˘Sonje, L. Bati˘ci´c, M. Abram, and Đ. C. Grbe˘sa, "Diagnostic accuracy of three SARS-CoV2 antibody detection assays , neutralizing effect and longevity of serum antibodies," *J Virol Methods*, vol. 293, no. 114173, pp. 1–7, 2021, doi: 10.1016/j.jviromet.2021.114173.

[232] K. Jiang, L. S. Schadler, R. W. Siegel, X. Zhang, and M. Terrones, "Protein immobilization on carbon nanotubes via a two-step process of diimide-activated amidation," *J Mater Chem*, vol. 14, pp. 37–39, 2004.

[233] A. I. López-Lorente, B. M. Simonet, and M. Valcárcel, "Raman spectroscopic characterization of single walled carbon nanotubes : in fl uence of the sample aggregation state," *Analyst*, vol. 139, pp. 290–298, 2014, doi: 10.1039/c3an00642e.

[234] J. S. Terry *et al.*, "Development of a SARS-CoV-2 nucleocapsid specific monoclonal antibody," *Virology*, vol. 558, pp. 28–37, 2021, doi: 10.1016/j.virol.2021.01.003.

[235] X. Li *et al.*, "Enhancing the performance of paper-based electrochemical impedance spectroscopy nanobiosensors: An experimental approach," *Biosens Bioelectron*, vol. 177, no. 112672, pp. 1–8, 2021, doi: 10.1016/j.bios.2020.112672.

[236] A. Ali *et al.*, "Sensing of COVID-19 Antibodies in Seconds via Aerosol Jet Printed Three Dimensional Electrodes," *medRxiv*, pp. 1–40, 2020.

[237] M. Z. Rashed *et al.*, "Rapid detection of SARS-CoV-2 antibodies using electrochemical impedance-based detector," *Biosens Bioelectron*, vol. 171, no. 112709, pp. 1–6, 2021, doi: 10.1016/j.bios.2020.112709.

[238] L. Liv, "Electrochemical immunosensor platform based on gold-clusters, cysteamine and glutaraldehyde modified electrode for diagnosing COVID-19," *Microchemical Journal*, vol. 168, no. 106445, pp. 1–7, 2021, doi: 10.1016/j.microc.2021.106445.

[239] D. Brinati, A. Campagner, D. Ferrari, M. Locatelli, G. Banfi, and F. Cabitza, "Detection of COVID-19 Infection from Routine Blood Exams with Machine Learning: A Feasibility Study," *J Med Syst*, vol. 44, no. 8, pp. 1–12, 2020, doi: 10.1007/s10916-020-01597-4.

[240] M. Plebani, "Errors in clinical laboratories or errors in laboratory medicine?," *Clin Chem Lab Med*, vol. 44, no. 6, pp. 750–759, 2006, doi: 10.1515/CCLM.2006.123.

[241] J. Peña-Bahamonde, H. N. Nguyen, S. K. Fanourakis, and D. F. Rodrigues, "Recent advances in graphene-based biosensor technology with applications in life sciences," *Journal of Nanobiotechnology*, vol. 16, no. 1. BioMed Central Ltd., Sep. 22, 2018. doi: 10.1186/s12951-018-0400-z.

[242] V. Georgakilas *et al.*, "Functionalization of graphene: Covalent and non-covalent approaches, derivatives and applications," *Chemical Reviews*, vol. 112, no. 11. pp. 6156–6214, Nov. 14, 2012. doi: 10.1021/cr3000412.

[243] H. A. Alhazmi *et al.*, "Graphene-based biosensors for disease theranostics: Development, applications, and recent advancements," *Nanotechnology Reviews*, vol. 11, no. 1. De Gruyter Open Ltd, pp. 96–116, Jan. 01, 2021. doi: 10.1515/ntrev-2022-0009.

[244] C. Alatzoglou *et al.*, "Development of a Multi-Enzymatic Biocatalytic System through Immobilization on High Quality Few-Layer bio-Graphene," *Nanomaterials*, vol. 13, no. 1, Jan. 2023, doi: 10.3390/nano13010127.

[245] C. V. Kumar and A. Pattammattel, "BioGraphene Direct Exfoliation of Graphite in a Kitchen Blender for Enzymology Applications," in *Methods in Enzymology*, vol. 571, Academic Press Inc., 2016, pp. 225–244. doi: 10.1016/bs.mie.2016.03.009.

[246] A. Pattammattel and C. V. Kumar, "Kitchen Chemistry 101: Multigram Production of High Quality Biographene in a Blender with Edible Proteins," *Adv Funct Mater*, vol. 25, no. 45, pp. 7088–7098, Dec. 2015, doi: 10.1002/adfm.201503247.

[247] D. P. Oran and E. J. Topol, "Prevalence of asymptomatic SARS-CoV-2 infection. A narrative review," *Ann Intern Med*, vol. 173, no. 5, pp. 362–368, Sep. 2020, doi: 10.7326/M20-3012.

[248] A. Shields *et al.*, "SARS-CoV-2 seroprevalence and asymptomatic viral carriage in healthcare workers: A cross-sectional study," *Thorax*, vol. 75, no. 12, pp. 1089–1094, Dec. 2020, doi: 10.1136/thoraxjnl-2020-215414.

[249] P. V'kovski, A. Kratzel, S. Steiner, H. Stalder, and V. Thiel, "Coronavirus biology and replication: implications for SARS-CoV-2," *Nature Reviews Microbiology*, vol. 19, no. 3. Nature Research, pp. 155–170, Mar. 01, 2021. doi: 10.1038/s41579-020-00468-6.

[250] F. Li, "Structure, Function, and Evolution of Coronavirus Spike Proteins," *Annual Review of Virology*, vol. 3. Annual Reviews Inc., pp. 237–261, Sep. 29, 2016. doi: 10.1146/annurev-virology-110615-042301.

[251] C. Wu *et al.*, "Analysis of therapeutic targets for SARS-CoV-2 and discovery of potential drugs by computational methods," *Acta Pharm Sin B*, vol. 10, no. 5, pp. 766–788, May 2020, doi: 10.1016/j.apsb.2020.02.008.

[252] F. Amanat *et al.*, "A serological assay to detect SARS-CoV-2 seroconversion in humans," *Nat Med*, vol. 26, no. 7, pp. 1033–1036, Jul. 2020, doi: 10.1038/s41591-020-0913-5.

[253] C. W. Farnsworth and N. W. Anderson, "SARS-CoV-2 Serology: Much Hype, Little Data," *Clin Chem*, vol. 66, no. 7, pp. 875–877, Jul. 2020, doi: 10.1093/clinchem/hvaa107.

[254] M. Lipsitch, D. L. Swerdlow, and L. Finelli, "Defining the Epidemiology of Covid-19 — Studies Needed," *New England Journal of Medicine*, vol. 382, no. 13, pp. 1194–1196, Mar. 2020, doi: 10.1056/nejmp2002125.

[255] Q. X. Long *et al.*, "Antibody responses to SARS-CoV-2 in patients with COVID-19," *Nat Med*, vol. 26, no. 6, pp. 845–848, Jun. 2020, doi: 10.1038/s41591-020-0897-1.

[256] A. Petherick, "Developing antibody tests for SARS-CoV-2," *The Lancet*, vol. 395, no. 10230, pp. 1101–1102, 2020, [Online]. Available: www.thelancet.com

[257] N. Sethuraman, S. S. Jeremiah, and A. Ryo, "Interpreting Diagnostic Tests for SARS-CoV-2," *JAMA - Journal of the American Medical Association*, vol. 323, no. 22. American Medical Association, pp. 2249–2251, Jun. 09, 2020. doi: 10.1001/jama.2020.8259.

[258] P. Tiberghien, X. de Lamballerie, P. Morel, P. Gallian, K. Lacombe, and Y. Yazdanpanah, "Collecting and evaluating convalescent plasma for COVID-19 treatment: why and

how?," *Vox Sanguinis*, vol. 115, no. 6. Blackwell Publishing Ltd, pp. 488–494, Aug. 01, 2020. doi: 10.1111/vox.12926.

[259] E. Cesewski and B. N. Johnson, "Electrochemical biosensors for pathogen detection," *Biosensors and Bioelectronics*, vol. 159. Elsevier Ltd, Jul. 01, 2020. doi: 10.1016/j.bios.2020.112214.

[260] X.-F. Cai *et al.*, "A Peptide-based Magnetic Chemiluminescence Enzyme Immunoassay for Serological Diagnosis of Coronavirus Disease 2019 (COVID-19)," *J Infect Dis*, vol. 222, no. 2, pp. 189–193, 2020.

[261] J. Xiang *et al.*, "Evaluation of Enzyme-Linked Immunoassay and Colloidal Gold-Immunochromatographic Assay Kit for Detection of Novel Coronavirus (SARS-Cov-2) Causing an Outbreak of Pneumonia (COVID-19)," *MedRxiv.*, 2020, doi: 10.1101/2020.02.27.20028787.

[262] T. Bertok *et al.*, "Electrochemical Impedance Spectroscopy Based Biosensors: Mechanistic Principles, Analytical Examples and Challenges towards Commercialization for Assays of Protein Cancer Biomarkers," *ChemElectroChem*, vol. 6, no. 4. Wiley-VCH Verlag, pp. 989–1003, Feb. 15, 2019. doi: 10.1002/celc.201800848.

[263] J. Leva-Bueno, S. A. Peyman, and P. A. Millner, "A review on impedimetric immunosensors for pathogen and biomarker detection," *Medical Microbiology and Immunology*, vol. 209, no. 3. Springer, pp. 343–362, Jun. 01, 2020. doi: 10.1007/s00430-020-00668-0.

[264] S. Vogt, Q. Su, C. Gutiérrez-Sánchez, and G. Nöll, "Critical View on Electrochemical Impedance Spectroscopy Using the Ferri/Ferrocyanide Redox Couple at Gold Electrodes," *Anal Chem*, vol. 88, no. 8, pp. 4383–4390, May 2016, doi: 10.1021/acs.analchem.5b04814.

[265] A. R. Cardoso, G. Cabral-Miranda, A. Reyes-Sandoval, M. F. Bachmann, and M. G. F. Sales, "Detecting circulating antibodies by controlled surface modification with specific target proteins: Application to malaria," *Biosens Bioelectron*, vol. 91, pp. 833–841, May 2017, doi: 10.1016/j.bios.2017.01.031.

[266] A. R. Cardoso *et al.*, "An ultra-sensitive electrochemical biosensor using the Spike protein for capturing antibodies against SARS-CoV-2 in point-of-care," *Mater Today Bio*, vol. 16, Dec. 2022, doi: 10.1016/j.mtbio.2022.100354.

[267] L. Dai, D. W. Chang, J. B. Baek, and W. Lu, "Carbon nanomaterials for advanced energy conversion and storage," *Small*, vol. 8, no. 8. pp. 1130–1166, Apr. 23, 2012. doi: 10.1002/smll.201101594.

[268] L. de Souza Freire *et al.*, "An Electrochemical Immunosensor Based on Carboxylated Graphene/SPCE for IgG-SARS-CoV-2 Nucleocapsid Determination," *Biosensors (Basel)*, vol. 12, no. 12, Dec. 2022, doi: 10.3390/bios12121161.

[269] A. C. Marques, A. R. Cardoso, R. Martins, M. G. F. Sales, and E. Fortunato, "Laser-Induced Graphene-Based Platforms for Dual Biorecognition of Molecules," *ACS Appl Nano Mater*, vol. 3, no. 3, pp. 2795–2803, Mar. 2020, doi: 10.1021/acsanm.0c00117.

[270] S. N. Korobeynikov, V. V. Alyokhin, and A. V. Babichev, "On the molecular mechanics of single layer graphene sheets," *Int J Eng Sci*, vol. 133, pp. 109–131, Dec. 2018, doi: 10.1016/j.ijengsci.2018.09.001.

[271] D. G. Papageorgiou, I. A. Kinloch, and R. J. Young, "Mechanical properties of graphene and graphene-based nanocomposites," *Progress in Materials Science*, vol. 90. Elsevier Ltd, pp. 75–127, Oct. 01, 2017. doi: 10.1016/j.pmatsci.2017.07.004.

[272] S. Ahadian *et al.*, "Facile and green production of aqueous graphene dispersions for biomedical applications," *Nanoscale*, vol. 7, no. 15, pp. 6436–6443, Apr. 2015, doi: 10.1039/c4nr07569b.

[273] G. Martins *et al.*, "Novel approach based on GQD-PHB as anchoring platform for the development of SARS-CoV-2 electrochemical immunosensor," *Anal Chim Acta*, vol. 1232, Nov. 2022, doi: 10.1016/j.aca.2022.340442.

[274] B. A. Braz *et al.*, "Graphene-Binding Peptide in Fusion with SARS-CoV-2 Antigen for Electrochemical Immunosensor Construction," *Biosensors (Basel)*, vol. 12, no. 10, Oct. 2022, doi: 10.3390/bios12100885.

[275] S. Fauziah, A. Karlsson, and H. Gustavsson, "Density Functional Theory (DFT) Study of Molecularly Imprinted Polymer (MIP) Methacrylic Acid (MAA) with D-Glucose Density Functional Theory (DFT) Study of Molecularly Imprinted Polymer (MIP) Methacrylic Acid (MAA) with D- Glucose," pp. 0–6, 2017, doi: 10.1088/1757-899X/214/1/012004.

[276] C. Sabu, T. K. Henna, V. R. Raphey, K. P. Nivitha, and K. Pramod, "Biosensors and Bioelectronics Advanced biosensors for glucose and insulin," *Biosensors and Bioelectronic*, vol. 141, no. January, p. 111201, 2019, doi: 10.1016/j.bios.2019.03.034.

[277] H. Teymourian, A. Barfidokht, and J. Wang, "Electrochemical glucose sensors in diabetes management: An updated review (2010-2020)," *Chem Soc Rev*, vol. 49, no. 21, pp. 7671–7709, 2020, doi: 10.1039/d0cs00304b.

[278] Z. Peng *et al.*, "Blood glucose sensors and recent advances: A review," *J Innov Opt Health Sci*, vol. 15, no. 2, 2022, doi: 10.1142/S1793545822300038.

[279] A. H. Free and H. M. Free, "Self testing, an emerging component of clinical chemistry.," *Clin Chem*, vol. 30, no. 6, pp. 829–838, 1984, doi: 10.1093/clinchem/30.6.829.

[280] T. Henning, "Commercially Available Continuous Glucose Monitoring Systems," in *In Vivo Glucose Sensing*, John Wiley., D. D. Cunningham and J. A. Stenken, Eds., 2009, pp. 113–156. doi: 10.1002/9780470567319.ch5.

[281] K. A. Razak, Z. A. Zulkifli, N. S. Ridhuan, and N. M. Nor, "The effect of gold nanoparticles modified electrode on the glucose sensing performance The Effect of Gold Nanoparticles Modified Electrode onThe Glucose Sensing Performance," vol. 020015, no. July, 2017, doi: 10.1063/1.4993334.

[282] Y. Yoshimi, A. Narimatsu, K. Nakayama, S. Sekine, K. Hattori, and K. Sakai, "Development of an enzyme-free glucose sensor using the gate effect of a molecularly imprinted polymer," *Journal of Artificial Organs*, vol. 12, no. 4, pp. 264–270, 2009, doi: 10.1007/s10047-009-0473-4.

[283] M. Farid, L. Goudini, F. Piri, A. Zamani, and F. Saadati, "Molecular imprinting method for fabricating novel glucose sensor : Polyvinyl acetate electrode reinforced by MnO 2 / CuO loaded on graphene oxide nanoparticles," *Food Chem*, vol. 194, pp. 61–67, 2016, doi: 10.1016/j.foodchem.2015.07.128.

[284] X. Li *et al.*, "Impedimetric Enzyme-Free Detection of Glucose via a Computation-Designed Molecularly Imprinted Electrochemical Sensor Fabricated on Porous Ni Foam," *Electroanalysis*, vol. 29, no. 5, pp. 1243–1251, 2017, doi: 10.1002/elan.201600721.

[285] S. Cho, H. Noh, M. Won, C. Cho, and K. Bok, "Biosensors and Bioelectronics A selective glucose sensor based on direct oxidation on a bimetal catalyst with a molecular imprinted polymer," *Biosensors and Bioelectronic*, vol. 99, no. August 2017, pp. 471–478, 2018, doi: 10.1016/j.bios.2017.08.022.

[286] T. Kajisa and T. Sakata, "Biological and Medical Applications of Materials and Interfaces Molecularly Imprinted Artificial Biointerface for Enzyme-Free Glucose Transistor Molecularly Imprinted Artificial Biointerface for Enzyme-Free Glucose Transistor Department of Materials Scien," *ACS Appl Mater Interfaces*, pp. 1–39, 2018, doi: 10.1021/acsami.8b13317.

[287] A. Diouf, B. Bouchikhi, and N. El, "Materials Science & Engineering C A nonenzymatic electrochemical glucose sensor based on molecularly imprinted polymer and its application in measuring saliva glucose," *Materials Science & Engineering C*, vol. 98, no. December 2018, pp. 1196–1209, 2019, doi: 10.1016/j.msec.2019.01.001.

[288] E. Sehit, J. Drzazgowska, D. Buchenau, C. Yesildag, M. Lensen, and Z. Altintas, "Ultrasensitive nonenzymatic electrochemical glucose sensor based on gold nanoparticles and molecularly imprinted polymers," *Biosens Bioelectron*, vol. 165, no. July, p. 112432, 2020, doi: 10.1016/j.bios.2020.112432.

[289] B. Chang and S. Park, "Electrochemical Impedance Spectroscopy," vol. 3, pp. 207–229, 2010, doi: 10.1146/annurev.anchem.012809.102211.

[290] P. Dauphin-ducharme, N. Arroyo-curras, M. Kurnik, G. Ortega, H. Li, and K. W. Plaxco, "A Simulation-based Approach to Determining Electron Transfer Rates using Square-Wave Voltammetry," 2017, doi: 10.1021/acs.langmuir.7b00359.

[291] D. Tonelli, E. Scavetta, and I. Gualandi, "Electrochemical Deposition of Nanomaterials for Electrochemical Sensing," 2019, doi: 10.3390/s19051186.

[292] H.-C. Chiang, Y. Wang, Q. Zhang, and K. Levon, "Optimization of the Electrodeposition of Gold Nanoparticles for the Application of Highly Sensitive ," *Biosensors (Basel)*, vol. 9, no. 50, pp. 1–11, 2019.

[293] X. Kan *et al.*, "Molecularly imprinted polymers based electrochemical sensor for bovine hemoglobin recognition," *Sens Actuators B Chem*, vol. 168, pp. 395–401, 2012, doi: 10.1016/j.snb.2012.04.043.

[294] A. R. Cardoso, A. P. M. Tavares, and M. G. F. Sales, "In-situ generated molecularly imprinted material for chloramphenicol electrochemical sensing in waters down to the nanomolar level," *Sens Actuators B Chem*, vol. 256, pp. 420–428, Mar. 2018, doi: 10.1016/J.SNB.2017.10.114.

[295] R. S. Gomes, B. A. Gomez-Rodríguez, R. Fernandes, M. G. F. Sales, F. T. C. Moreira, and R. F. Dutra, "Plastic antibody of polypyrrole/multiwall carbon nanotubes on screen-printed electrodes for cystatin C detection," *Biosensors (Basel)*, vol. 11, no. 6, 2021, doi: 10.3390/bios11060175.

[296] T. S. C. R. Rebelo, R. Costa, A. T. S. C. Brandão, a. F. Silva, M. G. F. Sales, and C. M. Pereira, "Molecularly imprinted polymer SPE sensor for analysis of CA-125 on serum," *Anal Chim Acta*, vol. 1082, pp. 126–135, 2019, doi: 10.1016/j.aca.2019.07.050.

[297] a. Ramanavičius, a. Ramanavičiene, and a. Malinauskas, "Electrochemical sensors based on conducting polymer-polypyrrole," *Electrochim Acta*, vol. 51, no. 27, pp. 6025–6037, 2006, doi: 10.1016/j.electacta.2005.11.052.

[298] S. Sadki, P. Schottland, N. Brodie, and G. Sabouraud, "The mechanisms of pyrrole electropolymerization," *Chem Soc Rev*, vol. 29, no. 5, pp. 283–293, 2000, doi: 10.1039/a807124a.

[299] S. Resende, M. F. Frasco, and M. G. F. Sales, "A biomimetic photonic crystal sensor for label-free detection of urinary venous thromboembolism biomarker," *Sens Actuators B Chem*, vol. 312, no. March, p. 127947, 2020, doi: 10.1016/j.snb.2020.127947.

[300] K. Kantarovich, I. Tsarfati, L. A. Gheber, K. Haupt, and I. Bar, "Writing droplets of molecularly imprinted polymers by nano fountain pen and detecting their molecular interactions by surface-enhanced Raman scattering," *Anal Chem*, vol. 81, no. 14, pp. 5686–5690, Jul. 2009, doi: 10.1021/ac900418x.

[301] R. M. Roland and S. A. Bhawani, "Synthesis and Characterization of Molecular Imprinting Polymer Microspheres of Piperine: Extraction of Piperine from Spiked Urine," *J Anal Methods Chem*, vol. 2016, 2016, doi: 10.1155/2016/5671507.

[302] J. Ye, Y. Chen, and Z. Liu, "A Boronate Affinity Sandwich Assay: An Appealing Alternative to Immunoassays for the Determination of Glycoproteins," *Angewandte Chemie - International Edition*, vol. 53, no. 39, pp. 10386–10389, Jul. 2014, doi: 10.1002/anie.201405525.

[303] G. V. Martins, A. C. Marques, E. Fortunato, and M. G. F. Sales, "8-hydroxy-2′-deoxyguanosine (8-OHdG) biomarker detection down to picoMolar level on a plastic antibody film," *Biosens Bioelectron*, vol. 86, pp. 225–234, Dec. 2016, doi: 10.1016/j.bios.2016.06.052.

[304] F. T. C. Moreira *et al.*, "Detection of cardiac biomarker proteins using a disposable based on a molecularly imprinted polymer grafted onto graphite." [Online]. Available: www.himedialabs.com/

[305] V. Leskovac, S. Trivić, G. Wohlfahrt, J. Kandrač, and D. Peričin, "Glucose oxidase from Aspergillus niger: The mechanism of action with molecular oxygen, quinones, and one-electron acceptors," *International Journal of Biochemistry and Cell Biology*, vol. 37, no. 4. Elsevier Ltd, pp. 731–750, 2005. doi: 10.1016/j.biocel.2004.10.014.

[306] G. Wohlfahrt, S. Witt, J. Hendle, D. Schomburg, H. M. Kalisz, and H.-J. Hecht, "1.8 and 1.9 A° resolution structures of thePenicillium amagasakiense and Aspergillus nigerglucose oxidases as a basis for modelling substrate complexes," *Acta Crystallographica Section D*, vol. D55, pp. 969–977, 1999.

[307] P. MacHeroux, B. Kappes, and S. E. Ealick, "Flavogenomics - A genomic and structural view of flavin-dependent proteins," *FEBS Journal*, vol. 278, no. 15. pp. 2625–2634, Aug. 2011. doi: 10.1111/j.1742-4658.2011.08202.x.

[308] M. A. R. Khan, F. T.C. Moreira, J. Riu, and M. G. F. Sales, "Plastic antibody for the electrochemical detection of bacterial surface proteins," *Sens Actuators B Chem*, vol. 233, pp. 697–704, Oct. 2016, doi: 10.1016/j.snb.2016.04.075.

[309] A. P. M. Tavares, N. S. Ferreira, L. A. A. N. A. Truta, and M. G. F. Sales, "Conductive Paper with Antibody-Like Film for Electrical Readings of Biomolecules," *Sci Rep*, vol. 6, May 2016, doi: 10.1038/srep26132.

[310] R. Cohen, R. E. Bitton, N. S. Herzallh, Y. Cohen, and O. Yehezkeli, "Utilization of FAD-Glucose Dehydrogenase from T. emersonii for Amperometric Biosensing and Biofuel Cell Devices," *Anal Chem*, vol. 93, no. 33, pp. 11585–11591, Aug. 2021, doi: 10.1021/acs.analchem.1c02157.

[311] P. Bollella and E. Katz, "Enzyme-based biosensors: Tackling electron transfer issues," *Sensors (Switzerland)*, vol. 20, no. 12. MDPI AG, pp. 1–32, Jun. 01, 2020. doi: 10.3390/s20123517.

[312] S. D. Wijayanti, F. Schachinger, R. Ludwig, and D. Haltrich, "Electrochemical and biosensing properties of an FAD-dependent glucose dehydrogenase from Trichoderma virens," *Bioelectrochemistry*, vol. 153, Oct. 2023, doi: 10.1016/j.bioelechem.2023.108480.

⟨2023⟩

ANA CARDOSO

NANOZYME+/DRIVING NANOZYMES TO-WARDS STEREOCHEMICAL RECOGNI-TION: APPLICATION TO BIOMOLECULES OF IN-TERESTS IN HEALTH

NOVA SCHOOL OF SCIENCE & TECHNOLOGY

⟨2023⟩

ANA RITA AIRES CARDOSO

NANOZYME+/DRIVING NANOZYMES TO-WARDS STEREOCHEMICAL RECOG-NITION: APPLICATION TO BIOMOLECULES OF IN-TERESTS IN HEALTH